Chem Soc Rev

REVIEW ARTICLE

View Article Online
View Journal | View Issue

Check for updates

Cite this: *Chem. Soc. Rev.*, 2020, **49**, 7167

Small molecule recognition of disease-relevant RNA structures†

Samantha M. Meyer, Christopher C. Williams, Yoshihiro Akahori, Toru Tanaka, Haruo Aikawa, Yuquan Tong, Jessica L. Childs-Disney and Matthew D. Disney *

Targeting RNAs with small molecules represents a new frontier in drug discovery and development. The rich structural diversity of folded RNAs offers a nearly unlimited reservoir of targets for small molecules to bind, similar to small molecule occupancy of protein binding pockets, thus creating the potential to modulate human biology. Although the bacterial ribosome has historically been the most well exploited RNA target, advances in RNA sequencing technologies and a growing understanding of RNA structure have led to an explosion of interest in the direct targeting of human pathological RNAs. This review highlights recent advances in this area, with a focus on the design of small molecule probes that selectively engage structures within disease-causing RNAs, with micromolar to nanomolar affinity. Additionally, we explore emerging RNA-target strategies, such as bleomycin A5 conjugates and ribonuclease targeting chimeras (RIBOTACs), that allow for the targeted degradation of RNAs with impressive potency and selectivity. The compounds discussed in this review have proven efficacious in human cell lines, patient-derived cells, and pre-clinical animal models, with one compound currently undergoing a Phase II clinical trial and another that recently garnerd FDA-approval, indicating a bright future for targeted small molecule therapeutics that affect RNA function.

Received 17th May 2020

DOI: 10.1039/d0cs00560f

rsc.li/chem-soc-rev

Open Access Article. Published on 25 September 2020. Downloaded on 8/9/2025 2:37:59 AM. This article is licensed under a Creative Commons Attribution-NonCommercial 3.0 Unported Licence.

1. Introduction

RNA is a critical component of the Central Dogma, best known for its roles in transcription and translation. However, non-coding (nc) RNAs play important functions critical for the regulation of cell homeostasis and normal biology.[1] These ncRNAs, such as microRNAs (miRNAs), small nucleolar RNAs (snoRNAs), small nuclear RNAs (snRNAs), transfer RNAs (tRNAs), long non-coding RNAs (lncRNAs), *etc.* (Fig. 1) are highly structured[1] and offered the first clues that RNA structures may play vital roles in human biology beyond the encoding and synthesis of protein. Indeed, this hypothesis has been proven true as RNA structures have been linked to both normal biology and disease pathology.[2,3]

The variability and complexity of RNA structures has been widely explored, leading to the appreciation that RNAs range from being largely disordered (dynamic) to adopting simple

Department of Chemistry, The Scripps Research Institute, 130 Scripps Way, Jupiter, FL, 33458, USA. E-mail: disney@scripps.edu

† Electronic supplementary information (ESI) available. See DOI: 10.1039/d0cs00560f

Samantha M. Meyer

Samantha M. Meyer received her BS in Biochemistry and Molecular Biology from the University of Wisconsin – Eau Claire in 2019. The following fall she began doctoral studies under the guidance of Prof. Matthew D. Disney at The Scripps Research Institute in Jupiter, Florida. Her current research focuses on targeting disease-causing RNAs with small molecules, with an emphasis on expanding the versatility of RIBOTACs.

Christopher C. Williams

Christopher C. Williams received his BA in Chemistry from Hamilton College (2017). He conducts his graduate studies under the guidance of Prof. Matthew D. Disney at The Scripps Research Institute in Florida, where he explores RNA-small molecule binding interactions in the context of infectious disease.

Open Access Article. Published on 25 September 2020. Downloaded on 8/9/2025 2:37:59 AM.
This article is licensed under a Creative Commons Attribution-NonCommercial 3.0 Unported Licence.

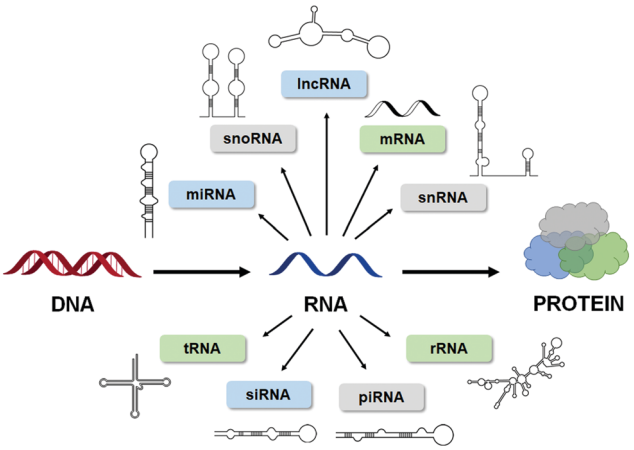

Fig. 1 RNA is highly structured. The Central Dogma of biology, showcasing the numerous types of structured RNAs that have been identified to date.

structures such as loops and bulges (secondary structure) to creating highly intricate pseudoknots, G-quadruplexes, and coaxial stacking (tertiary structure). The influence of these structures has been explored in the context of bacterial gene expression and riboswitches[4] and in viral replication and infection.[5] In the context of human biology, structured RNAs influence translational regulation,[6–8] alternative splicing,[9,10] and even enzymatic catalysis,[11–14] further demonstrating their intimate involvement in maintaining healthy biology. As these topics will not be reviewed in depth here, we direct the reader to the references cited above for additional detail.

Predictably, disruption of RNA structure *via* mutation, formation of unnatural RNA structures, *e.g.*, by insertions or expansions, or aberrant expression, leads to dysregulation of cellular processes, resulting in disease. For example, dysregulation of miRNAs, short regulatory RNAs that modulate gene expression *via* the RNA-induced silencing complex (RISC),[7] have

Yoshihiro Akahori

Yoshihiro Akahori received his PhD in Synthetic Organic Chemistry (2014) from the Nagoya City University, supervised by Prof. Seiichi Nakamura. While there he worked on synthesizing oxygenated natural terpenoids. He then joined Daiichi Sankyo Co., Ltd where he engaged in drug discovery research. Since 2020, he has worked at The Scripps Research Institute with Prof. Matthew D. Disney. His current research focuses on developing small molecules that target RNA.

Toru Tanaka

Toru Tanaka received his PhD in Organic Chemistry (2016) from Kyoto Pharmaceutical University under the guidance of Prof. Masayuki Yamashita, where he worked on using sulfoxonium methylide skeletal transformation reactions to open cyclopropane and cyclobutene rings. Since 2020, he has worked as a postdoctoral fellow with Prof. Matthew D. Disney. His current research focuses on the design and synthesis of small molecules that bind RNA.

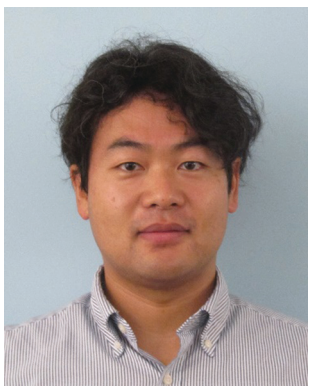

Haruo Aikawa

Haruo Aikawa was awarded his PhD in Chemistry from Tohoku University, Japan, in 2009, under Drs. Yoshinori Yamamoto and Naoki Asao. Dr. Aikawa also worked on peptide chemistry in the lab of Dr. Hirokazu Tamamura at Tokyo Medical and Dental University. His research on nucleic acid-binding molecules began in 2013 in the lab of Dr. Kazuhiko Nakatani at Osaka University. In 2018, he joined Dr. Matthew D. Disney's lab at The Scripps Research Institute in Florida as a postdoctoral fellow. His current research themes are regulation of RNA biology by small molecules targeting repeat expansion disorders and miRNAs.

Yuquan Tong

Yuquan Tong received his BS in Chemical and Biomolecular Engineering from the University of Illinois at Urbana – Champaign in 2019. Under the supervision of Prof. Matthew D. Disney, he started his doctoral studies at The Scripps Research Institute in Florida, working on small molecules targeting RNA. His current research focuses on targeting mRNAs of "undruggable" disease-causing proteins, including alpha synuclein and tau.

This journal is © The Royal Society of Chemistry 2020

Open Access Article. Published on 25 September 2020. Downloaded on 8/9/2025 2:37:59 AM.
This article is licensed under a Creative Commons Attribution-NonCommercial 3.0 Unported Licence.

been associated with, among others, cardiovascular disease, inflammatory disorders, and cancer.[7,15,16] Additionally, structured RNAs have been implicated in several neurological disorders, as reviewed in Bernat *et al.*,[17] a well-known example being RNA repeat expansion/microsatellite disorders. This class of disorders is responsible for over 30 human diseases including Huntington's disease (HD), amyotrophic lateral sclerosis (ALS), fragile X-associated tremor and ataxia syndrome (FXTAS), and myotonic dystrophies type 1 and 2 (DM1 and DM2).[17] The biological consequences of these repeat expansions will be reviewed in detail below.

To date, two main therapeutic strategies have been employed to target disease-causing RNAs: antisense oligonucleotides (ASOs) and small molecules.[18] ASOs are single-stranded nucleotide sequences designed to complementarily base pair a target RNA's primary sequence. ASOs, which often contain modified phosphate backbones and sugar motifs to protect against cellular degradation, either repress translation by sterically blocking ribosomal loading onto the RNA or induce degradation of the target RNA *via* Ribonuclease H (RNase H).[19] RNase H recognizes the RNA–DNA heteroduplex and hydrolyzes the phosphodiester bonds of the RNA strand, cleaving it.[19] Conversely, small molecules are designed to target RNA structure instead of sequence, much like how small molecules are designed to target proteins *via* structure-based recognition. Small molecule binding of an RNA target can modulate disease biology, thus creating avenues to further explore RNA-disease biology and potential therapeutics against RNA-associated disorders.[18]

This review provides a general overview of recently developed RNA-targeting small molecules, highlighting advances in the field that continue to push towards the development of potent and selective small molecule lead therapeutics. A focus is placed on small molecules targeting miRNA biogenesis, lncRNAs, mRNAs encoding intrinsically disordered proteins (IDPs), and repeat expansion disorders. This review details both the pathomechansims caused by the RNA's structure and how small molecules can alleviate this pathology. Additionally, emergent modalities such as RNA-targeted cleaver and degrader compounds, including ribonuclease targeting chimeras (RIBOTACs), are reviewed in detail, highlighting the selectivity and potency of these compounds. There is still much to be learned about small molecules targeting RNA before these probes can be converted into lead medicines, but a solid foundation has been laid to enable clinical advancement across multiple indications. (See Table 1 for a complete list of diseases mentioned in this review and the abbreviations used to define them.) A tutorial on targeting RNA structures derived from sequence with small molecules can be found in ref. 20.

Table 1 Commonly mentioned diseases and abbreviations

Disease	Abbreviation
Triple negative breast cancer	TNBC
Fragile X-associated tremor and ataxia syndrome	FXTAS
Spinal muscular atrophy	SMA
Frontotemporal dementia	FTD
Parkinsonism linked to chromosome 17	FTDP-17
Myotonic dystrophy type 1	DM1
Myotonic dystrophy type 2	DM2
C9orf72-associated frontotemporal dementia and amyotrophic lateral sclerosis	c9FTD/ALS
Parkinson's disease	PD

2. Small molecule targeting of miRNAs

MiRNAs are short 20–25 nucleotide (nt) sequences of RNA that negatively regulate gene expression through translational repression of their mRNA targets, dictated by sequence complementarity to the 3′ untranslated region (UTR) of the mRNA target. These RNAs are actively involved in regulation of cellular processes including proliferation, development, differentiation, and apoptosis. Like other types of RNAs, miRNAs are transcribed as primary transcripts (pri-miRs) that are processed into precursor miRNAs (pre-miRs), both of which fold into hairpin structures. These structures are cleaved sequentially by the nucleases Drosha and Dicer to produce the final, single-stranded mature miRNA (Fig. 2A).[7]

Biogenesis begins with the Drosha:DiGeorge syndrome critical region 8 (DGCR8) microprocessor complex that excises a portion of the pri-miR at the open stranded end of the hairpin, yielding a pre-miR of ~70 nucleotides in length. The pre-miR is then exported from the nucleus *via* exportin 5.[21] In the cytoplasm, pre-miR is further processed at the hairpin loop by the enzyme Dicer, which acts as a molecular ruler, yielding a double stranded miRNA.[22] The miRNA is then loaded into the argonaute (AGO)/RISC complex where the guide strand stays successfully loaded and the complementary strand is degraded.[23] After biogenesis, the RISC complex regulates gene expression either through translational inhibition *via* steric hinderance of ribosomal loading or *via* stimulation of complete mRNA decay.[24–26]

Due to the complexity of miRNA interaction networks (*i.e.*, multiple miRNAs often act upon one mRNA, and one miRNA can regulate multiple mRNAs),[27,28] dysregulation of miRNA expression has been associated with a variety of human diseases, especially cancer.[29–31] Examples of how RNA-binding small molecules have been designed and optimized to bring about potent and selective regulators of miRNA function are discussed in detail below.

2.1 Neomycin–nucleobase conjugates targeting oncogenic miRNAs

Neomycin–nucleobase conjugates are small molecules that target disease-causing miR-372 and -373 (Fig. 2C and Table S1, ESI†).[32] These bifunctional conjugates consist of (i) an artificial nucleobase designed to specifically recognize an RNA base pair of the double-stranded region of pre-miRNA and (ii) an aminoglycoside shown to have strong binding affinity to stem-loop RNA motifs. Artificial nucleobases engage in the formation of Hoogsteen-type triplex DNA helices,[33] and when conjugated to basic amino acids, form compounds with high affinity and selectivity for the stem loop structure of human immunodeficiency virus type 1 (HIV-1) transactivation response element (TAR) RNA.[34] Aminoglycoside antibiotics, which alone constitute

Open Access Article. Published on 25 September 2020. Downloaded on 8/9/2025 2:37:59 AM.
This article is licensed under a Creative Commons Attribution-NonCommercial 3.0 Unported Licence.

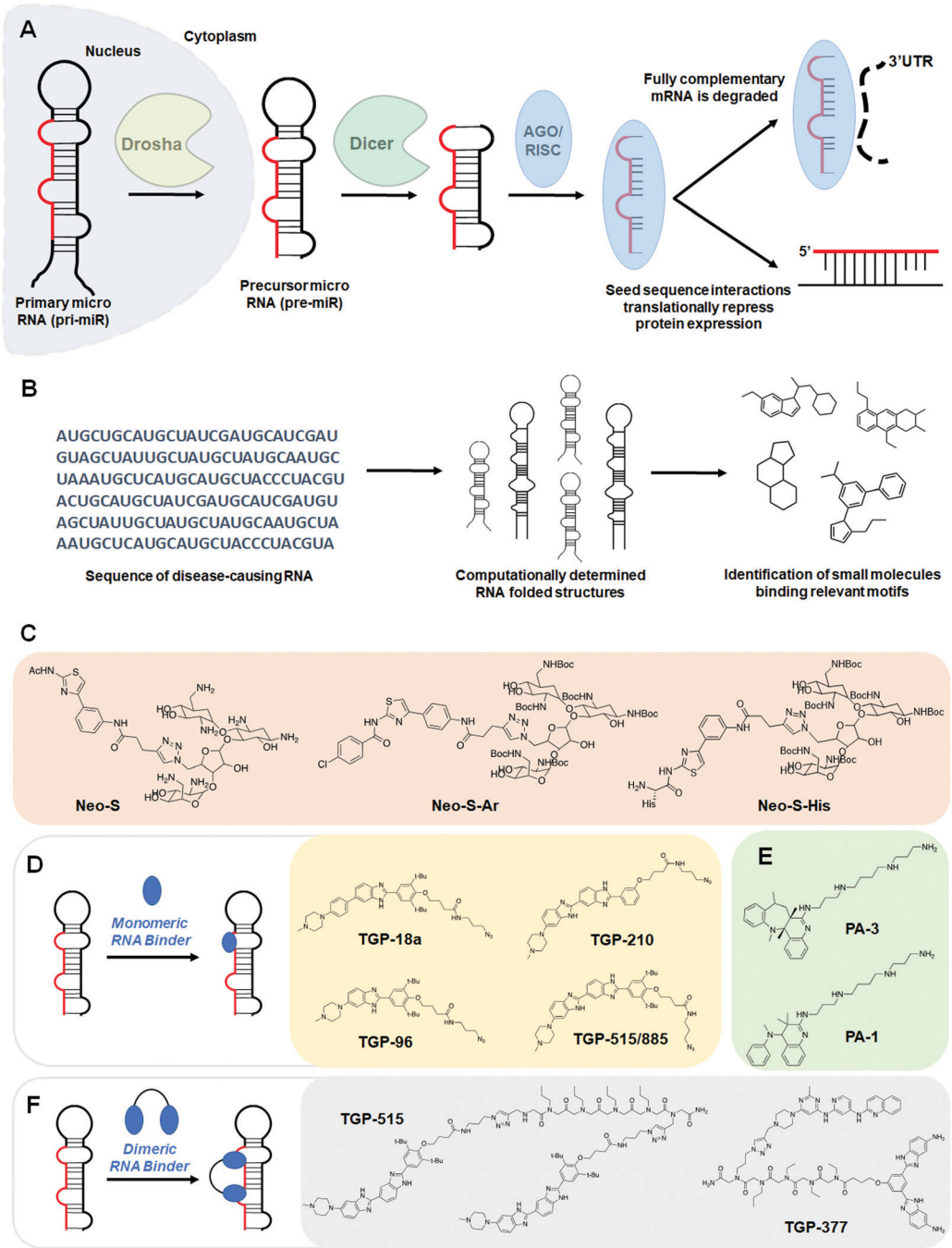

Fig. 2 Small molecule targeting of miRNAs. (A) Schematic of the biogenesis of miRNAs. Primary miRNAs (pri-miR) are processed by the nuclear RNase III Drosha and exported to the cytoplasm, affording precursor miRNAs (pre-miR), which are then processed by the RNase III endonuclease Dicer. The miRNA duplex is loaded into the AGO/RISC complex, where the duplex is dissociated and acts through either translational repression or mRNA degradation to downregulate target proteins. (B) Workflow schematic of the Inforna hit identification process. (C) Structures of neomycin conjugates that inhibit miRNA biogenesis. (D) Schematic of monomeric RNA binder mode of action, blocking functional processing sites on miRNA. Representative chemical structures of these monomers are also shown. (E) Structures of polyamines that inhibit miRNA biogenesis. (F) Dimeric RNA binders have improved potency and selectivity by binding to a functional site and nearby druggable motif simultaneously. Structures of representative miRNA-targeting dimers are shown.

a class of widely prescribed medicines targeting the decoding A-site in prokaryotic rRNA to inhibit protein translation, bind stem-loop structured RNAs along the major groove of the RNA duplex.

On the basis of these findings, the Duca lab rationalized conjugation of the aminoglycoside neomycin with an artificial nucleobase would yield chemical matter capable of binding the stem-loop sequences of miR-372 and -373.[32] These first-generation conjugate compounds fortuitously bound the Dicer processing sites of pre-miR-373 and pre-miR-372, inhibiting their biogenesis *in vitro*, as determined by a cell-free Förster resonance energy

 This journal is © The Royal Society of Chemistry 2020

Open Access Article. Published on 25 September 2020. Downloaded on 8/9/2025 2:37:59 AM. This article is licensed under a Creative Commons Attribution-NonCommercial 3.0 Unported Licence.

transfer (FRET) based assay, and reduced oncogenic burden in cells. The **Neo-S** conjugate inhibited Dicer cleavage *in vitro* and rescued expression of the miRNA-regulated protein Large Tumor Suppressor homologue 2 (LATS2). However, **Neo-S** was not entirely selective and affected expression of miR-17-5p, -21, and -200b in a dose-dependent manner, albeit to a lesser extent than miR-372 and -373 (Table S1, ESI†).

Through medicinal chemistry efforts, Vo *et al.*[35] synthesized and evaluated the properties of second generation compounds with the aim of improving potency and selectivity. Using a cell-free FRET based assay, they learned that select modifications of the artificial nucleobase motif yielded little to no improvement in inhibitory activity. Extended linker length proved deleterious and between a selection of other aminoglycosides, neomycin still remained the best at inhibiting Dicer processing. Preliminary evaluation of compounds offered two new structures for examination in further studies, the first of which quickly fell out of favor due to unspecific binding to both the stem and loop regions of pre-miR-372 and evidence of binding to double-stranded DNA and tRNA. The second structure, **Neo-S-Ar**, with an improved IC_{50} relative to **Neo-S** (1.0 μM *versus* 2.4 μM for **Neo-S**), decreases miR-372 and -373 levels in cells in a dose-dependent manner, but much like **Neo-S**, inhibits Dicer processing of pre-miR-17 and -21 and affects levels of miR-200b in AGS (human Caucasian gastric adenocarcinoma) cells (Table S1, ESI†). The authors noted that **Neo-S** and **Neo-S-Ar** only elicit a phenotypic response in AGS cells, which overexpress miR-372 and -373, and not in MKN74 (human gastric tubular adenocarcinoma) cells, which do not overexpress these oncogenic miRNAs. Despite imperfect selectivity, these efforts provided a lead for further drug optimization.

With the aim of improving potency and selectivity for the miR-372 and -373 targets, Vo *et al.*[36] reasoned that because amino acids are natural ligands of RNA and easily interact with negatively charged RNA structures/sequences, appending one such amino acid could improve potency and selectivity.[37] The lab had also shown that basic amino acids, including arginine, lysine, and histidine are particularly effective in the design of selective RNA ligands,[34,38] inspiring **Neo-S-His**, which had improved selectivity for pre-miR-372 over previous generations (**Neo-S** and **Neo-S-Ar**) (Table S1, ESI†).[36] Conjugation of different amino acids appended at various positions on the neomycin–nucleobase scaffold were synthesized, but **Neo-S-His** was the only compound selective for pre-miR-372 over DNA. Treatment of AGS cells with **Neo-S-His** showed the compound inhibited cell growth by ~40% and even though the compound also affected expression levels of oncogenic miR-21, aberrant expression of miR-21 has been shown to have no effect on the proliferation of AGS cells, indicating this off-target did not contribute to the observed *anti*-proliferative effects. Furthermore, expression levels of other miRNAs, including miR-371, -373, -17, and -200b, were not affected by **Neo-S-His**, unlike previous generations of the compound (Table S1, ESI†).

2.2 Polyamines targeting oncogenic miRNAs

In addition to neomycin–nucleobase conjugates, Staedel *et al.*[39] screened a 640-member library for inhibition of Dicer-mediated pre-miR-372 processing to identify novel scaffolds with enhanced potency and selectivity. The top hits were all polyamines, the most potent of which, **PA-1**, inhibited growth of AGS cells, but not MKN74 cells (Fig. 2E and Table S1, ESI†). Treatment of AGS cells with **PA-1** also resulted in a dose-dependent accumulation of the downstream protein LATS2, much like the first-generation neomycin–nucleobase conjugate series. **PA-1**, however, binds and affects expression levels of miRs other than miR-372 in AGS cells (Table S1, ESI†). Binding studies of **PA-1** revealed that RNA binding was enhanced most significantly by interactions between the polyamine chain and the RNA phosphate backbone, and less significantly by π–π interactions between the dihydroquinoline motif and specific nucleotides.[40] Therefore, a strained analog of **PA-1**, **PA-3**, featured a fused benzazepine-dihydroquinoline motif appended to the polyamine chain. Using the previously employed cell-free FRET based assay, it was shown that **PA-3** inhibited Dicer processing of pre-miR-372 twice as well as **PA-1**. Compared to **PA-1** and other newly synthesized analogs, **PA-3** showed (i) the most selective inhibition of Dicer-mediated processing of miR-372, (ii) the most selective binding of pre-miR-372 in the presence of a large excess of tRNA and DNA, and (iii) the greatest selectivity for pre-miR-372 and pre-miR-373 over other pre-miRNAs in terms of activity and affinity (Table S1, ESI†). Furthermore, thermodynamic binding profiles of the polyamine/pre-miR-372 complex revealed that **PA-3** bears the highest enthalpic contribution.

2.3 Design of monomeric small molecules targeting disease-causing miRNAs

Additional small molecules targeting miRNAs have been identified by the lead identification strategy dubbed Inforna.[41] (For a more in-depth, tutorial review of Inforna and its utilization please see ref. 20.) Inforna comprises a database of experimentally selected RNA motif-small molecule interactions and mines the structural motifs in a chosen disease-related RNA target, deduced from its sequence, for overlap with the database (Fig. 2B). Inforna allows for transcriptome-wide probing of bioactive small molecules that target RNA without target bias (a target agnostic approach). This ''bottom-up'' strategy has enabled the design of modularly assembled small molecules that bind RNAs linked to human disease, proving particularly successful in the targeting of disease-causing miRNAs. One such example includes the design of Targapremir-18a (**TGP-18a**), named for its targeting of pre–miR–18a (Fig. 2D and Table S1, ESI†).[42] *In vitro* studies showed that **TGP-18a** inhibits Dicer processing of multiple members of the miR-17-92 cluster, namely pre-miR-17, pre-miR-18a, and pre-miR-20a, which share a common bulge at the Dicer site and adjacent structural similarity. Using RT-qPCR, these *in vitro* results were corroborated in DU145 prostate cancer cells, in which miR-18a is overexpressed. Importantly, inhibition de-represses serine/threonine protein kinase 4 (STK4) and rescues phenotype, *i.e.*, triggers apoptosis. Interestingly, these studies used Inforna to identify potential miRNA off-targets, that is other miRNAs with binding sites for **TGP-18a**, albeit with less avidity. The potential off-targets are expressed at much lower levels than the miRNAs in the miR-17-92 cluster, on average about 10-fold

Open Access Article. Published on 25 September 2020. Downloaded on 8/9/2025 2:37:59 AM.
This article is licensed under a Creative Commons Attribution-NonCommercial 3.0 Unported Licence.

less (Table S1, ESI†). Not only were these miRNAs unaffected by **TGP-18a**, target engagement studies show that they were not bound by the small molecule, demonstrating that differences in target expression level can be exploited to enhance the observed selectivity.

Another example of a miRNA target proven druggable through the use of Inforna is miR-96 (Table S1, ESI†).[43] Velagapudi *et al.*[43] showed the compound **Targaprimir-96** (**TGP-96**) reduces miR-96 levels (*via* inhibition of Drosha processing) at least as selectively as a locked nucleic acid (LNA). In one example, when dosed at concentrations high enough to silence approximately 90% of miR-96 expression, the miR-96 LNA also silenced ~50% of miR-183 expression, owing to the overlapping seed sequences of the two miRNAs (only the first nucleotide differs). In contrast, **TGP-96** only silenced miR-182 expression by ~15% when dosed at concentrations that silenced miR-96 expression by ~90% (Table S1, ESI†). Inhibition of miR-96 biogenesis by **TGP-96** de-repressed downstream protein expression of Forkhead box O1 (FOXO1), a putative tumor suppressor regulated by miR-96,[44] and stimulated apoptosis in MCF-7 breast cancer cells. Importantly, these studies confirmed that **TGP-96** acts along the miR-96-FOXO1 circuit by knocking down FOXO1 expression with an siRNA. Indeed, knockdown of FOXO1 reduces **TGP-96** activity.

In complementary studies, Costales *et al.*[45] designed **TGP-210**, a miR-210 binding small molecule that inhibits Dicer processing (Table S1, ESI†). MiR-210 controls hypoxia inducible factors (HIFs) through the negative regulation of glycerol-3-phosphate dehydrogenase 1-like (GPDL1).[46] *In vitro* and in triple negative breast cancer (TNBC) MDA-MB-231 cells, cultured under hypoxic conditions, **TGP-210** dose-dependently inhibited Dicer processing of pre-miR-210. In cells, this inhibition resulted in rescue of GPDL1 expression, reduction of levels of HIF1-α, and triggering of apoptosis. **TGP-210** was selective across a panel of hypoxia-associated miRNAs, as determined by RT-qPCR of treated MDA-MB-231 cells (Table S1, ESI†).

A technique termed Chemical-Cross Linking and Isolation by Pull Down (Chem-CLIP)[47] was then used to confirm direct target engagement of pre-miR-210 by **TGP-210**. In this technique, the small molecule of interest (in this case **TGP-210**) was appended with cross-linking (ex. chlorambucil) and purification (ex. biotin) modules. Upon compound binding to the target RNA, proximity-induced cross-linking occurs, which results in a complex that can be purified *via* pull-down with streptavidin beads. The RNAs enriched in the pull-down fraction, relative to the starting lysate, can be determined either through RT-qPCR or RNA-seq to confirm the compound's cellular target. Although expression levels of other mature miRNAs had been shown to be unaffected by **TGP-210**, Chem-CLIP experiments demonstrated binding does occur to other miRNAs. These studies showed that binding to a functional site is required for bioactivity and confirmed the observation by Velagapudi *et al.*[42] that expression level influences the degree of target occupancy. *In vivo* studies in NOD/SCID mice showed that treatment with **TGP-210** effectively reduces tumor growth *via* inhibition of miR-210 levels, de-repression of GPDL1, and reduction of HIF1-α levels.

2.4 Design of dimeric small molecules targeting disease-causing miRNAs

The observed selectivity for **TGP-210** was fortuitous, as off-targets were bound significantly less avidly and/or at non-functional sites and their expression levels were significantly lower than the desired target. However, such factors are unlikely to align for most targets. Therefore, facile methods to enhance small molecule potency and selectivity would be beneficial. As a test case, Costales *et al.*[48] explored **TGP-515/885**, a monomeric compound designed using Inforna that binds with dual selectively to the Drosha processing sites of both miR-515 and -885 (Fig. 2D and Table S1, ESI†). While both hairpin miRNA structures bear similar sequences at the Drosha processing sites, miR-515 folds with an additional internal loop adjacent to the Drosha processing site that also binds **TGP-515/885**. Dimerization of **TGP-515/885** yields **TGP-515**, which binds both the Drosha processing site and the adjacent internal loop to confer selectivity for pri-miR-515 over pri-miR-885 (Fig. 2F). Indeed, **TGP-515** bound miR-515 avidly while discriminating against pri-miR-885 *in vitro* and in cells (Table S1, ESI†). Its >200-fold enhancement in affinity compared to **TGP-515/885** translated into a >10-fold boost in potency in cells. Experiments in MCF-7 cells revealed that across all miRNAs, the entire transcriptome, and the proteome, **TGP-515** was selective for its RNA target.

Interestingly, cellular inhibition of miR-515 biogenesis de-repressed sphingosine kinase 1 (SK1), responsible for the synthesis of the second messenger sphingosine 1-phosphate (S1P), both of which were upregulated by **TGP-515** treatment. Activation of this circuit triggers migratory and proliferative characteristics of MCF-7 cells. However, it also enhances levels of human epidermal growth factor receptor 2 (HER2) levels, sensitizing HER2 negative cells (MCF-7 cells) to HER2-targeting precision medicines. Taken all together, this study shows that Inforna can inform how to design a specific compound from a dual-selective monomeric fragment.

In addition to the design of homodimeric molecules, Inforna can be used to design heterodimeric compounds which bind avidly to miRNAs.[49] Vascular endothelial growth factor A (VEGFA) stimulates angiogenesis in human endothelial cells and is a sought after target in the treatment of heart failure.[50–52] MiR-377 regulates VEGFA expression, and repression of miR-377 by an antisense oligonucleotide has been shown to rescue VEGFA expression and stimulate angiogenesis.[53,54] Inforna-based design afforded **TGP-377**, which binds pre-miR-377 at the Dicer site and another bulge directly adjacent (Fig. 2F and Table S1, ESI†).[49] Expression levels of miR-377 from human umbilical vein endothelial cells (HUVEC) treated with **TGP-377** were knocked down with an IC_{50} of ~500 nM, 10-fold more potently than the lead small molecule monomer (Table S1, ESI†). Accumulation of pre-miR-377 was also observed, demonstrating **TGP-377** acts through inhibition of Dicer processing and correspondingly rescues VEGFA expression. A miRNA profiling experiment showed that **TGP-377** targets miR-377 selectively, including

 This journal is © The Royal Society of Chemistry 2020

Open Access Article. Published on 25 September 2020. Downloaded on 8/9/2025 2:37:59 AM.
This article is licensed under a Creative Commons Attribution-NonCommercial 3.0 Unported Licence.

among miR-377 isoforms (Table S1, ESI†). Global proteomics analysis revealed that **TGP-377** affects only 160 of over 4000 unique proteins. A bioinformatic STRING analysis uncovering protein association networks showed, unsurprisingly, cell proliferative pathways including FGFR, Hedgehog, MAP kinase, and ERK were upregulated. Furthermore, **TGP-377** induced a pro-angiogenic phenotype in HUVEC cells as evidenced by increased tubule branching density by ~50% relative to control. As gene therapy is the only known treatment strategy to increase VEGFA expression, **TGP-377** represents the first small molecule to do so.[50–52,55]

3. Small molecule recognition of lncRNAs

LncRNAs are eukaryotic transcripts >200 nt in length that do not encode a protein.[56] These RNAs play key regulatory roles in cellular processes such as proliferation, differentiation, and development, the aberrant expression of which can lead to cancer,[57] neurodegenerative[58] and neuromuscular[59] disorders, and immune disorders.[60,61] LncRNAs are promising therapeutic targets because of their differential expression between cancerous and normal tissues and their important roles in carcinogenesis.[62] Not surprisingly, small molecule screening against lncRNAs has been attracting attention.[63–65] In this section, we describe examples of small molecule regulation of lncRNAs.

3.1 Small molecule recognition of the lncRNA HOTAIR

The lncRNA HOX transcript antisense RNA (HOTAIR) is involved in several cellular processes associated with carcinogenesis, such as those affecting cell mobility, proliferation, apoptosis, invasion, aggression, and metastasis.[66] Additionally, HOTAIR recruits chromatin-modifying complexes, such as polycomb repressive complex 2 (PRC2) and lysine-specific histone demethylase 1 (LSD1) to modulate the cancer epigenome and suppress tumor suppressor genes.[67]

Ren *et al.*[68] used *in silico* high-throughput screening to identify **ADQ** as a potent small molecule binder of HOTAIR (Fig. 3A and Table S1, ESI†). In multiple cancer cell lines, **ADQ** increased expression of nemo like kinase (NLK), a transcriptional target of HOTAIR, in a luciferase assay. Electrophoretic mobility shift assay (EMSA) confirmed **ADQ** directly binds HOTAIR. To further confirm the functional domains of **ADQ**, full-length HOTAIR, the 5′ domain, or a mutant 5′ domain construct were stably transfected into U87 and MDA-MB-231 cells. The **ADQ**-mediated dissociation of HOTAIR and enhancer of zeste 2 polycomb repressive complex 2 subunit (EZH2) was confirmed using full-length HOTAIR but was not observed with the mutant 5′ domain in which the **ADQ** binding site was ablated (Fig. 3B).

3.2 Small molecule recognition of the lncRNA MALAT1

The lncRNA metastasis-associated lung adenocarcinoma transcript 1 (MALAT1) has recently been identified to be upregulated and coupled to tumorigenesis in several cancers.[69] MALAT1 has been linked to several physiological processes, including alternative splicing, nuclear organization, and epigenetic modulation of gene expression.[70] A study in colorectal cancer cells showed that an ~1500 nt segment at the evolutionarily conserved 3′ end of MALAT1 was sufficient to increase invasion and proliferation, implying that this region enables its oncogenic function.[71] The recent structural characterization of a 74 nt region at the 3′ end of MALAT1 by X-ray diffraction confirmed a unique, bipartite triple helix where the U-rich stem-loop sequesters the A-rich tail, a phenomenon proposed to prevent exonucleolytic degradation (Fig. 3B).[72,73] Notably, the deletion of this segment decreased accumulation of the MALAT1 transcript. A comparable decrease in accumulation was also observed upon mutation of a Hoogsteen-positioned uridine, thought to disrupt the triple-helix structure, indicating that subtle alterations in the stability of this structure can lead to significant changes in transcript level.

Donlic *et al.*[74] have identified small molecule binders of MALAT1 through *in vitro* assays. They used furamidine, the tunable diphenylfuran (DPF)-based scaffold, as a starting point because furamidine is known to bind to triple helix structures

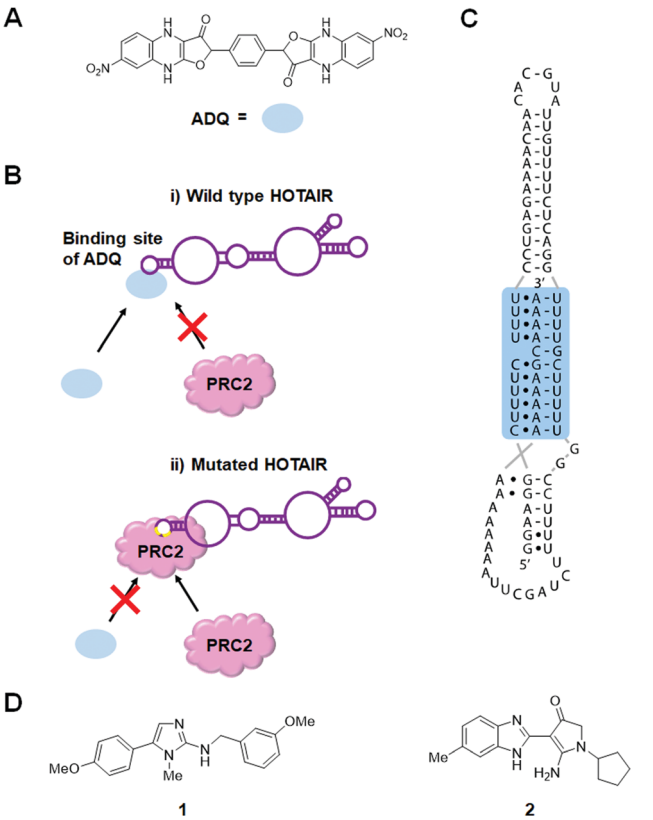

Fig. 3 Small molecule inhibition of lncRNAs. (A) Chemical structure of **ADQ**. (B) **ADQ** binds to the 5′ domain of HOTAIR and suppresses trimethylation of histone H3 lysine 27 (H3K27) in the promoter region of nemo like kinase (NLK) by weakening HOTAIR's ability to recruit and bind enhancer of zeste 2 polycomb repressive complex 2 subunit (EZH2), the enzymatic component of the PRC2 complex, thus restoring expression of NLK. (C) MALAT1 triple helix structure. (D) Chemical structures of MALAT1 small molecule binders.

Open Access Article. Published on 25 September 2020. Downloaded on 8/9/2025 2:37:59 AM. This article is licensed under a Creative Commons Attribution-NonCommercial 3.0 Unported Licence.

of various DNAs.[75,76] They synthesized a DPF scaffold-based small molecule library, diversified in subunit composition and positioning, to explore the recognition of MALAT1.

Using a small molecule microarray (SMM) strategy, Abulwerdi *et al.*[64] reported the discovery of two structurally unrelated derivatives (**1** and **2**) that target the triplex region of MALAT1 (Fig. 3C and Table S1, ESI†). Compound **1** was selective for MALAT1 and nuclear paraspeckle assembly transcript 1 (NEAT1), which has a similar structure to MALAT1 (Table S1, ESI†). FRET, isothermal titration calorimetry (ITC) and nuclear magnetic resonance (NMR) spectroscopic experiments confirmed **1** binds to MALAT1 *in vitro*. However, understanding of the inhibitory mechanism of **1** is limited by the lack of knowledge surrounding the actual mechanism of triplex-mediated protection. Additional research in this area will prove advantageous for the design of therapeutics targeting oncogenic lncRNAs and provide further support for target engagement.

4. Small molecule rescue of repeat-associated transcriptional repression in fragile X syndrome

Currently without a cure, fragile X syndrome (FXS) is the most common hereditary disorder that causes mental retardation, resulting from >200 CGG triplet repeats [full mutation allele; $r(CGG)^{exp}$] in the 5′ UTR of the fragile X mental retardation 1 (*FMR1*) gene on the X chromosome.[77] The *FMR1* promoter is epigenetically silenced through elevated levels of DNA CpG methylation and repressive histone marks H3K9me2, H3K9me3, H3K27me3, and H4K20me3, as well as lower levels of active histone marks H3K9ac, H3K4me2, and H4K16ac. Silencing progresses during embryonic development with the consequent loss of fragile X mental retardation protein (FMRP) encoded by the *FMR1* gene.[77] Although the mechanism of disease progression of FXS is not fully understood at present, a small molecule targeting the FXS RNA has been discovered that rescued repeat-associated epigenetic silencing.

4.1 Small molecule prevents the formation of RNA:DNA hybrids

Colak *et al.*[78] reported that treatment of human embryonic stem cells (hESCs) from FXS patients with **1a**, which was discovered using Inforna,[79] can prevent epigenetic silencing during neuronal differentiation (Table S1, ESI†). Knockdown of *FMR1* mRNA in hESCs decreased silencing histone marks, suggesting the *FMR1* transcript is involved in the gene silencing process of its own gene. In the presence of **1a**, repressive histone marks induced by differentiation also decreased. Since the compound thermodynamically stabilizes the $r(CGG)^{exp}$ hairpin by binding to its 1 × 1 GG internal loops, it was speculated that the unfolded *FMR1* mRNA is responsible for epigenetic silencing. To support this hypothesis, they performed chromatin isolation by RNA purification, a technique used to identify DNA sequences which bind to a specific RNA sequence. These studies showed the *FMR1* DNA adjacent to the genomic CGG repeat is highly enriched only in the absence of **1a**. Furthermore, treatment with RNase H, which selectively digests RNA:DNA duplexes, significantly reduced the enrichment of the *FMR1* promoter. Based on these results, a mechanism was proposed by which *FMR1* mRNA containing extended CGG repeats binds to complementary DNA to form the RNA:DNA duplex that induces epigenetic silencing of the *FMR1* promoter (Fig. 4A). It was also suggested that **1a** promotes CGG stem-loop formation of the *FMR1* transcript and thus prevents the formation of the RNA:DNA duplex. In addition, because silencing decreases *FMR1* mRNA expression, RNA:DNA duplex formation would be engaged only at the initiation of silencing. In fact, **1a** has no effect on silenced cells, as subsequent gene silencing is maintained by other factors.

4.2 Small molecule targeting of $r(CGG)^{exp}$ in combination with 5-azadeoxycytidine

In 2016, Kumari *et al.*[80] proposed that **1a** also has an inhibitory effect on histone methyltransferase polycomb repressive complexes 2 (PRC2) recruitment. Treatment of FXS patient cells with 5-azadeoxycytidine (AZA), an inhibitor of DNA methyltransferase 1, has been reported to demethylate the *FMR1* promoter and reactivate the *FMR1* gene.[81,82] Although AZA withdrawal causes re-silencing of the *FMR1* gene, this can be greatly delayed in the presence of **1a**, but not by inhibiting the RNA:DNA hybrid. Rather, **1a** inhibits association of $r(CGG)^{exp}$ with PRC2, interfering with its recruitment to unmethylated CpG motifs and thus slowing *FMR1* resilencing in FXS patient cells (Table S1, ESI†).[79,83] It is assumed that H3K27 in the *FMR1* promoter is methylated by the aberrantly recruited histone methyltransferase. Indeed, it was observed that inhibitors of EZH2, the enzymatic component of PRC2, affect the maintenance of the reactivated state similar to how **1a** does. Knockdown of *FMR1* mRNA also reduced EZH2 levels associated with the *FMR1* gene. Taken together, these data support that **1a** is a dual functioning compound, preventing DNA:RNA hybrid formation and the recruitment of PRC2 by binding to the $r(CGG)^{exp}$ stem-loop (Fig. 4B).

5. Small molecules modulate alternative splicing

Alternative splicing is a complex, elegant cellular process that allows for variation in protein isoforms to modulate protein function.[84] During the splicing process, exons can be included or excluded, giving rise to a variety of splicing isoforms afforded from a single pre-mRNA.[84] Mutations that change splicing patterns unsurprisingly cause human diseases including muscular atrophy,[85,86] tauopathies,[87] β-thalassemia,[88] progeria,[89] and Pompe disease.[90]

5.1 Small molecules modulate *SMN2* splicing

Spinal muscular atrophy (SMA) is caused by mutations in the *SMN1* gene that decrease levels of survival motor neuron (SMN) protein produced in the spinal cord.[86] In humans, *SMN1* and *SMN2* are the two genes that encode for SMN, but the majority

 This journal is © The Royal Society of Chemistry 2020

Open Access Article. Published on 25 September 2020. Downloaded on 8/9/2025 2:37:59 AM.
This article is licensed under a Creative Commons Attribution-NonCommercial 3.0 Unported Licence.

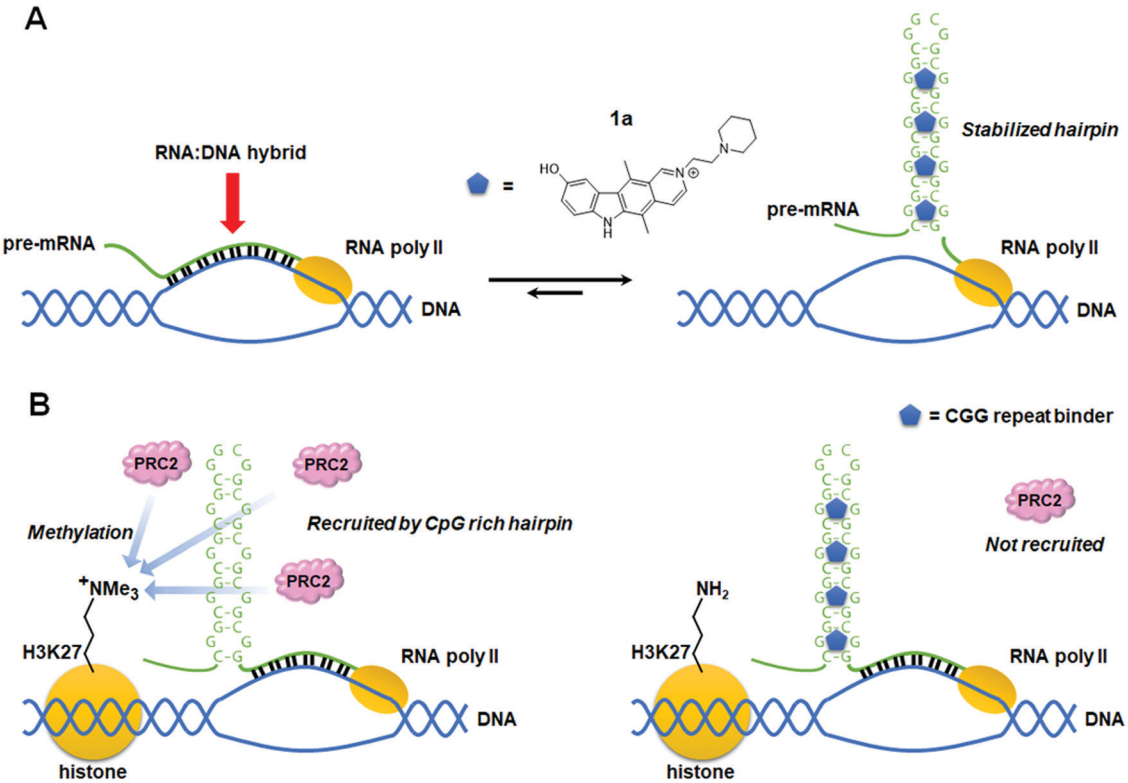

Fig. 4 Proposed mode of action of an r(CGG)^{exp} repeat binder that prevents epigenetic silencing of the *FMR1* promoter in fragile X syndrome (FXS). (A) Schematic mechanism showing stabilized r(CGG)^{exp} hairpins restrict formation of the RNA:DNA hybrids responsible for epigenetic silencing of *FMR1*. (B) Schematic mechanism showing binding of a small molecule to the r(CGG)^{exp} hairpin preventing recruitment of polycomb repressive complex 2 (PRC2), a H3K27 methylation enzyme complex.

of SMN protein is translated from the full-length mRNA produced from the *SMN1* pre-mRNA.[91] Due to a C-to-U transition at position 6 on exon 7, exon 7 skipping is dominant in the splicing of *SMN2* pre-mRNA,[92] producing a truncated SMN protein with a reduced half-life.[93] Currently, there are three treatment options for SMA: **nusinersen**, an ASO that regulates *SMN2* splicing to produce the full-length SMN protein;[94] onasemnogene abeparvovec, an adeno-associated virus (AAV) carrying the normal *SMN1* gene;[95] and **risdiplam** (PTC/Roche), an orally avaliable small molecule that was recently FDA-approved.[96,97] Another small molecule therapeutic candidate, **branaplam** (Novartis), is also currently undergoing clinical trials (Fig. 5A and Table S1, ESI†).[96] **Risdiplam** and **branaplam** generate the SMN protein *via* regulation of *SMN2* splicing. Since both compounds were discovered from phenotypic screening, a series of studies on their modes of action (MOAs) were reported and are discussed below.

5.1.1 Small molecule stabilization of exon 7 5′ splice site–U1 snRNP complex. Palacino *et al.*[98] investigated **branaplam's** MOA by using the active derivative, **NVS-SM2**, as a proxy (Table S1, ESI†). Since it is known that mutations at the end of *SMN2* exon 7[86,99] and in breast cancer 1 (*BRCA1*) exon 18[100] induce exon skipping, the authors tested the ability of **NVS-SM2** to modulate the splicing of these two exons, the latter as a counter screen of small molecule selectivity. While **NVS-SM2** rescued *SMN2* exon 7 splicing, it failed to rescue *BCRA1* exon 18 splicing. To define the *SMN2* RNA sequence that interacts with **NVS-SM2**, the authors utilized a set of *SMN2-BCRA1* chimeric genes to pinpoint the sequence necessary for **NVS-SM2** interaction. Only one chimeric gene, containing 21 nucleotides of the 5′ splice site in *SMN2* exon 7 fused to *BRCA1*, showed exon inclusion activity when treated with **NVS-SM2**, suggesting **NVS-SM2** interacts with the 5′ splice site of *SMN2* exon 7. Interestingly, the GA sequence at the end of exon 7 was found to be critical for the activity of **NVS-SM2**, as determined by base mutation experiments of the 5′ splice site. A RefSeq comparison revealed nGA sequences at the 3′ ends of exons are rare, suggesting the U1 small nuclear ribonucleoprotein (snRNP), a splice site-recognizing RNP, is involved in the mode of action of **NVS-SM2**. Size-exclusion chromatography confirmed that exon 7′s 5′ splice site bound to U1 snRNP only when **NVS-SM2** was present. In addition, total correlated spectroscopy (TOCSY) NMR showed that chemical-shift perturbations were observed at residues proximal to the nGA motif. Combining all these data with the crystal structure of U1 snRNP,[101,102] it was proposed **NVS-SM2** has a novel mode of action by which it stabilizes a ternary complex between the small molecule, U1 snRNP, and the 5′ splice site, particularly at the major groove of the –1A RNA bulge (Fig. 5B and Table S1, ESI†).

Risdiplam's MOA was defined using a derivative dubbed **SMN-C5** and a duplex model of the 5′ splice site/U1 snRNP complex (Table S1, ESI†).[103] The model consisted of 11 nt of the 5′ splice site hybridized to 11 nt of the U1 snRNA. The three-dimensional

Open Access Article. Published on 25 September 2020. Downloaded on 8/9/2025 2:37:59 AM.
This article is licensed under a Creative Commons Attribution-NonCommercial 3.0 Unported Licence.

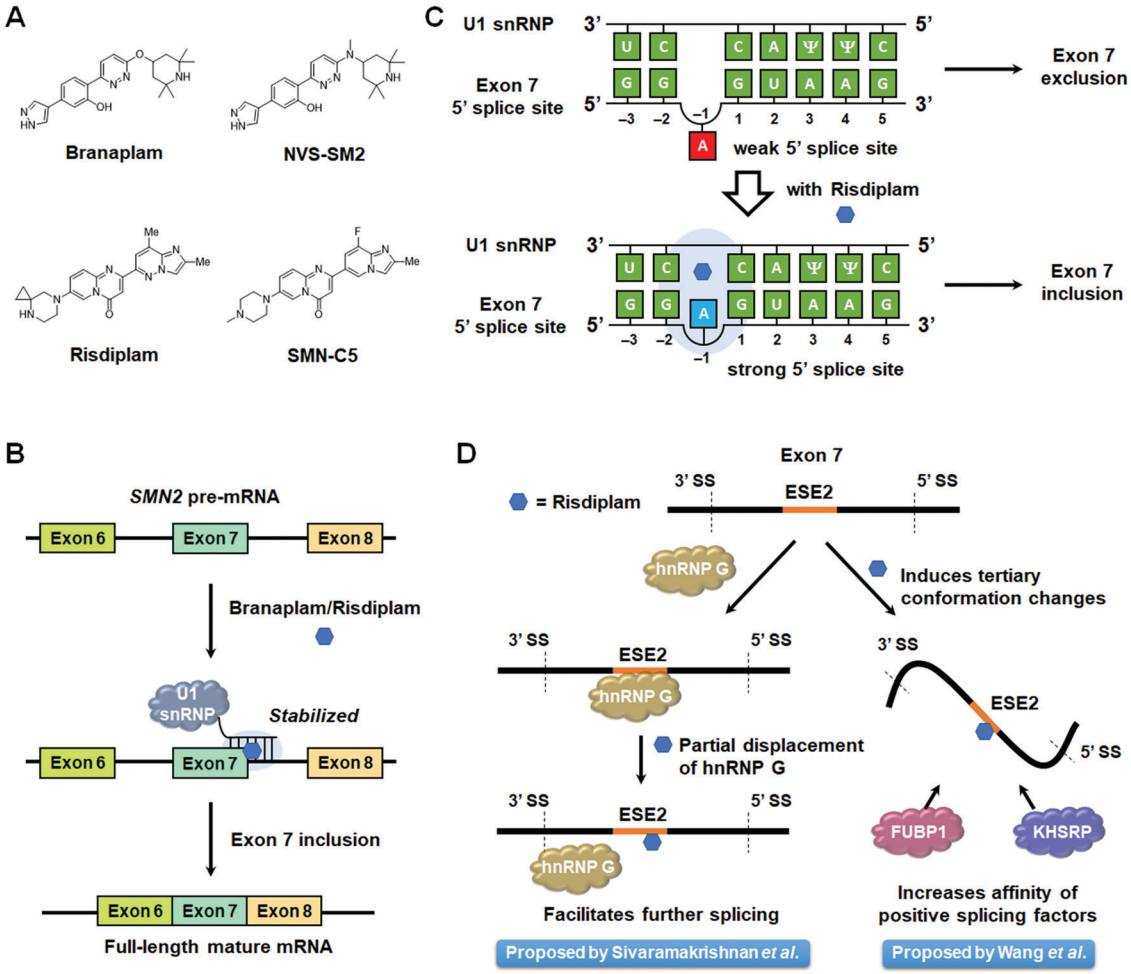

Fig. 5 Mode of action of small molecule splicing modulators targeting *SMN2 pre-mRNA*. (A) Structures of small molecule splicing modulators targeting *SMN2* pre-mRNA and the derivatives used to study their mechanisms of action. (B) Schematic mechanism of small molecules facilitating *SMN2* exon 7 inclusion by stabilizing the complex between *SMN2* exon 7, the 5′ splice site (SS), and the U1 snRNP. (C) Schematic representation of 5′ splice site bulge repair mediated by **risdiplam**. (D) Competing modes of action proposed for **risdiplam**.

structure of this model with and without **SMN-C5** was defined by NMR spectroscopy, constrained by nuclear Overhauser effects (NOEs). In the binding model of the apo form, the unpaired adenine in the 5′ splice site is located in the minor groove. Upon **SMN-C5** binding to the RNA's major groove, the bulged adenine is pushed back into the duplex, stabilized by the hydrogen bond formed between the carbonyl group of **SMN-C5** and the amino group of the adenine. Previous structural studies have shown that the U1 snRNP zinc finger stabilizes the minor groove at exon–intron junction of RNA duplexes.[101,102] Modeling the apo duplex in the zinc finger produces an obvious steric clash between the bulged adenine and the zinc finger. In contrast, the **SMN-C5**-bound duplex alleviates this clash, improving the accessibility of the minor groove. Collectively, these studies suggest that **SMN-C5** improves splice site recognition by U1 snRNP, facilitating exon 7 inclusion and expression of functional, full length SMN protein (Table S1, ESI†).

5.1.2 Small molecule interaction with exonic splicing enhancer 2 (ESE2) in *SMN2* exon 7 recruits splicing factors. **Risdiplam** modulates the alternative splicing of other exons such as striatin 3 (*STRN3*) exon 8, among others. Sivaramakrishnan *et al.*[104] searched for common sequence motifs around these exons (*STRN3* exon 8 and *SMN2* exon 7) and found the sequences of their 5' splice site are an exact match, while they share similar exonic splicing enhancer (ESE) sequences juxtaposed to a purine rich sequence. ESE sequences are known to recruit positive splicing factors and thus aid in the splicing process.[105] These results suggested that **SMN-C5** may have an additional mode of action besides ternary complex formation with the 5' splice site and U1 snRNP. Surface plasmon resonance (SPR) studies indicated binding of **SMN-C5**, but not **NVS-SM1**, to the ESE2 in *SMN2* pre-mRNA. In addition, NMR spectroscopy showed large chemical-shift perturbations of the ESE2 RNA were induced by addition of **SMN-C5**, resulting in the formation of broad imine signals, indicative of a small molecule-induced conformational change.

The authors then sought to identify potential protein components that may be contributing to *SMN2* exon 7 skipping using a pull-down experiment. Ten proteins were enriched only in the presence of **SMN-C5**, among them heterogenous nuclear

 This journal is © The Royal Society of Chemistry 2020

Open Access Article. Published on 25 September 2020. Downloaded on 8/9/2025 2:37:59 AM. This article is licensed under a Creative Commons Attribution-NonCommercial 3.0 Unported Licence.

ribonucleoprotien (hnRNP) G, a known positive splicing factor that interacts with ESE2.[106] Unexpectedly, **SMN-C5** partially competes with hnRNP G for ESE2 binding, and small molecule binding alters the RNA structure of the region to which hnRNP G normally binds. Thus, one hypothesis is that partial displacement of hnRNP G by **SMN-C5** facilitates the progression of the splicing process (Fig. 5D).

Wang *et al.*[107] also reported that **SMN-C2** and **SMN-C3**, derivatives of **risdiplam**, act on ESE2. *SMN2* exon 7 is known to form two stem-loops, terminal stem-loop 1 (TSL1) and terminal stem-loop 2 (TSL2), that have an inhibitory effect on splicing.[108] Both cell-free and cell-based selective 2′ hydroxyl acylation analyzed by primer extension (SHAPE) analysis showed that the addition of **SMN-C2** altered the reactivity of some bases in TSL1, suggesting this compound induces conformational changes of this inhibitory loop. Further, proteomics analysis using a photo-cross-linking probe revealed enrichment of far upstream element binding protein 1 (FUBP1)[109] and far upstream element binding protein 2 (KHSRP).[110] Fluorescence polarization assays with **SMN-C2** and recombinant FUBP1 induced higher polarization in the presence of ESE2. These results indicated that **SMN-C2**, FUBP1, and exon 7 form a ternary complex. Furthermore, EMSA showed the formation of FUBP1–exon 7 complexes are enhanced in a dose-dependent manner by **SMN-C3**. Based on these results, it was concluded that derivatives of **risdiplam** interact with ESE2 to induce conformational changes in exon 7 and improve the binding affinity of positive splicing factors (Fig. 5D).

In summary, **risdiplam** has been proposed to have two modes of action: (i) stabilizing the RNA duplex of exon 7 5′ splice site and U1 snRNP and (ii) inducing conformational changes of exon 7 ESE2 to facilitate the formation of a complex with positive splicing factors. These two modes of action may contribute to **risdiplam**'s high selectivity.

5.2 Small molecule modulation of *MAPT* pre-mRNA splicing

The small molecules described above direct *SMN2* splicing towards exon 7 inclusion. However, many diseases are caused by aberrant exon inclusion and therapeutic benefit is achieved by exclusion of exons. One such example is tauopathies, caused by aggregation of the protein tau, a regulator of microtubule stability that is highly expressed in neurons.[111] The microtubule-associated protein tau (*MAPT*) gene encoding tau is composed of 16 exons and is known to produce six isoforms by alternative splicing.[87] Exclusion of exon 10 produces the 3R isoform, with three microtubule binding domains (MBDs), while inclusion produces the aggregation-prone 4R isoform, with four MBDs.[112] The ratio of 3R tau to 4R tau is nearly equal in healthy adults (Fig. 6A).[113] However, in frontotemporal dementia (FTD) and Parkinsonism linked to chromosome 17 (FTDP-17), genetic mutations of the *MAPT* gene increase the rate of exon 10 inclusion, and hence the ratio of 4R/3R tau.[114] This causes aggregation of tau proteins and ultimately neuronal death.[114]

The 5′ splice site of *MAPT* exon 10 forms a stem-loop, known as a splicing regulatory element (SRE).[115,116] Genetic mutations in the SRE destabilize its structure, increasing the rate of exon 10 inclusion in the mature transcript.[115–117] For example, DDPAC is an intronic mutation in which the 14th C downstream from the 5′ splice site is mutated to U, therefore mutating a GC base pair to a GU base pair, thermodynamically destabilizing the SRE by 1.2 kcal mol^{-1}.[117] This results in an ~30 : 1 ratio of 4R : 3R tau isoforms. Thus, thermodynamic stabilization of the tau SRE *via* small-molecule targeting could be a viable therapeutic option.

One of the first studies to demonstrate the ligandability of the SRE in tau exon 10 showed the anticancer drug, **mitoxantrone** (MTX) binds and stabilizes the SRE, resulting in decreased production of the tau 4R isoform (Table S1, ESI†).[118] Zheng *et al.*[118] reported the NMR structure of the tau pre-mRNA-MTX complex, showing MTX interacts with the bulged region of the SRE stem-loop. The elucidation of this structure highlighted the importance of structure-based recognition between RNA and small molecule ligands as it showed the three-dimensional shape of the RNA was necessary for binding to MTX.[118] Additional structure–activity relationships (SAR) were used to optimize MTX's ability to decrease exon 10 inclusion, leading to compounds with enhanced affinity for tau pre-mRNA and increased potency for reducing the levels of 4R tau (Table S1, ESI†).[119]

More recently, Chen *et al.*[120] reported that stabilizing the SRE by small molecule binding to the A bulge present in the SRE structure could inhibit recognition by U1 snRNP and promote exon 10 exclusion in wild-type (WT) and DDPAC tau. Tanimoto score-based similarity searching using a previously reported Inforna hit[121] as a query identified **A-1** as a modulator of the 4R/3R tau ratio (Fig. 6B and Table S1, ESI†). To improve physical properties of **A-1**, *in silico*-based hit expansions were conducted. As a result, **A-2**, **A-3**, and **A-4** were obtained from the pharmacophore modeling of **A-1**, and **A-5** was obtained from structure-based design using the three-dimensional structure of the SRE (Table S1, ESI†).

All five compounds not only decrease the 4R/3R ratio by 50% at 10–25 μM, but also had improved physicochemical properties, including potential for blood–brain barrier (BBB) penetrance, compared to **A-1** (Table S1, ESI†). In particular, the average central nervous system multiparameter optimization (CNS-MPO) score for **A-3**, **A-4**, and **A-5** was 4.8; CNS-MPO scores >4 indicate high potential for brain pentrance.[122]

Target engagement studies using Chem-CLIP confirmed **A-5** binds directly to the *MAPT* pre-mRNA SRE. Furthermore, melting curve analysis showed that hit compounds specifically increased the melting temperature (T_m) of tau SRE, providing experimental evidence that small molecule binding to the A bulge indeed thermodynamically stabilizes the tau SRE and prevents recognition by U1 snRNP (Fig. 6C). To further elucidate the binding mode, three-dimensional structures of the apo-SRE and the compound bound SRE (**A-1**, **A-2**, and **A-5**) were characterized by NMR spectroscopy. In both cases, the RNA duplex was consistent with an A-form helical structure, and all compounds bound to a cavity around the bulged adenine, despite having different binding modes. Altogether, these studies demonstrated that compounds identified using Inforna can be converted to more

Open Access Article. Published on 25 September 2020. Downloaded on 8/9/2025 2:37:59 AM.
This article is licensed under a Creative Commons Attribution-NonCommercial 3.0 Unported Licence.

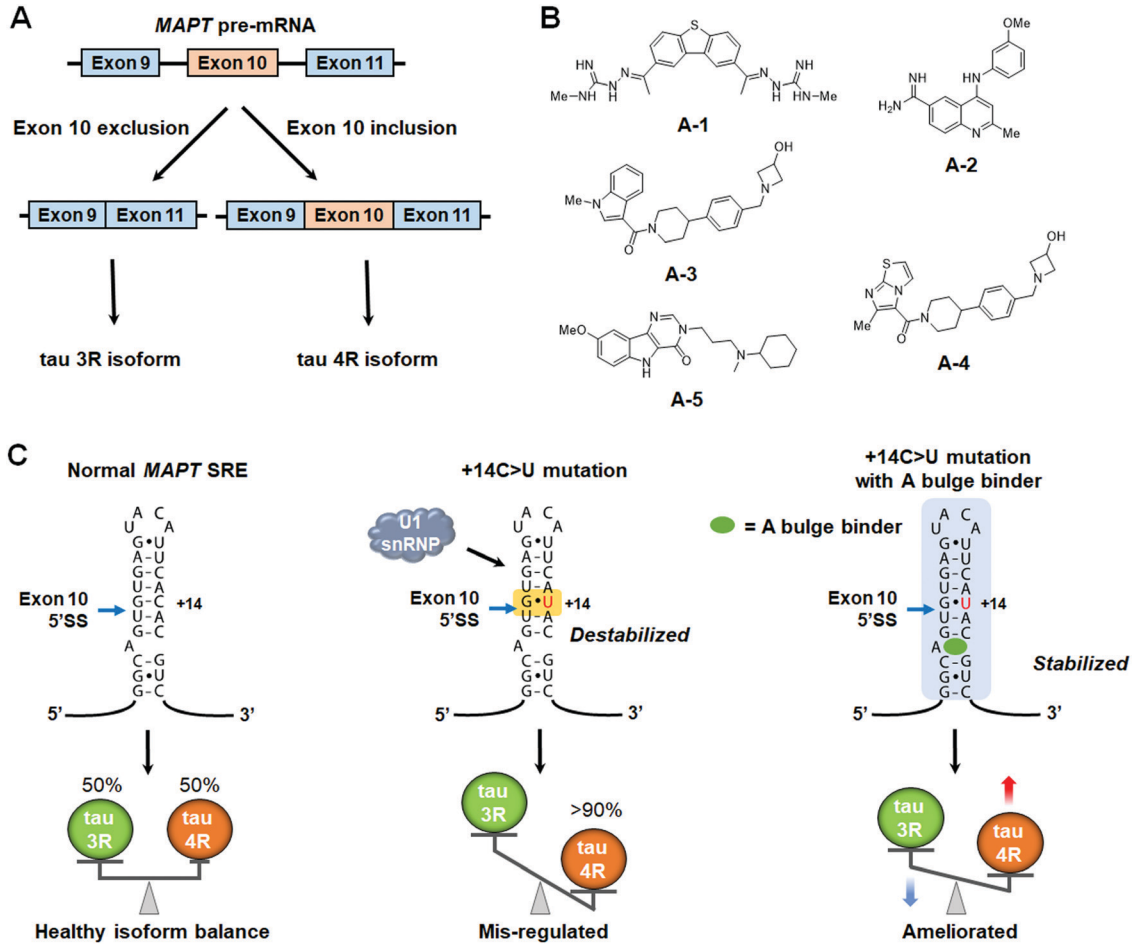

Fig. 6 Small molecule modulation of *MAPT* pre-mRNA splicing. (A) Alternative splicing of *MAPT* exon 10 yields tau 3R and 4R isoforms. (B) Structures of small molecule splicing modulators that bind to the A-bulge of the *MAPT* splicing regulatory element (SRE). (C) Schematic representations showing the effect of U1 snRNP accessibility to the *MAPT* SRE on tau 3R/4R isoform balance.

potent and drug-like compounds possessing the designed RNA-centric mechanism of action.

As is presented here, small molecules can modulate the alternative splicing of pre-mRNAs selectively, either by binding to RNA structural motifs or stabilizing complexes between pre-mRNA and splicing factors. Since aberrant alternative splicing has been associated with various diseases, including rare hereditary diseases,[123] central nervous system disorders,[124,125] and cancers,[126,127] further studies in this field could lead to the development of potent and selective small molecules that can direct splicing outcomes.

6. Small molecules targeting RNA repeat expansion disorders

RNA repeat expansion, or microsatellite, disorders are characterized by long abnormal stretches of repeating RNA nucleotides that can be harbored in intronic, coding, or untranslated regions of pre-mRNAs. These expanded repeats often fold into hairpin structures that interfere with normal RNA processing, leading to disease. Indeed, RNA repeat expansions are responsible for over 30 human diseases, with a large majority being neurodegenerative and neuromuscular in nature.[17] Repeats contribute to disease *via* various mechanisms, including: (i) RNA gain-of-function in which RNA-binding proteins (RBPs) are sequestered and inactivated; (ii) formation of nuclear foci; and (iii) production of toxic proteins, either as a result of canonical translation of an open reading frame (ORF) or as a result of repeat-associated non-ATG (RAN) translation (discussed in Section 8, "Small Molecules Targeting RNA Repeat Expansions Inhibit RAN Translation").

A common RNA gain-of-function pathomechanism in microsatellite disorders is the formation of RNA–protein complexes between the hairpin structures of repeating RNA and RBPs. However, there are various ways by which these complexes lead to disease (Fig. 7). For example, the sequestration of endogenous splicing factors by RNA repeats leads to deregulation of alternative pre-mRNA splicing that affects overall cellular protein levels and homeostasis. Additionally, RNA–protein complexes aggregate in the nucleus in toxic RNA foci, affecting nucleocytoplasmic transport. Thus, the driving idea behind small molecule therapeutics for these disorders is that binding of small molecules competes with RBPs for the disease-causing RNA target, liberating them to fulfill their normal function.

 This journal is © The Royal Society of Chemistry 2020

Open Access Article. Published on 25 September 2020. Downloaded on 8/9/2025 2:37:59 AM.
This article is licensed under a Creative Commons Attribution-NonCommercial 3.0 Unported Licence.

In this section, we focus on four neurodegenerative diseases and their associated RNA–protein complexes: (i) the r(CUG)^{exp}–muscleblind-like 1 (MBNL1) complex in myotonic dystrophy type 1 (DM1) where the repeating nucleotides are indicated in parentheses and "exp" denotes "expanded"; (ii) the r(CCUG)^{exp}–MBNL1 complex causative of myotonic dystrophy type 2 (DM2); (iii) the r(CGG)^{exp}–DGCR8 complex that forms a scaffold for splicing regulators Src-associated in mitosis 68 kDa protein (Sam68) and hnRNP in FXTAS; and (iv) the r(G$_4$C$_2$)^{exp}–hnRNP H complex in *C9orf72*-associated frontotemporal dementia and amyotrophic lateral sclerosis (c9FTD/ALS).

6.1 Small molecule inhibition of the r(CUG)^{exp}–MBNL1 complex in DM1

DM1 is an adult-onset neuromuscular disorder caused by an expanded repeating CUG sequence [r(CUG)^{exp}] in the 3′ UTR of dystrophia myotonica protein kinase (*DMPK*) mRNA (Fig. 8A). The expanded RNA affects disease biology by folding into a hairpin structure with a periodic array of internal loops that sequester proteins (RNA gain-of-function), such as the splicing factor MBNL1. Sequestration of MBNL1 deregulates the alternative splicing of the protein's natural substrates, which are directly correlated with disease symptoms. For example, MBNL1 regulates the alternative splicing of the muscle-specific chloride ion channel (CLCN1). In DM1-affected cells, CLCN1's aberrant splicing causes loss of the chloride ion channel from the surface of muscle cells, altering conductance and resulting in myotonia. MBNL1 also self-regulates splicing of its own exon 5. In normal cells, exon 5 is included in the mature mRNA sequence ~45% of the time (Fig. 8B). In DM1-affected cells however, exon 5 is included 85% of the time. In addition, r(CUG)^{exp}–MBNL1 complexes aggregate and form RNA foci in the nucleus that lead to reduction of nucleocytoplasmic transport and result in cytotoxicity.[128,129] Being that the r(CUG)^{exp} hairpin plays a key role in DM1 pathology, this structure has become a promising target for small molecule therapeutics.

In 2013, Rzuczek *et al.*[130] identified a *bis*-benzimidazole derivative (**H**) as a 1 × 1 UU internal loop RNA binder. To target the repeating chain of UU internal loops present in r(CUG)^{exp}, they synthesized a series of **H**-dimers with various linkers. After assessing rescue of DM1-associated splicing, cellular permeability, cytotoxicity, and proteolytic stability of

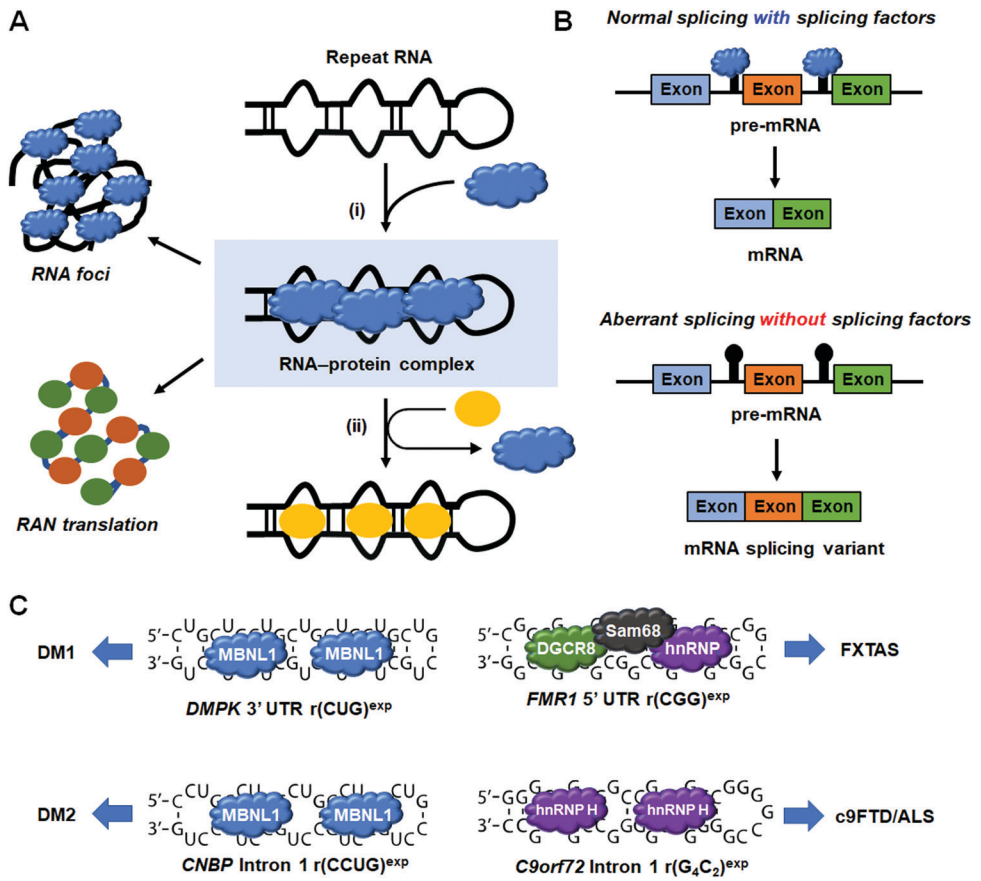

Fig. 7 Small molecule binding of RNA repeat expansions releases sequestered RNA-binding proteins (RBPs). (A) Schematic of RBP sequestration by RNA repeat expansions. (i) RBPs, such as splicing factors, are sequestered by RNA repeat expansions, contributing to disease pathology. (ii) Small molecules competitively bind to RNA repeats and release sequestered proteins, resulting in rescue of splicing defects, reduction in RNA foci, and repression of repeat-associated non-ATG (RAN) translation. (B) Schematic of alternative splicing resulting from the presence or absence of endogenous splicing factors. (C) The RNA:protein complexes that contribute to myotonic dystrophy type 1 (DM1), myotonic dystrophy type 2 (DM2), fragile X-associated tremor and ataxia syndrome (FXTAS), and *C9orf72*-associated frontotemporal dementia and amyotrophic lateral sclerosis (c9FTD/ALS).

Open Access Article. Published on 25 September 2020. Downloaded on 8/9/2025 2:37:59 AM.
This article is licensed under a Creative Commons Attribution-NonCommercial 3.0 Unported Licence.

the compounds, **2H-K4NMe** was identified as the most promising ligand (Table S1, ESI†). **2H-K4NMe** showed >30-fold binding selectivity to r(CUG)$_{12}$ over other RNA sequences, with a K_d of 13 nM (Table S1, ESI†). Further, **2H-K4NMe** rescued the cardiac troponin T (*cTNT*) splicing defect at a 5 μM dose.

Based on these findings they developed the dimer **2H-K4NMeS**, which displayed enhanced metabolic stability over **2H-K4NMe** (Table S1, ESI†).[131] **2H-K4NMeS** has K_d's of 280 nM and 12 nM for r(CUG)$_{12}$ and r(CUG)$_{109}$, respectively, indicating cooperative binding (Table S1, ESI†). Treatment of DM1-patient-derived cells with as little as 100 nM of **2H-K4NMeS** improved the *MBNL1* exon 5 pre-mRNA splicing defects (Fig. 8D). **2H-K4NMeS** also rescued splicing defects of other MBNL1-regulated splicing events, such as calcium/calmodulin dependent protein kinase II gamma (*CAMK2G*) exon 14 and nuclear receptor corepressor 2 (*NCOR2*) exon 45a splicing, and to a similar extent as *MBNL1* exon 5. This study clearly showed that RNA-binding small molecules can free MBNL1 from RNA–protein complexes at reasonable concentrations for therapeutic use, thereby normalizing splicing events.

Another mechanism by which RNA–protein complexes contribute to DM1 pathology is by aggregating into RNA foci in the nucleus (Fig. 8C). RNA-binding small molecules are expected to disrupt RNA foci by competitively binding to the RNA, preventing protein binding or releasing bound proteins from the complex. Indeed, **2H-K4NMeS** decreased the number of foci present in cells by ~50% when treated at 1 μM.[131] As expected, the activity of **2H-K4NMeS** for improving nucleocytoplasmic transport defects was also observed using a firefly *luciferase* reporter with r(CUG)$_{800}$ in the 3′ UTR. Disruption of RNA foci was also reported after treatment of cells with compound **3**.

To study target engagement, **2H-K4NMeS** was converted into a Chem-CLIP probe, **2H-K4NMeS-CA-Biotin**.[131] This molecule potently rescued splicing defects and reduced the number of

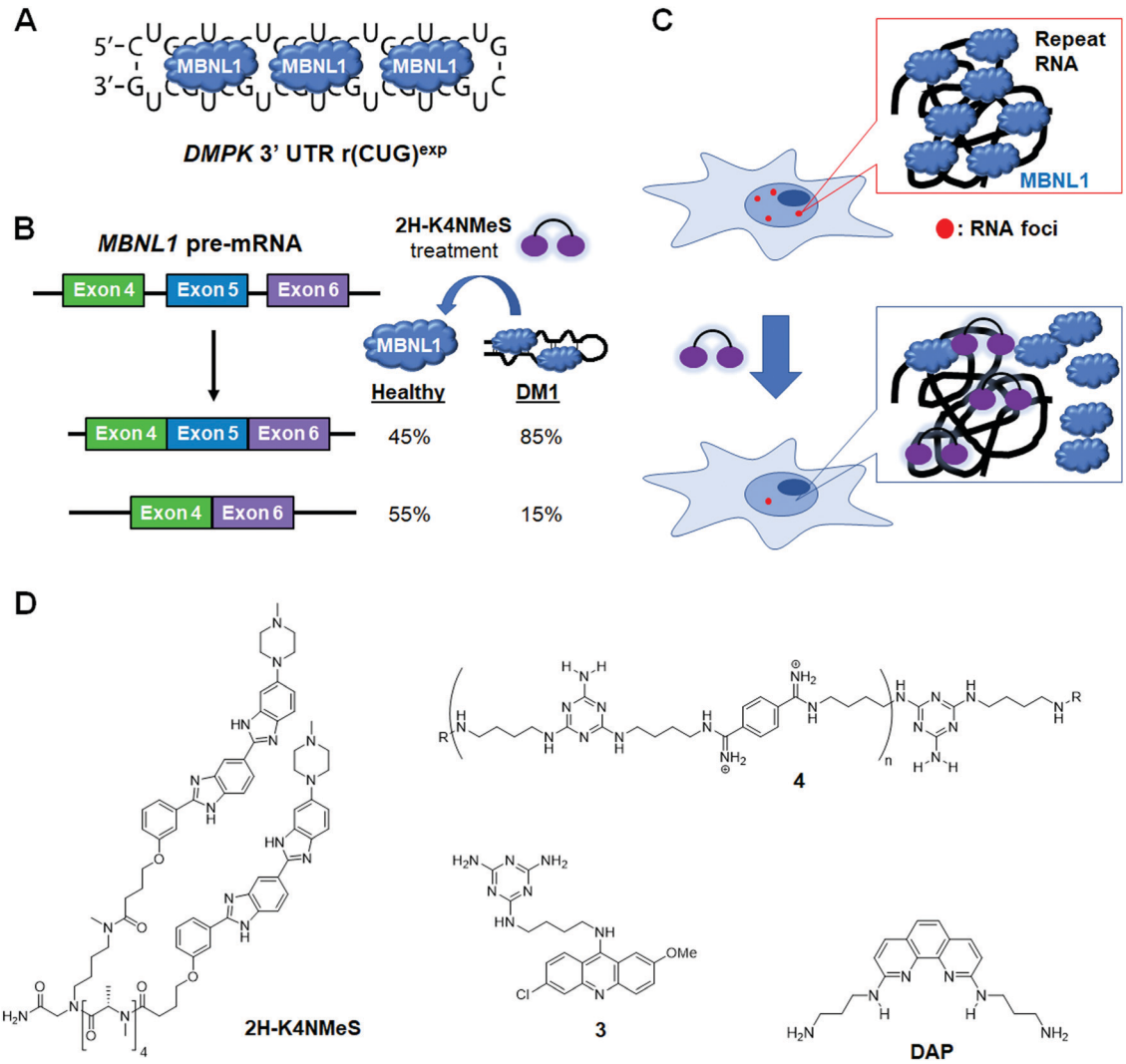

Fig. 8 Small molecule targeting of r(CUG)^{exp}, the RNA causative of myotonic dystrophy type 1 (DM1). (A) r(CUG)^{exp} sequesters MBNL1 protein, which regulates alternative pre-mRNA splicing. (B) MBNL1 regulates self-splicing of its own exon 5. Sequestration of MBNL1 by r(CUG)^{exp} results in exon 5 being included in the mature *MBNL1* transcript too frequently, contributing to DM1 pathology. (C) Schematic representation of RNA foci formation and disruption by small molecule binding. (D) Structures of compounds that bind r(CUG)^{exp}.

 This journal is © The Royal Society of Chemistry 2020

Open Access Article. Published on 25 September 2020. Downloaded on 8/9/2025 2:37:59 AM.
This article is licensed under a Creative Commons Attribution-NonCommercial 3.0 Unported Licence.

nuclear foci when DM1 patient-derived cells were dosed at a 10 nM concentration. In pulled down factions, an ~13 000-fold enrichment of *DMPK* mRNA was observed, as compared to the starting cell lysate. Using the competitive version of Chem-CLIP, C-Chem-CLIP, in which increasing concentrations of **2H-K4NMeS** were co-treated with a constant concentration of **2H-K4NMeS-CA-Biotin**, confirmed **2H-K4NMeS** and **2H-K4NMeS-CA-Biotin** share the same binding site in cells. The specific binding site was further defined by Chem-CLIP-Map,[132] confirming binding of the UU internal loops of r(CUG)^{exp} in the *DMPK* mRNA.

More interestingly, Rzuczek *et al.*[131] demonstrated target-templated oligomerization of an **H**-dimer in cells (Fig. 9). The designed **H**-dimer was modified with azide and alkyne moieties at opposite ends of the molecule, allowing oligomerization upon binding r(CUG)^{exp} through click chemistry. This oligomerization only occurred in DM1 cells, as healthy cells lack the repeating RNA necessary to template the reaction. This *in situ*-produced oligomer rescued splicing defects at concentrations as low as 100 pM in DM1 patient-derived cells.

Arambula *et al.*[133] developed acridine–triaminotriazine conjugate **3** targeting the r(CUG)^{exp} (Table S1, ESI†). They designed **3** based on the complementary Janus-wedge hydrogen bonding between triaminotriazine and the UU internal loops of r(CUG)^{exp}. This bonding is further stabilized by stacking interactions of the acridine moiety (Fig. 8D). ITC, using a model RNA hairpin, r(CUG)$_4$, revealed **3** has a K_d of 430 nM and 1 : 1 binding stoichiometry (Table S1, ESI†). However, **3** also binds with similar avidity to d(CTG)$_2$ duplex with a K_d of 390 nM. *In vitro*, **3** inhibits r(CUG)$_4$–MBNL1 complex formation with an IC_{50} of 52 μM and a K_i of 6 μM to r(CUG)$_4$, similar to values observed for r(CUG)$_{12}$. To capitalize on the multiple binding sites (UU internal loops) of the target, bivalent derivatives of **3** were developed.[134] A bivalent ligand containing an oligoamino linker was deemed the most superior with improved properties such as aqueous solubility and cell permeability compared to monomeric **3**. The dimer inhibited formation of RNA foci in a transfected cellular model of DM1 at 20 μM, and almost complete disruption at 50 μM.

In 2016, Luu *et al.*[135] demonstrated that dimerization of a dimeric compound which has two triaminotriazines linked with bisimidate produced a potent inhibitor of the r(CUG)^{exp}–MBNL1 complex. This intricate "dimer of dimers", has 1000-fold improved potency *in vitro* (K_i of 25 nM) compared to the original dimer. This molecule reduced RNA foci by ~20% when treated at 1 μM in cells, significantly improved splicing defects of insulin receptor (*IR*) exon 11 (10 μM dose in cells), and alleviated disease phenotypes in a *Drosophila* model of DM1. However, due to the compounds high molecular weight, it had issues with cellular uptake. To overcome this weakness, Lee *et al.*[136] developed oligomeric ligand **4**, composed of triaminotriazine units (targeting the UU internal loops of r(CUG)^{exp}) and bisimidate units (targeting the major groove of RNA) (Fig. 8D and Table S1, ESI†). Although **4** is still too large to permeate the cell membrane, its poly-cationic nature makes it membrane penetrant by endocytosis. Using 200 nM of **4**, they showed full rescue of *IR* mis-splicing and a decrease in foci number in a transfected model of DM1. However, **4** also inhibits transcription of d(CTG)^{exp}, indicating the compound is not specific for the RNA repeat (Table S1, ESI†). They used adult DM1 *Drosophila* (CTG_{480}) to investigate the *in vivo* effects of **4** by measuring the improvement of climbing defects observed after treatment with the compound. Approximately 80% of untreated files show significant defects in their ability to climb, but this was rescued by treatment with **4** (80 μM; 37% fail to climb). In addition, in a liver-specific DM1 mouse model containing 960 interrupted CUG repeats, **4** decreased the levels of the transgene, likely due to the compound's inhibitory effect on d(CTG)^{exp} transcription, improved pre-mRNA splicing defects, and reduced RNA foci formation, highlighting the compound's potential in preclinical animal models.

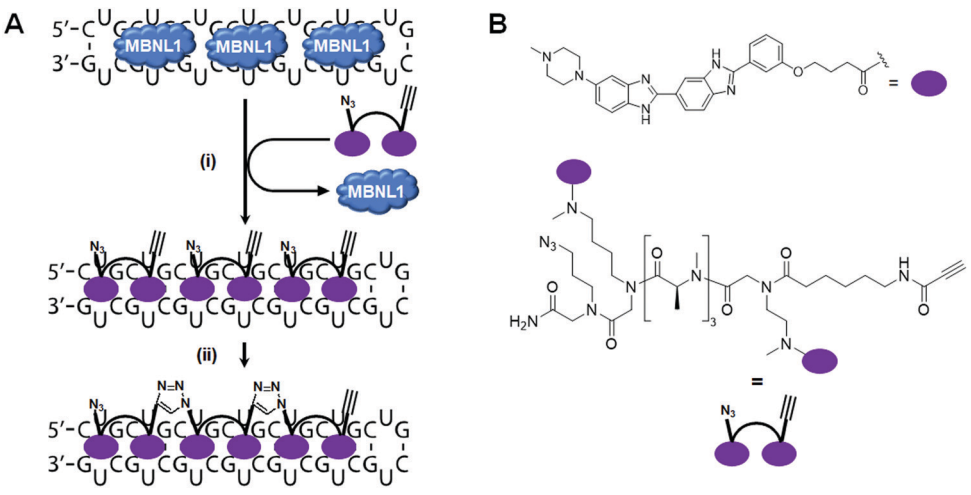

Fig. 9 RNA-templated ligand oligomerization catalyzed by r(CUG)^{exp}. (A) *In cellulis* click chemistry, templated by the RNA repeat expansion, forms an oligomeric compound on-site, that is bound to the r(CUG)^{exp} RNA target. (i) MBNL1 sequestered by r(CUG)^{exp} is released upon binding of the dimeric click compound. (ii) The azide terminus of one dimer reacts with the alkyne terminus of another dimer in close proximity to synthesize an oligomer *in cellulis*. (B) Structures of the RNA binding motif and dimeric click compound that oligomerizes *in cellulis*.

Open Access Article. Published on 25 September 2020. Downloaded on 8/9/2025 2:37:59 AM.
This article is licensed under a Creative Commons Attribution-NonCommercial 3.0 Unported Licence.

As another example of an r(CUG)^{exp} binding molecule, Li *et al.*[137] designed a 1,10-phenanthroline derivative (**DAP**) and studied its effect by *in vitro* translation (Fig. 8D and Table S1, ESI†). Using a transfected template RNA with r(CUG)$_{20}$ inserted between *Renilla* luciferase (*R*luc) and *firefly* luciferase (*F*luc) showed treatment with **DAP** suppressed translation of *F*luc downstream of the repeat sequence in a concentration-dependent manner. The translation of *R*luc was also moderately affected by **DAP** treatment. The selectivity of **DAP** was assessed by SPR and melting temperature, revealing **DAP** shows preferential binding to r(CUG)$_9$ and r(CCG)$_9$ among r(CXG)$_9$ sequences (X = A, U, G, or C) (Table S1, ESI†). Furthermore, electrospray ionization time-of-flight mass spectrometry (ESI-TOF MS) analysis showed **DAP** binds to r(CUG)$_9$ with an RNA:compound ratio of 1 : 4.

6.2 Small molecule inhibition of the r(CCUG)^{exp}–MBNL1 complex in DM2

DM2 is caused by r(CCUG)^{exp} in intron 1 of CCHC-type zinc finger nucleic acid binding protein (*CNBP*) pre-mRNA (Fig. 10A). As observed in DM1, r(CCUG)^{exp} sequesters MBNL1, causing MBNL1-dependent splicing defects and RNA foci formation, but also causes aberrant splicing of *CNBP* intron 1 (intron retention). To target DM2, Lee *et al.*[138] developed a dimeric kanamycin compound (**5**) that inhibits formation of r(CCUG)$_{12}$–MBNL1 complexes *in vitro* with an IC$_{50}$ of ∼90 nM (∼2500-fold more potent than the monomer; IC$_{50}$ = ∼220 μM) (Table S1, ESI†). Compound **5** demonstrated good cellular permeability and localized to both the nucleus and cytoplasm. In DM2 fibroblasts, **5** (10 μM) successfully rescued *IR* splicing defects and significantly reduced the number of RNA foci (Fig. 10B and C).[139] These activities were further improved by the incorporation of a cleavage module on the ligand (discussed in Section 10.4, "Targeted Cleavage of r(CCUG)^{exp} by a Small Molecule–Bleomycin A5 Conjugate").

Similar to the case shown with DM1 (Fig. 9), incorporation of azide and alkyne moieties into the kanamycin RNA-binding module afforded target-templated oligomerization in DM2 patient-derived cells.[140] When DM2 fibroblasts were treated with this clickable molecule (1 μM), the number of foci observed was reduced by ∼45% and *IR* exon 11 splicing defects were rescued by approximately the same percentage. These results clearly indicated the activity of the compound was far improved by on-site, *in situ* oligomerization. This oligomeric molecule also affected aberrant splicing of *CNBP* mRNA by inhibiting binding of MBNL1 to intron 1, thus allowing the intron to be properly spliced out of *CNBP* pre-mRNA (discussed in Section 7, "Small Molecules Shunt Toxic RNA to Endogenous Decay Pathways").

6.3 Small molecule inhibition of the r(CGG)^{exp}–protein complexes in FXTAS

In FXTAS, expanded r(CGG) repeats of lengths >55 but <200 (premutation allele) in the 5′ UTR of *FMR1* mRNA cause disease (Fig. 11A). The repeat folds into a hairpin structure with repeating 1 × 1 GG internal loops that sequester several proteins, such as DGCR8, Sam68, and hnRNP. Because these proteins have important roles in RNA biogenesis, their sequestration alters pre-mRNA splicing, thus resulting in disease.

Disney *et al.*[79] previously identified compound **1a** as a binder to r(CGG)^{exp} by screening compounds using a time-resolved fluorescence resonance energy transfer (TR-FRET) assay that monitors r(CGG)$_{12}$–DGCR8Δ complex formation and SAR (Fig. 11C and Table S1, ESI†). In particular, **1a** disrupted the r(CGG)$_{12}$–DGCR8Δ complex with an IC$_{50}$ of 12 μM, in the presence of competitor tRNA. Sequestration of Sam68 by r(CGG)^{exp} dysregulates splicing of *SMN2* mRNA, therefore the ability of **1a** to improve Sam68-regulated splicing defects was assessed (Fig. 11B). In transfected COS7 cells, r(CGG)^{exp} causes *SMN2* exon 7 to be included too frequently (∼70% compared to 30% in healthy cells). Upon

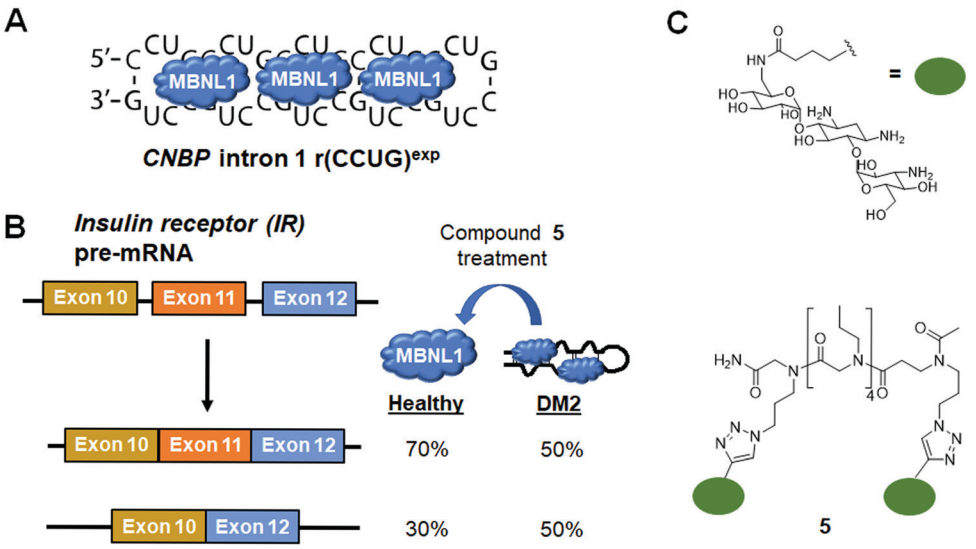

Fig. 10 Small molecule targeting of r(CCUG)^{exp}, the causative agent of myotonic dystrophy type 2 (DM2). (A) r(CCUG)^{exp} sequesters MBNL1. (B) MBNL1 regulates splicing of insulin receptor (*IR*) exon 11. Aberrant splicing results in exon 11 being excluded from the mature *IR* transcript, contributing to DM2 pathology. (C) Structures of the kanamycin RNA-binding motif and dimeric compound that bind r(CCUG)^{exp}.

 This journal is © The Royal Society of Chemistry 2020

Open Access Article. Published on 25 September 2020. Downloaded on 8/9/2025 2:37:59 AM.
This article is licensed under a Creative Commons Attribution-NonCommercial 3.0 Unported Licence.

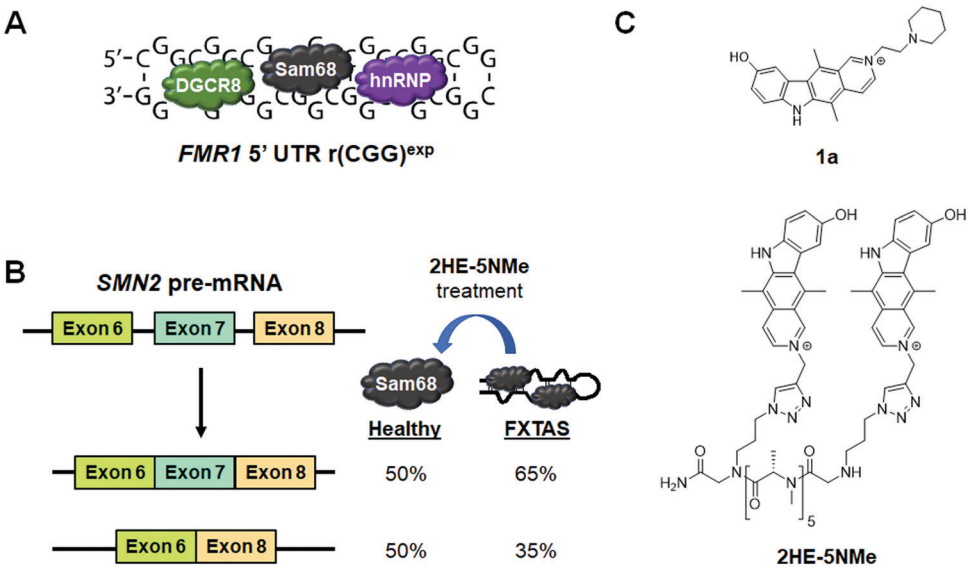

Fig. 11 Small molecule targeting of r(CGG)^{exp}, the RNA causative of fragile X-associated tremor ataxia syndrome (FXTAS). (A) r(CGG)^{exp} sequesters proteins such as DGCR8, Sam68, and hnRNP. (B) Sam68 regulates splicing of *SMN2* exon 7. Thus, its sequestration results in increased exon 7 inclusion in the mature *SMN2* transcript, contributing to FXTAS pathology. (C) Structures of compounds that bind to r(CGG)^{exp}.

treatment of these cells with **1a** (20 μM), improvement of the *SMN2* splicing defect was observed while improvement of another Sam68-regulated splicing event, apoptosis regulator Bcl-X (*Bcl-x*) exon 2, was observed upon treatment with 100 μM of **1a** (Table S1, ESI†). **1a** (10 μM) also reduced the number of RNA foci, as studied by RNA fluorescence *in situ* hybridization (FISH).[79]

As discussed previously, dimerization of RNA-binding modules is a powerful and easy method to obtain highly potent and selective compounds. Thus, a dimeric derivative of **1a**, **2HE-5NMe**, was designed and studied (Fig. 11C and Table S1, ESI†).[141] Inhibition of the r(CGG)$_{12}$–DGCR8Δ complex by **2HE-5NMe** was assessed by TR-FRET and revealed the compound inhibits complex formation with 6-fold greater activity than monomeric **1a** (IC_{50} = 3.5 μM in the presence of tRNA). Further, **2HE-5NMe** has 16-fold higher affinity for r(CGG)$_{12}$ (K_d = 50 ± 0.6 nM) than **1a**, which translates into a 3-fold higher occupancy *in cellulis*, as revealed by Chem-CLIP studies (Table S1, ESI†).[141]

The activity of **2HE-5NMe** for rescuing splicing defects was assessed by exon 7 inclusion in *SMN2* mRNA. Treatment of **2HE-5NMe** at 50 μM rescued exon 7 inclusion levels back to those observed in wild type cells, demonstrating a >10-fold increase in activity over **1a**. While **1a** can inhibit foci formation but not disrupt existing foci, **2HE-5NMe** has the ability to do both (~70% reduction at 50 μM). It should be noted that most foci in this study were dissolved within 1 h of treatment and fully dissolved after 4 h. Recovery of *SMN2* splicing defects were observed in parallel to this time course. The effect of these compounds on RAN translation is discussed in Section 8.2, "Small Molecules Targeting the r(CGG)^{exp} in *FMR1* Inhibit RAN Translation".

6.4 Small molecule inhibition of the r(G$_4$C$_2$)^{exp}–hnRNP H complex in c9FTD/ALS

An expanded repeat of G_4C_2 [r(G$_4$C$_2$)^{exp}] in intron 1 of *C9orf72* mRNA is the most common genetic cause of the neurodegenerative disease c9FTD/ALS (Fig. 12A). The structure of r(G$_4$C$_2$)^{exp} has been well-studied, revealing the repeating RNA can adopt two main structures, a hairpin with an array of internal loops and a G-quadruplex. Because the hairpin form of r(G$_4$C$_2$)^{exp} forms the same 1 × 1 GG internal loops as r(CGG)^{exp}, Su *et al.*[142] hypothesized that **1a** might also bind to r(G$_4$C$_2$)^{exp}. Using **1a** as a lead, a library of chemically similar compounds was created and screened for binding r(G$_4$C$_2$)$_8$ using a dye displacement assay. The screen revealed **1a** and two additional compounds, **6** and **7**, bind r(G$_4$C$_2$)^{exp} (Fig. 12B and Table S1, ESI†), with K_ds of 9.7, 10, and 16 μM, respectively (Table S1, ESI†). To assess the biological activities of each compound, foci formation was evaluated in r(G$_4$C$_2$)$_{66}$-expressing COS7 cells. Compounds **1a** and **6**, but not **7**, showed a 3-fold reduction of foci-positive cells. This reduction in foci by **1a** can be traced to its direct engagement of r(G$_4$C$_2$)^{exp}, as determined by Chem-CLIP, which revealed an 80-fold enrichment of r(G$_4$C$_2$)$_{66}$ in the pulled down fractions, as compared to 18S rRNA.[142] C-Chem-CLIP studies where r(G$_4$C$_2$)$_{66}$-expressing COS7 cells were co-treated with **1a** and its Chem-CLIP probe verified target engagement by the parent compound.[142]

Interestingly, *C9orf72* mRNA is bidirectionally transcribed and thus repeats from the sense [r(G$_4$C$_2$)^{exp}] and antisense [r(G$_2$C$_4$)^{exp}] strand are produced. Like the sense strand, r(G$_2$C$_4$)^{exp} also forms nuclear inclusions. However, the antisense foci were not reduced by the treatment of **1a**, confirming its selectivity for the sense strand. Furthermore, **1a** showed significant reduction of RNA foci-positive cells in three *C9ORF72*+ induced neuron (iNeuron) lines.

In a subsequent study,[143] **1a** was further optimized, affording **8** (Fig. 8 and Table S1, ESI†). Compound **8** binds to r(G$_4$C$_2$)$_8$ with a K_d of 0.26 μM, while showing ~300-fold weaker binding to antisense r(G$_2$C$_4$)$_8$ and ~540-fold weaker binding to base-pair control r(G$_2$C$_2$)$_8$ (Table S1, ESI†). With the remarkable binding

Open Access Article. Published on 25 September 2020. Downloaded on 8/9/2025 2:37:59 AM.
This article is licensed under a Creative Commons Attribution-NonCommercial 3.0 Unported Licence.

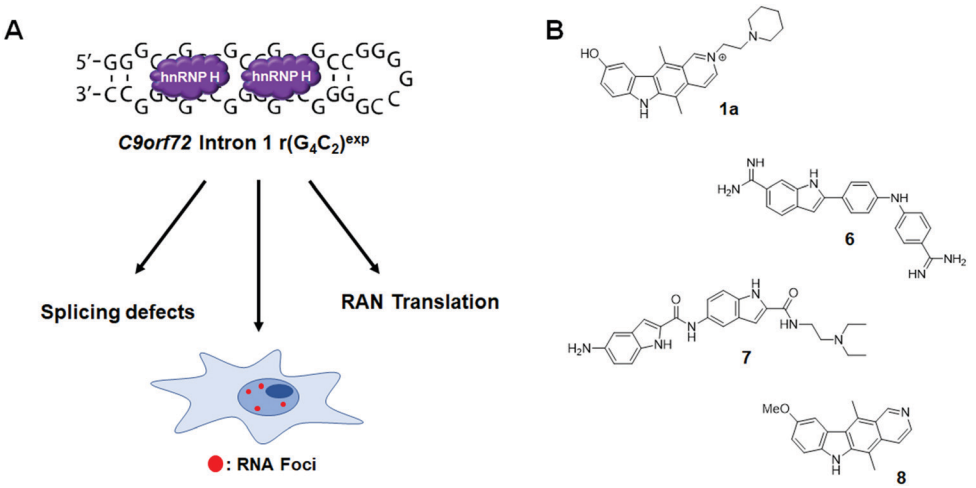

Fig. 12 Small molecule targeting of $r(G_4C_2)^{exp}$, the most common genetic cause of *C9orf72*-associated frontotemporal dementia and amyotrophic lateral sclerosis (c9FTD/ALS). (A) $r(G_4C_2)^{exp}$ sequesters hnRNP H, resulting in splicing defects. The repeat expansion also undergoes RAN translation and forms RNA foci. (B) Structures of compounds that bind to $r(G_4C_2)^{exp}$. Compound **1a** also binds to $r(CGG)^{exp}$ due to the 5′-CGG/3′-GGC binding site shared between the two repeats.

affinity of **8**, the binding mechanism was further investigated by NMR spectroscopy. In brief, **8** stacks between GG internal loops and closing GC base pairs to stabilize the closing base pairs with π–π interactions. *In vitro*, **8** inhibited the $r(G_4C_2)_8$-hnRNP H complex with an IC_{50} of 19 μM and reduced both the number of foci-positive cells and the number of foci present per cell by half in HEK293T cells transfected with a plasmid encoding $r(G_4C_2)_{66}$ (5 μM dose). Therefore, **8** is a potent and selective small molecule capable of alleviating disease-associated phenotypes in cellular models of c9ALS/FTD. The inhibition of RAN translation by **8** is discussed in Section 8.3, "Small Molecules Targeting the $r(G_4C_2)^{exp}$ in *C9orf72* Inhibit RAN Translation". Most importantly, these studies with **8** revealed that the hairpin form of $r(G_4C_2)^{exp}$, not the G-quadruplex, is RAN translated.

7. Small molecules shunt toxic RNAs to endogenous decay pathways

As discussed in Section 6.2 ("Small Molecule Inhibition of the $r(CCUG)^{exp}$-MBNL1 Complex in DM2"), $r(CCUG)^{exp}$ causes *CNBP* intron 1 retention. Although formation of nuclear foci and splicing defects have been well studied in DM2, intron retention was only recently discovered by the Swanson group (~40% retained in DM2-affected cells *vs.* ~10% in healthy cells) (Fig. 13A).[144] Intronic regions of pre-mRNAs are normally subjected to endogenous decay upon liberation, but in DM2 the intron containing the repeat expansion remains present in the mature mRNA transcript.[145] Shortly after this discovery, **5**, previously reported to target $r(CCUG)^{exp}$ and alleviate DM2-associated defects, was employed as a chemical probe to investigate the mechanism of intron retention (Table S1, ESI†).[140] These studies showed that binding of MBNL1 causes intron retention and that small molecules can alleviate this retention by shunting the intron to endogenous decay pathways.

Treatment of DM2 patient-derived cells with **5** (1–10 μM) led to ~15–20% of the retained intron being eliminated, while no effect was observed on *CNBP* mature mRNA levels (Fig. 13B),[140] suggesting a mechanism by which small molecule binding of the $r(CCUG)^{exp}$ shunts pathogenic RNAs to endogenous quality control pathways. Notably, there are a variety of disease-causing RNA repeats harbored in introns that lead to intron retention, such as c9FTD/ALS caused by $r(G_4C_2)^{exp}$ and Fuchs endothelial corneal dystrophy (FED) caused by $r(CUG)^{exp}$. Small molecule intervention in these cases may have similar cooperative effects with endogenous RNA decay mechanisms to be therapeutically advantageous.

8. Small molecules targeting RNA repeat expansions inhibit RAN translation

8.1 RAN translation in microsatellite diseases

An additional pathomechanism found in some neurodegenerative RNA repeat expansion disorders, such at $r(CGG)^{exp}$ and $r(G_4C_2)^{exp}$, is RAN translation.[146–150] In this phenomenon, repeat expansions serve as non-canonical translation initiation sites, thus giving rise to homopolymeric, as in the case of $r(CGG)^{exp}$,[149,150] or dipeptide repeat (DPR) proteins, as in the case of $r(G_4C_2)^{exp}$.[146,148] These proteins are intrinsically disordered and form neurotoxic aggregates that contribute to disease pathology.[151] Therefore, small molecules that inhibit RAN translation are of high therapeutic importance.

8.2 Small molecules targeting the $r(CGG)^{exp}$ in *FMR1* inhibit RAN translation

In FXTAS, RAN translation produces the homopolymeric protein poly(G) (Fig. 14A).[149,150] As **1a** and **2HE-5NMe** (Fig. 14B and Table S1, ESI†) were shown to bind $r(CGG)^{exp}$ selectively both

 This journal is © The Royal Society of Chemistry 2020

Open Access Article. Published on 25 September 2020. Downloaded on 8/9/2025 2:37:59 AM.
This article is licensed under a Creative Commons Attribution-NonCommercial 3.0 Unported Licence.

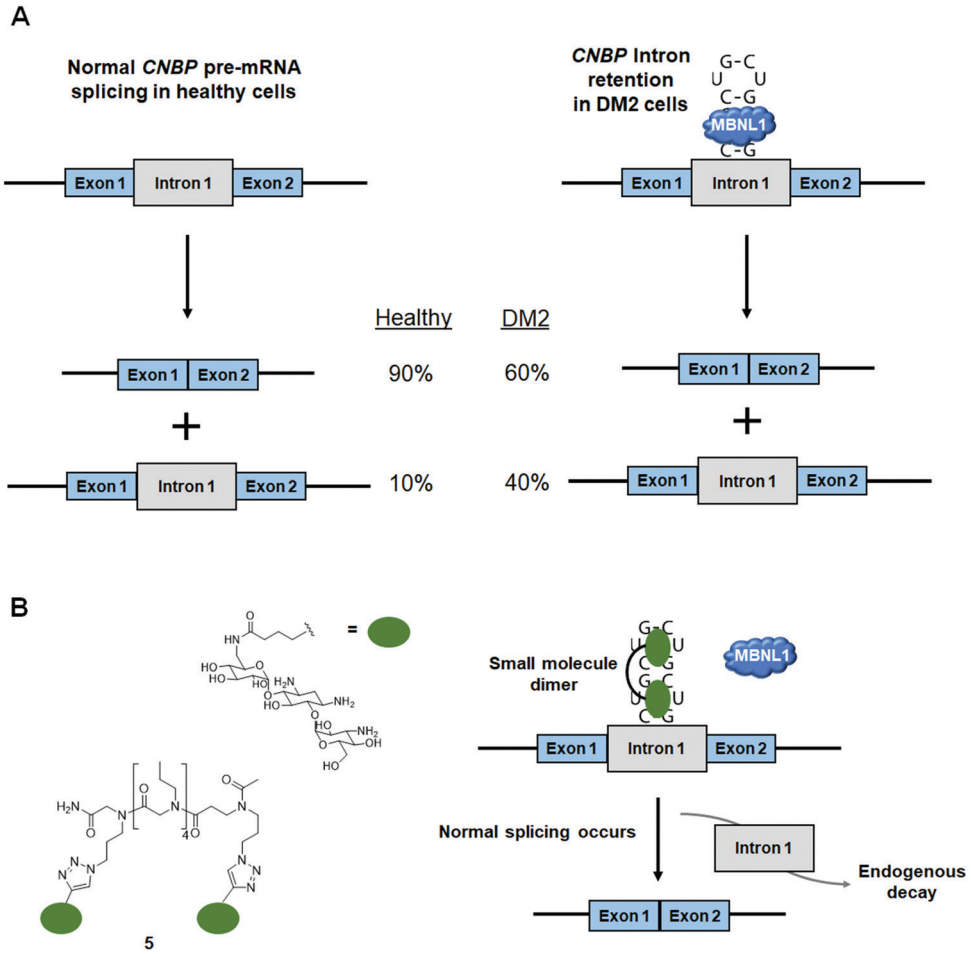

Fig. 13 Small molecule binding causes toxic RNAs to be shunted to endogenous decay pathways. (A) MBNL1 sequestration by r(CCUG)^{exp} results in *CNBP* intron 1 retention. (B) Small molecule binding frees MBNL1 and allows for proper intron splicing to occur. The excised intron is shunted to endogenous decay pathways.

in vitro and *in cellulis* (as determined by Chem-CLIP),[79,141] their ability to inhibit RAN translation was also assessed. Interestingly, both **1a** and **2HE-5NMe** thermally stabilize r(CGG)$_{12}$ (by 1.4 and 0.9 kcal mol^{-1} respectively),[141] suggesting they may prevent ribosomal readthrough or loading and thereby inhibit RAN translation. In agreement with their similar degree of stabilization of r(CGG)$_{12}$, **1a** and **2HE-5NMe** inhibited RAN translation to a similar extent (~80% inhibition at 50 μM) as well as reduced the number of poly(G) nuclear inclusions.[141] Notably, both compounds reduced polysome loading onto r(CGG)$_{88}$, as hypothesized.[79,141] Importantly, neither compound affects mRNA levels or canonical translation of the downstream ORF.[79,141]

To date, the most potent inhibitor of r(CGG)^{exp} RAN translation is the covalent cross-linker **2H-5-CA-Biotin** (Table S1, ESI†).[152] **2H-5-CA-Biotin** selectively engaged the RNA target in cells and inhibited RAN translation at a dose of only 500 nM (~40% decrease in poly(G) levels) while not affecting canonical translation of the downstream ORF.[152] Additionally, polysome profiling indicated that **2H-5-CA-Biotin** disrupts polysome loading onto r(CGG)^{exp}-containing transcripts.

8.3 Small molecules targeting the r(G$_4$C$_2$)^{exp} in *C9orf72* inhibit RAN translation

In c9FTD/ALS, RAN translation gives rise to five DPRs.[151] Poly(GA) and poly(GR) are translated from the sense strand [r(G$_4$C$_2$)^{exp}], while poly(PA) and poly(PR) are translated from the antisense strand [r(G$_2$C$_4$)^{exp}].[153] Poly(GP) is RAN translated from both strands and is highly expressed in the central nervous system. Additionally, it is the most soluble of the DPRs, making its detection facile (Fig. 14A).[146,151,154] In agreement with its ability to alleviate another c9FTD/ALS-associated defect (nuclear inclusions), **1a** dose-dependently reduced levels of poly(GP) by 10%, 18%, and 47% in iNeurons treated at 25, 50, or 100 μM, respectively.[142] Likewise, the **1a** derivative **8** dose-dependently inhibited RAN translation in HEK293T cells expressing r(G$_4$C$_2$)$_{66}$ (IC$_{50}$ = 1.6 ± 0.20 μM), while having no effect on canonical translation (Fig. 14B).[143] Polysome profiling upon treatment with **8** showed the amount of r(G$_4$C$_2$)$_{66}$ transcripts loaded into polysomes was significantly decreased for high and low molecular weight polysomes and monosomes, indicating that **8** works by sterically blocking the assembly of ribosomes onto r(G$_4$C$_2$)^{exp}, thus reducing the levels of toxic DPRs produced.[143]

Open Access Article. Published on 25 September 2020. Downloaded on 8/9/2025 2:37:59 AM.
This article is licensed under a Creative Commons Attribution-NonCommercial 3.0 Unported Licence.

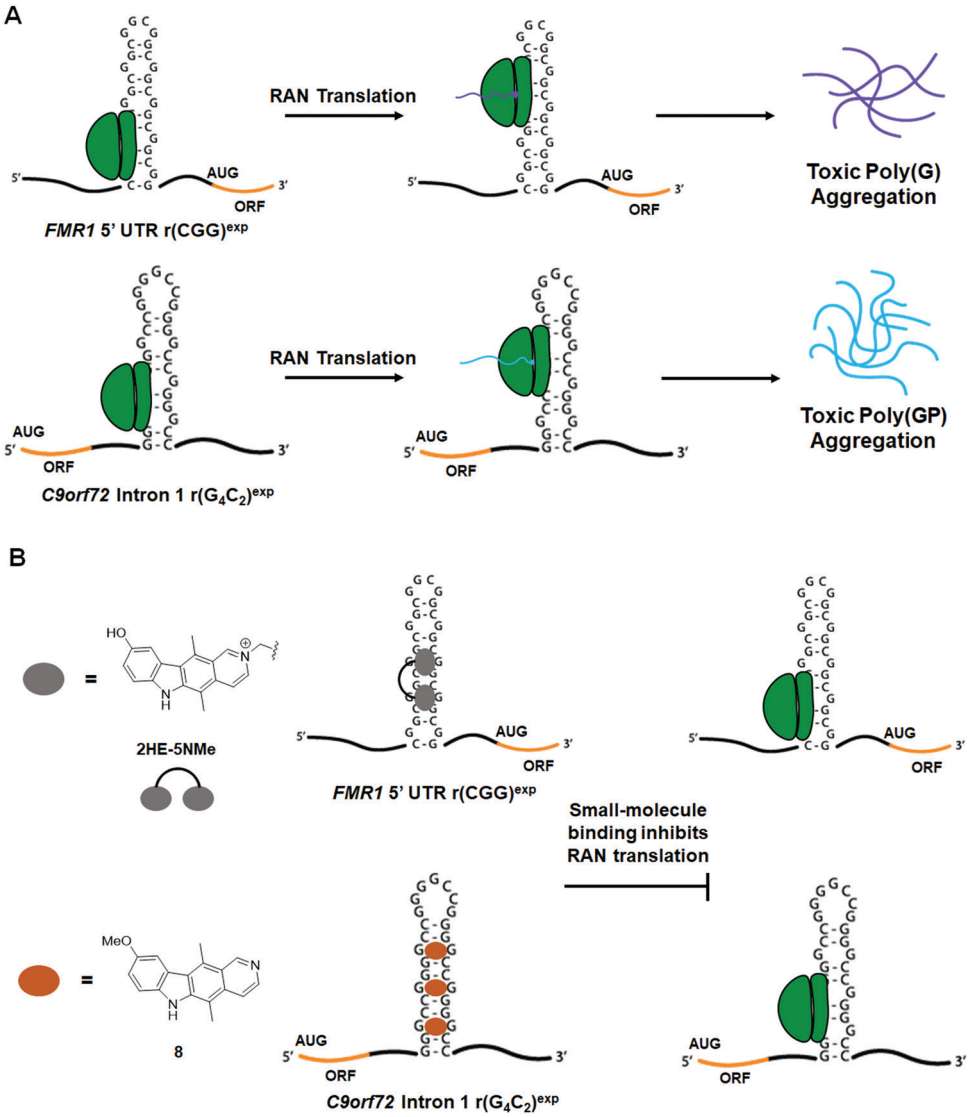

Fig. 14 Small molecule targeting of RNA repeat expansions reduces aberrarnt repeat-associated non-ATG (RAN) translation. (A) Schematic of RAN translation of *FMR1* due to r(CGG)^{exp} in the 5′ UTR and *C9orf72* due to r(G$_4$C$_2$)^{exp} in intron 1. (B) Small molecules targeting r(CGG)^{exp} and r(G$_4$C$_2$)^{exp} inhibit RAN translation.

9. Small molecules inhibit translation of traditionally undruggable proteins

Over the past decades, tremendous efforts have been invested in the development of small molecules targeting disease-causing proteins, and yet only 15% of proteins are considered "druggable" from genome-wide analysis.[155,156] One major roadblock in drugging the remaining 85% is their lack of defined structures that can serve as potential small molecule binding pockets.[157,158] To overcome this challenge, an alternative strategy, especially useful for proteins with aberrantly high expression levels, is to target their encoding mRNA specifically with small molecules and hence inhibit downstream translation. A recent example of this is the development of a small molecule targeting the α-synuclein mRNA,[159] which encodes an intrinsically disordered protein (IDP) key to the pathogenesis of Parkinson's disease (PD).[160]

The α-synuclein protein, encoded by the *SNCA* gene, can oligomerize to form fibrils across neurons in the brain as well as accumulate in Lewy bodies and Lewy neurites, contributing to the risk of developing PD (Fig. 15A).[161,162] Since individuals with multiplication of the *SNCA* gene locus develop dominantly inherited PD with a gene-dosage effect,[163] reducing the level of α-synuclein expression could be a promising disease-alleviating strategy.[164,165] As an IDP, α-synuclein is challenging to target. The *SNCA* mRNA, however, displays a functionally important and structurally defined 5′ UTR with an iron responsive element (IRE) that provides opportunities for small molecule targeting.[166,167] Indeed, employment of the sequence-based design and lead identification strategy, Inforna (discussed in Section 2.3, "Design of Monomeric Small Molecules Targeting Disease-Causing miRNAs"),[41] yielded a set of small molecules that bind the IRE region of *SNCA* mRNA. These initial hits were

 This journal is © The Royal Society of Chemistry 2020

Open Access Article. Published on 25 September 2020. Downloaded on 8/9/2025 2:37:59 AM.
This article is licensed under a Creative Commons Attribution-NonCommercial 3.0 Unported Licence.

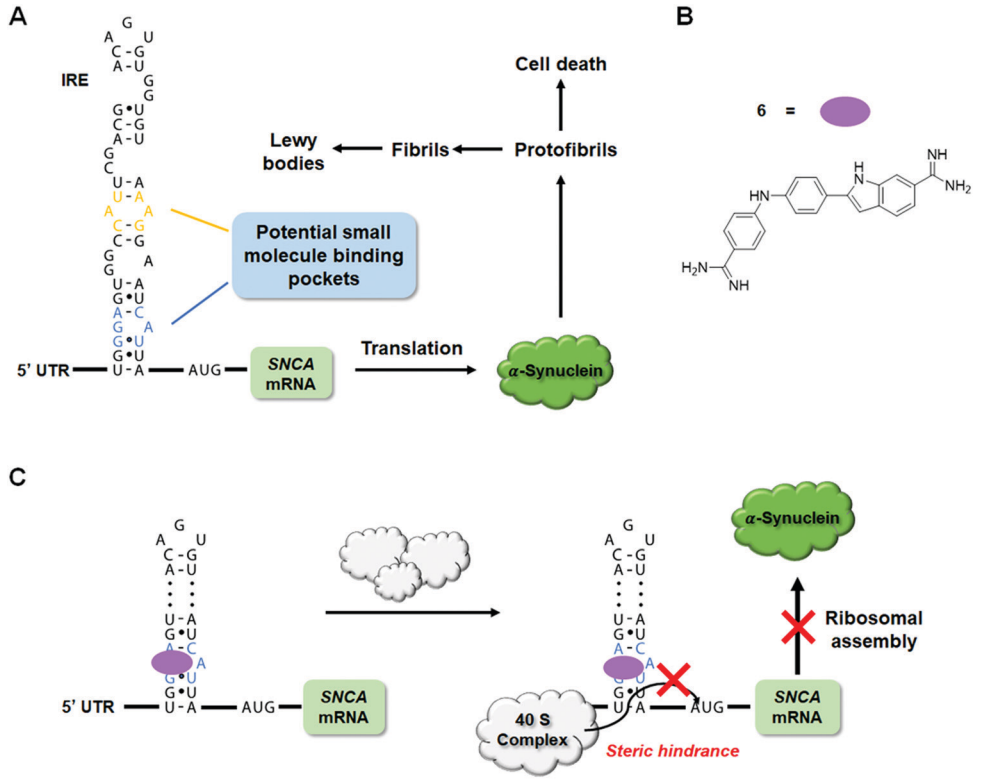

Fig. 15 RNA-targeted small molecules inhibit translation of traditionally undruggable proteins. (A) Schematic depiction of α-synuclein-mediated disease pathway. (B) Structure of **Synucleozid**, an Inforna-designed small molecule that binds the A-bulge of the *SNCA* IRE that regulates translation of the mRNA. (C) **Synucleozid** targets the IRE structure of *SNCA* mRNA and represses α-synuclein protein expression by inhibiting ribosomal assembly onto the *SNCA* transcript.

subjected to a western blot screen of α-synuclein inhibition potency in neuroblastoma cells, with the most potent compound, **Synucleozid**, exhibiting an IC_{50} ~500 nM (Fig. 15B and Table S1, ESI†).[159] To ensure that inhibition occurs at the translational and not transcriptional level, RT-qPCR was used to confirm the level of *SNCA* mRNA remained constant upon treatment of **Synucleozid**.

It should be noted, however, that observation of the expected biological effects can only support, not validate, the putative binding mode of a small molecule. To validate the A bulge of the IRE of *SNCA* mRNA as the binding site of **Synucleozid**, competitive binding assays and mutational analyses were performed. Indeed, mutations of the A bulge to either a U/G bulge or a base pair reduced the binding affinity of **Synucleozid** by 10-fold, while mutations of other non-canonical base pairs had no effect on **Synucleozid** binding avidity. Furthermore, ASO-Bind-Map[18,168] was used to confirm the binding of **Synucleozid** to the IRE both *in vitro* and *in cellulis*. Briefly, ASO-Bind-Map relies on ASO-mediated RNA cleavage, *via* RNase H, which can be inhibited by small molecule binding of the RNA target. Small molecule binding thermodynamically stabilizes the RNA and impedes ASO binding at the binding site. *In vitro*, protection from RNase H cleavage can be read out by gel electrophoresis while RT-qPCR or RNA-seq can be used to read out protection by the binding small molecule *in cellulis*. In this case, treatment of **Synucleozid** impeded cleavage of the IRE, indicating that **Synucleozid** indeed binds to the IRE and stabilizes its structure.

In addition to its intrinsic specificity for the binding pocket on RNA, the overall specificity of a small molecule depends on the prevalence of the structured pocket across the entire human transcriptome. In other words, a small molecule that is specific to its target binding pocket would still suffer from off-target effects if this binding pocket is shared by other non-target RNAs. The selectivity of **Synucleozid** was first assessed by studying its effect on mRNAs expressed in the nervous system that contain known IREs in their UTRs, including amyloid precursor protein (APP), prion protein (PrP), ferritin and the transferritin receptor (TfR). Upon treatment of **Synucleozid** (1 μM), no effect was observed upon APP, PrP, or TfR levels, but ferritin levels were reduced by ~50%. This reduction could be the result of an off-target effect of **Synucleozid** or could be due to compound-mediated rescue of autophagic and lysosomal dysfunction caused by an accumulation of α-synuclein in PD.[169] While future studies are necessary to elucidate **Synucleozid**'s effect on ferritin levels, the compound demonstrated overall high selectivity for *SNCA* mRNA due to its unique structure in the 5′ UTR. Moreover, the targeted 5′-G_G/3′-CAU region was searched across a database of structural elements expressed in the human transcriptome, including miRNA hairpin precursors (7436 motifs) and 2459 other known motifs from rRNA, RNase P RNA, U4/U6 snRNA, and nonredundant tRNAs.[159,170]

Open Access Article. Published on 25 September 2020. Downloaded on 8/9/2025 2:37:59 AM.
This article is licensed under a Creative Commons Attribution-NonCommercial 3.0 Unported Licence.

Remarkably, the bulge targeted by **Synucleozid** only occurs five times among these motifs (0.051%) and fortuitously, the potential miRNA off-targets are not expressed at appreciable levels.[170] Not surprisingly, **Synucleozid** had no effect on their expression. A transcriptome-wide assessment of **Synucleozid** treatment using RNA-seq revealed very few changes (55/20 034 genes changed; 0.3%).[159,171] Similarly, a proteome-wide selectivity analysis also showed limited changes (283/3300 proteins changed; 8%). Collectively, these data support the fundamental claim that RNAs can indeed form unique 3D structures suitable for targeting with small molecules, therefore expanding the druggability of proteins broadly. Notably, this assertion is bolstered by studies that direct the splicing outcome of *MAPT* exon 10 (tau), another IDP.[120]

10. Targeted cleavage of disease-causing RNAs using bleomycin A5-conjugates

10.1 Bleomycin A5 cleavage of miRNAs

Bleomycin A5 is a well-known, DNA-cleaving natural product[172] that also cleaves RNA (Fig. 16A).[173,174] Building on the foundational studies of Hecht,[173,174] it was recently determined that bleomycin A5 has two preferred RNA cleavage sites, AU rich regions, with longer stretches of AU base pairs correlating with more efficient RNA cleavage and purine-rich sequences.[175] Angelbello *et al.*[175] identified a compilation of 13 human miRNAs that contain AU-rich regions, seven of which have been tied to disease. Of these, pri-miR-10b has a 5′AUAUAU/3′UAUAUA

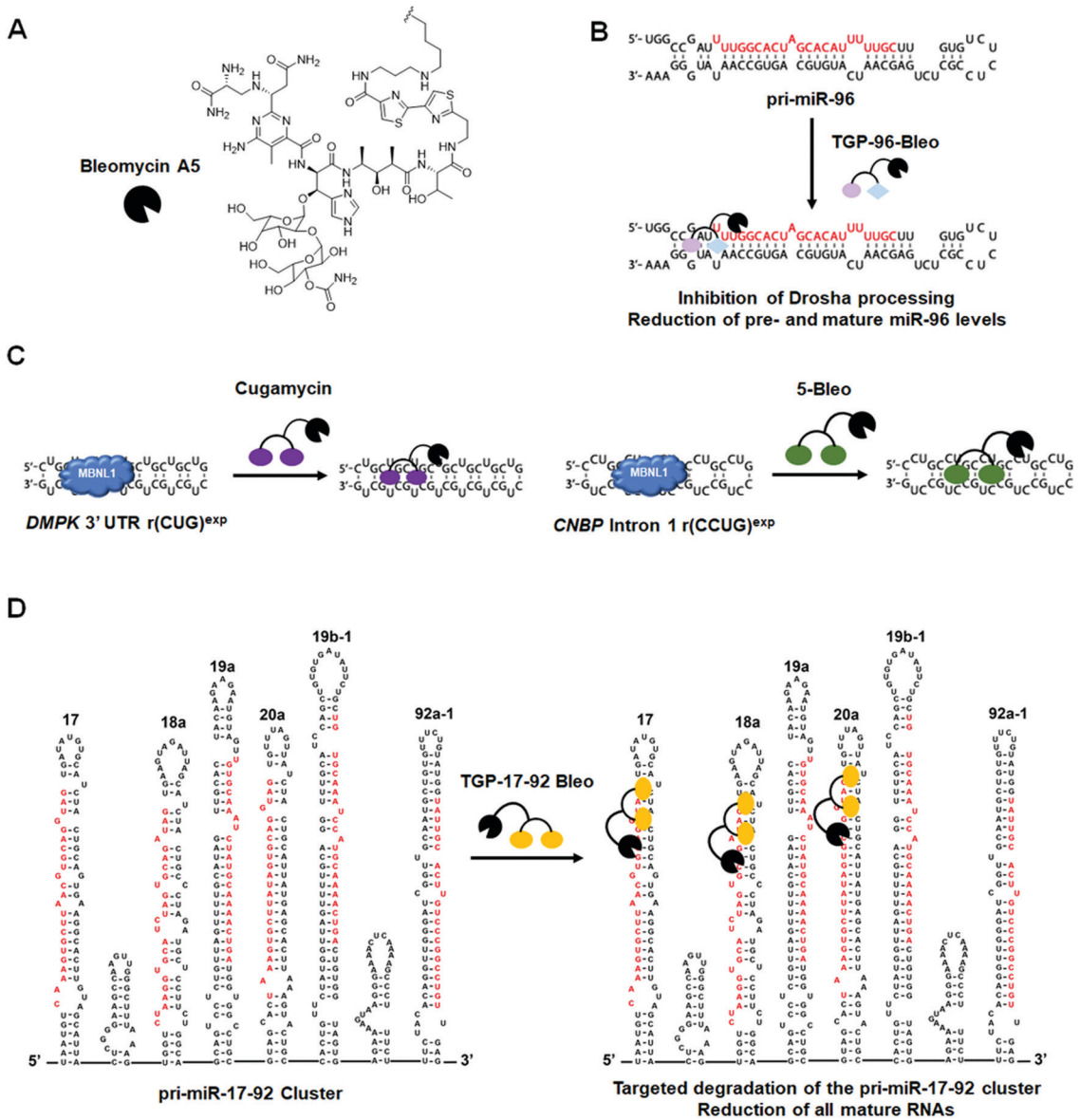

Fig. 16 Small molecule-bleomycin A5 conjugates cleave disease-causing RNAs in a targeted manner. (A) Structure of Bleomycin A5. (B) **TGP-96-Bleo** targets and cleaves oncogenic pri-miR-96. (C) Targeted degradation of r(CUG)^{exp} by **Cugamycin** and r(CCUG)^{exp} by **5-Bleo**. (D) Targeted degradation of the pri-miR-17-92 cluster by **TGP-17-92 Bleo**.

 This journal is © The Royal Society of Chemistry 2020

Open Access Article. Published on 25 September 2020. Downloaded on 8/9/2025 2:37:59 AM. This article is licensed under a Creative Commons Attribution-NonCommercial 3.0 Unported Licence.

sequence, creating a potential recognition site for bleomycin A5 cleavage. Indeed, bleomycin A5 cleaved pri-miR-10b at two locations, the predicted AU-rich region and a 5′GUG/3′CAC site near the Dicer processing site. This finding was not surprising as bleomycin A5 also prefers purine-rich sequences.[175]

Bleomycin A5 was then studied for cleavage of pri-miR-10b in two cellular models: (i) HeLa cells transfected with a plasmid encoding pri-miR-10b and (ii) the TNBC cell line MDA-MB-231 in which miR-10b is overexpressed.[176] Aberrant levels of miR-10b have been linked to both tumor invasion and metastasis in TNBC.[176] At nM concentrations, the compound cleaved pri-miR-10b in both cell types thereby reducing levels of mature miR-10b, as determined by RT-qPCR.

This study highlighted the ability of bleomycin A5 to cleave RNA in cells, opening the door for the development of small molecule-bleomycin conjugates that direct the natural product to cleave a specific RNA target. This work also emphasized that ncRNAs can be targets of known drugs and should therefore be considered in drug discovery screens.

10.2 Targaprimir-96-Bleo (TGP-96-Bleo): Targeted cleavage of pri-miR-96 by a small molecule–bleomycin A5 conjugate

The first example of using small molecule–bleomycin conjugates to cleave miRNAs came from Li *et al.*,[177] in which they used a heterodimeric–bleomycin A5 conjugate to target oncogenic pri-miR-96. Both the bleomycin derivative and its site of conjugation to the small molecule were carefully selected. Bleomycin contains four domains: (i) a metal-binding nucleic acid cleavage domain; (ii) a C-terminal DNA-binding domain; (iii) a linker connecting the cleavage and DNA-binding domains; and (iv) a carbohydrate domain important for cellular uptake of the molecule.[172] The derivative bleomycin A5 was chosen for conjugation to RNA-binding small molecules because the DNA-binding domain contains a butyl-1,4-diamine side chain that allows for easy conjugation of small molecules. Additionally, it has been shown that conjugation through bleomycin's C-terminal free amine reduces affinity for DNA *via* ablation of the amine's positive charge.[178,179] These studies suggest that small molecule–bleomycin A5 conjugates have the potential to selectively cleave RNA targets.

As discussed previously (in Section 2.3. "Design of Monomeric Small Molecules Targeting Disease-Causing miRNAs"), **TGP-96**[47] was designed using Inforna and is a potent binder of the pri-miR-96 Drosha processing site and adjacent 1 × 1 GG loop. Binding of **TGP-96** to pri-miR-96 inhibited the biogenesis of mature miR-96, derepressed FOXO1, and triggered apoptosis in MDA-MB-231 cells.[47] To further improve bioactivity, a small molecule cleaver was synthesized by conjugating **TGP-96** to bleomycin A5 (**TGP-96-Bleo**) *via* the C-terminal amine in the traditional DNA-binding domain of bleomycin A5, thus disrupting key interactions necessary for DNA recognition (Table S1, ESI†).[177] As bleomycin A5 has been shown to cleave AU base pairs,[175] and pri-miR-96 has AU base pairs in close proximity to **TGP-96**'s binding site, this conjugation strategy had a high potential for success.

Indeed, **TGP-96-Bleo** bound pri-miR-96 with a K_d of 64 ± 11 nM and cleaved the hairpin at the predicted AU base pairs, while no binding to DNA was observed (Fig. 16B and Table S1, ESI†).[177] A control compound lacking the RNA-binding modules cleaved plasmid DNA at levels 5-fold greater than those seen with **TGP-96-Bleo**,[177] indicating conjugation of bleomycin A5 to RNA binding modules reduces its affinity for DNA, lowering the potential for off-targets. This was further supported by visualizing γ-H2AX foci formation in cells, a marker for DNA double stranded breaks. Cells treated with the control compound lacking RNA-binding modules displayed ~2.3-fold more foci than cells treated with **TGP-96-Bleo**.[177] Notably, the concentrations of **TGP-96-Bleo** that cleaved DNA and induced double stranded DNA breaks are 20-fold higher than the concentrations that reduced mature miR-96 levels, *vide infra*.

Based on these promising results, **TGP-96-Bleo** was compared to **TGP-96** in MDA-MB-231 TNBC cells for reducing levels of mature miR-96. RT-qPCR analysis confirmed treatment with **TGP-96-Bleo** decreased the levels of both pri-miR-96 and mature miR-96.[177] As mentioned above, **TGP-96** decreased mature miR-96 levels but increased pri-miR-96 levels. These data are consistent with the mechanisms of action for the two compounds; **TGP-96-Bleo** as an RNA cleaver and **TGP-96** as an RNA binder. Target occupancy of **TGP-96-Bleo** for the predicted pri-miR-96 binding sites was confirmed *via* a competitive cleavage assay in which cells were co-treated with **TGP-96-Bleo** and **TGP-96**, with **TGP-96** added in increasing concentrations to compete off a constant concentration of **TGP-96-Bleo**. Treatment with **TGP-96-Bleo** also resulted in rescue of FOXO1 expression and subsequent activation of apoptotic pathways in MDA-MB-231 cells, demonstrating rescue of disease phenotypes by **TGP-96-Bleo**.[177] **TGP-96-Bleo** did not have an effect on any other miRNAs predicted to target FOXO1.[180]

To further profile the selectivity of **TGP-96-Bleo**, small molecule nucleic acid profiling by cleavage applied to RNA (RiboSNAP) was utilized against the 349 miRNAs expressed in MDA-MB-231 cells.[177] The results of this profiling showed miR-96 levels were the most drastically and significantly affected by **TGP-96-Bleo** treatment, highlighting the selectivity of this small molecule RNA cleaver (Table S1, ESI†). Additionally, this experiment showed DNA off-targets of bleomycin A5 can be ablated by conjugation to an RNA-binder and that small molecule cleaver compounds can be successfully used for cellular profiling. A variation of RiboSNAP, RiboSNAP-Map, in which cleavage fragments are analyzed to determine the exact binding site of a small molecule, was also debuted in this paper.[177] RiboSNAP-Map uses a gene specific forward primer and universal reverse primer to amplify cleavage products, which are then sequenced to determine the site of cleavage.[177] This method confirmed the **TGP-96-Bleo** cleavage site is in close proximity to the known binding sites of **TGP-96**, positioning bleomycin A5 to cleave the proximal AU base pairs of pri-miR-96.

The data presented in this paper demonstrate the utility of conjugating bleomycin A5 to selective RNA-binding small molecules for the targeted degradation of disease-relevant RNAs and introduces novel methods for cellular profiling and target engagement validation using these compounds.

Open Access Article. Published on 25 September 2020. Downloaded on 8/9/2025 2:37:59 AM. This article is licensed under a Creative Commons Attribution-NonCommercial 3.0 Unported Licence.

10.3 Cugamycin: Targeted cleavage of r(CUG)^{exp} by a small molecule–bleomycin A5 conjugate

Small molecule–bleomycin A5 conjugates can be used to target structured RNAs other than miRNAs. For example, another class of important RNA targets is the hairpin structures characteristic to microsatellite/repeat expansion disorders. The dimeric compound **2H-K4NMeS**, described above, that reverses DM1-associated defects was appended with bleomycin A5 to yield the small molecule cleaver, **Cugamycin** (Fig. 16C and Table S1, ESI†).[181] *In vitro* binding studies demonstrated **Cugamycin**'s selectivity for r(CUG)^{exp} (EC_{50} = 365 nM) over DNA, and cleavage studies confirmed bleomycin A5′s reduction in affinity for DNA when conjugated to an RNA-binding small molecule, as DNA cleavage was reduced by 4-fold as compared to bleomycin A5 (Table S1, ESI†).[181]

In DM1 patient-derived myotubes, **Cugamycin** localized to the nucleus and cleaved ~70% of r(CUG)^{exp}-containing *DMPK* transcripts (dosed at 1 μM), while having no effect on wild-type *DMPK* transcripts that contain only a few r(CUG) repeats (non-pathogenic).[181] Further, **Cugamycin** demonstrated allele selectivity; that is, it only cleaved the mutant *DMPK* allele (1300 repeats). In conjunction with this cleavage, **Cugamycin** rescued MBNL1-dependent alternative splicing by ~40%, leading to a ~30% reduction in MBNL1-r(CUG)^{exp} nuclear foci when treated at 1 μM. **Cugamycin** did not have an effect on NOVA-mediated splicing, indicating selectivity for the r(CUG)^{exp} target.[181] Additionally, selectivity was profiled by measuring cleavage of five additional mRNAs that contain short r(CUG) repeats (<20 repeats). All five transcripts were unaffected by **Cugamycin** treatment.[181] Of note, an antisense LNA gap-mer complementary to r(CUG)^{exp} reduced the levels of all five r(CUG) repeat-containing mRNAs, as well as wild-type *DMPK* levels.[181] Modeling of RNA structures present in these mRNAs, as well as r(CUG)^{exp}, indicated the hairpin structure adopted by r(CUG)^{exp} is not recapitulated by shorter repeat lengths, bolstering the notion that structure-binding small molecules can indeed be selective in patient-derived cells and that selectivity translates *in vivo* (discussed below).

Off-target DNA cleavage in DM1 myotubes was assessed by visualizing γ-H2AX foci after treatment with **Cugamycin**, a control compound lacking the RNA-binding modules, or bleomycin A5, all tested at concentrations at which **Cugamycin** cleaved r(CUG)^{exp} and improved DM1-associated defects. Both the control compound and bleomycin A5 caused formation of γ-H2AX foci, while **Cugamycin** had no effect.[181] This again demonstrates that conjugation of bleomycin A5 through its C-terminal amine ablated affinity for DNA.

Cugamycin was also tested *in vivo* using the *HSA*^{LR} mouse model of DM1.[181] This model contains 250 CTG repeats driven by the human skeletal actin (*HSA*) promoter and recapitulates DM1 disease phenotypes such as dysregulation of MBNL1-dependent splicing, loss of the muscle-specific chloride ion channel (CLCN1), and myotonia.[182,183] **Cugamycin** was *i.p.* injected every other day, at a dose of 10 mg kg^{-1}, for a total of 8 days. After treatment, an ~40% reduction in the levels of the *HSA* transgene [r(CUG)$_{250}$] was observed in tibialis anterior (TA) and gastrocnemius muscles, indicating that **Cugamycin** engaged its RNA target *in vivo*.[181] Lung fibrosis, a common side effect of bleomycin,[184] was not observed with **Cugamycin** treatment.

Rescue of aberrant alternative splicing in the TA and gastrocnemius muscles were also studied upon treatment with **Cugamycin**, showing that MBNL1-dependent splicing events *Mbnl1* exon 7 and *Clcn1* exon 7A were rescued by ~50%, while alternative splicing of integrin β-1 precursor (*Itgb1*) exon 17 and capping actin protein of muscle *z*-line subunit β (*Capzb*) exon 8, non MBNL1-dependent events, were unaffected.[181] Loss of the CLCN1 protein, due to aberrant alternative splicing and exon 7A inclusion contributes directly to myotonia.[183] Therefore, recuse of MBNL1-dependent splicing should increase CLCN1 protein expression on the cell surface, leading to a rescue of disease phenotype. Indeed, upon **Cugamycin** treatment, the levels of CLCN1 in TA muscle plasma membranes increased and an ~40% reduction in myotonia was observed.[181] These results were consistent across TA, gastrocnemius, and quadriceps muscles, indicating **Cugamycin** reaches DM1-affected tissues and rescues disease-associated phenotypes broadly.

Interestingly, **Cugamycin**'s parent compound, **2H-K4NMeS**, when delivered at the same dose and route of administration was unable to rescue MBNL1-dependent splicing or myotonia, indicating the cleavage capacity of **Cugamycin** is essential for *in vivo* efficacy.[181] These data also suggest that a cleavage-driven mechanism of action can provide a more prolonged and potent effect *in vivo* than a simple binding mode of action.

The ability of **Cugamycin** to rescue MBNL1-associated alternative splicing defects broadly and selectively was assessed by transcriptome-wide analysis of splicing events. By comparison to wild-type mice, the extent of the dysregulation of each splicing event in *HSA*^{LR} was measured. Angelbello *et al.*[181] identified 138 exons that are deregulated, reported as percent spliced in (Ψ), using mixture of isoforms (MISO)[185] analysis. Of these 138 exons, 134 of them showed Ψ values shifted back towards wild-type upon treatment with **Cugamycin**.[181] These data indicate that through **Cugamycin**'s selective recognition of r(CUG)^{exp}, the compound was able to globally rescue aberrant MBNL1-dependent alternative splicing in a mouse model of DM1. In addition to changes in alternative splicing, transcriptomic changes are also observed in DM1 mice. In particular, 326 genes are significantly dysregulated in *HSA*^{LR} mice.[181] Treatment with **Cugamycin** resulted in rescue of expression of 177 of these genes, highlighting the ability of the compound to normalize the transcriptome.[181] **Cugamycin** had no effect on the transcriptome of wild-type mice, as measured by RNA-seq, again highlighting the selectivity of this small molecule cleaver compound.

This study validated the strategy of using a small molecule-bleomycin A5 conjugate, **Cugamycin**, to target and cleave RNA repeats selectively in microsatellite/repeat expansion disorders, including in preclinical mouse models. **Cugamycin** showed remarkable potency *in vitro* and rescued DM1-associated phenotypes both in cells and *in vivo*. Additionally, the compound showed high selectivity for the *DMPK* mutant allele harboring r(CUG)^{exp} and demonstrated the ability to rescue MBNL1-dependent alternative

 This journal is © The Royal Society of Chemistry 2020

Open Access Article. Published on 25 September 2020. Downloaded on 8/9/2025 2:37:59 AM. This article is licensed under a Creative Commons Attribution-NonCommercial 3.0 Unported Licence.

splicing transcriptome-wide with no significant off-targets. The data presented in this study indicate the cleavage-mediated mechanism of action of **Cugamycin** is highly effective at rescuing DM1-associated disease phenotypes in a mouse model, suggesting **Cugamycin** is a strong lead candidate for further optimization into a preclinical compound.

10.4 Targeted cleavage of r(CCUG)^{exp} by a small molecule-bleomycin A5 conjugate

After the success observed with **Cugamycin**, a small molecule-bleomycin A5 conjugate was created to target the r(CCUG)^{exp} in intron 1 of *CNBP*, causative of DM2.[139] Building off a previously designer dimer (**5**)[139] (discussed in Sections 6.2 and 7), Benhamou *et al.*[139] conjugated bleomycin A5 through the natural product's C-terminal amine to afford **5-Bleo** (Table S1, ESI†). *In vitro* studies showed **5** and **5-Bleo** bind r(CCUG)$_{10}$ with similar affinities (~100 nM) and that **5-Bleo** cleaved RNA between 5′-GC steps in base paired regions adjacent to the compound's binding site (Fig. 16C and Table S1, ESI†).[139] This compound also demonstrated selectivity for the RNA target over DNA, consistent with the results from previous bleomycin A5 conjugates.[139,181]

While the dimer and cleaver compounds display similar binding affinities for r(CCUG)^{exp} (~100 nM) *in vitro*, in DM2 fibroblasts the cleaver reduced levels of intron 1-containing r(CCUG)^{exp} transcripts by an ~2.5-fold greater extent than the dimer, the binding of which shunts the intron down endogenous decay pathways (*i.e.*, has a different mode of action).[139] Mature *CNBP* mRNA levels were also reduced upon treatment of **5-Bleo**. Thus, the bleomycin A5 conjugate was able to more effectively reduce levels of mutant *CNBP* mRNA, compared to the binder, and cleaves the r(CCUG)^{exp} target. Off-target DNA cleavage was again assessed by visualizing the formation of γ-H2AX foci in DM2 fibroblasts. Treatment with **5-Bleo** did not result in a significant increase in foci at the active concentration, demonstrating the compound's selectivity *in cellulis*.[139]

Target engagement of **5-Bleo** was confirmed in cells using a competitive cleavage assay in which increasing concentrations of the dimer were co-treated with a constant concentration of **5-Bleo** and the levels of mature *CNBP* mRNA were measured. Increasing the concentration of the simple binding dimer led to an increase in *CNBP* mRNA levels (a reduction in cleavage), indicating **5-Bleo** and the dimer share the same RNA target and that the mechanism of **5-Bleo** is through direct cleavage of r(CCUG)^{exp}.[139]

Further cellular studies demonstrated **5-Bleo**'s enhanced ability to rescue MBNL1-dependent *IR* pre-mRNA splicing defects compared to the dimer. **5-Bleo** rescued splicing by ~50% at 5 μM, while the dimer only rescued splicing defects by ~20% at 10 μM, a 2-fold higher concentration.[139] Additionally, an ~50% reduction in r(CCUG)^{exp}-containing foci was observed upon treatment of **5-Bleo**. Evaluation of mature *CNBP* mRNA levels and *IR* splicing in healthy fibroblasts after treatment with **5-Bleo** showed no changes, confirming **5-Bleo**'s allele selectivity for the disease-causing r(CCUG)^{exp} as the shorter r(CCUG) repeats present in healthy fibroblasts were unaffected.[139]

11. Targeted degradation of disease-causing RNAs using RIBOTACs

The advent of proteolysis targeting chimeras (PROTACs)[186] demonstrated the ability to trigger protein degradation with small molecules. This concept has been broadened to other biomolecules, such as RNAs, as is the case of RIBOTACs.[187] RIBOTACs mediate RNA decay by recruiting endogenous RNases to degrade specific transcripts. In particular, RIBOTACs have been developed that recruit RNase L, a component of the antiviral immune response. RNase L is present in minute quantities in all cells as an inactive monomer. Upon viral infection, it is upregulated, dimerized and activated by 2′–5′ oligoadenylate [2′–5′ poly(A)].[188] RNase L is thus an intriguing enzyme for small molecule recruitment and targeted RNA destruction. That is, an RNA-binding small molecule coupled to an RNase L-recruiting module could locally recruit and activate RNase L to cleave the target selectively, without activation of the immune system.

11.1 Targaprimir-96 RIBOTAC (TGP-96 RIBOTAC): Targeting pri-miR-96 for degradation

As previously described in Section 2.3 (''Design of Monomeric Small Molecules Targeting Disease-Causing miRNAs''), **TGP-96** is a dimeric small molecule that binds pri-miR-96 and inhibits its biogenesis, thereby derepressing the transcription factor FOXO1 and triggering apoptosis in TNBC cells.[47] **TGP-96** was converted into a RIBOTAC (**TGP-96 RIBOTAC**) by appending a short 2′–5′ A_4 oligonucleotide as the RNase L recruiting module onto the compound (Fig. 17 and Table S1, ESI†).[187] *In vitro* binding assays confirmed the recruiting module does not affect the avidity of the compound for pri-miR-96's Drosha processing site (K_d = 20 nM) (Table S1, ESI†).[187] *In vitro* cleavage assays demonstrated the ability of **TGP-96 RIBOTAC** to recruit and dimerize RNase L, leading to the selective cleavage of pri-miR-96.[187] This cleavage was inhibited when **TGP-96** was added as a competitor, validating the binding sites of **TGP-96** and **TGP-96 RIBOTAC** are the same.

In MDA-MB-231 cells, despite having ~2-fold reduced cellular permeability compared to **TGP-96**, **TGP-96 RIBOTAC** reduced the levels of pri-miR-96 and mature miR-96, confirming compound mode of action.[187] RNase L-dependent cleavage was verified in multiple experiments: (i) immunoprecipitation with an RNase L antibody confirmed ternary complex formation between pri-miR-96, RNase L, and **TGP-96 RIBOTAC**; (ii) competitive cleavage between **TGP-96 RIBOTAC** and a derivative lacking the RNase L-recruiting module showed a dose-dependent decrease in cleavage of pri-miR-96, validating the ability of **TGP-96 RIBOTAC** to locally dimerize RNase L; and (iii) siRNA knockdown of RNase L ablated **TGP-96 RIBOTAC**'s ability to degrade pri-miR-96.[187]

Treatment of **TGP-96 RIBOTAC** in MDA-MB-231 cells resulted in modulation of the invasive phenotype associated with miR-96 in cancer. An ~2-fold increase in FOXO1 expression was observed upon treatment, consistent with inhibition of miR-96 biogenesis, and thus resulted in apoptosis.[187] This effect can be reversed upon over expression of pri-miR-96.

Open Access Article. Published on 25 September 2020. Downloaded on 8/9/2025 2:37:59 AM.
This article is licensed under a Creative Commons Attribution-NonCommercial 3.0 Unported Licence.

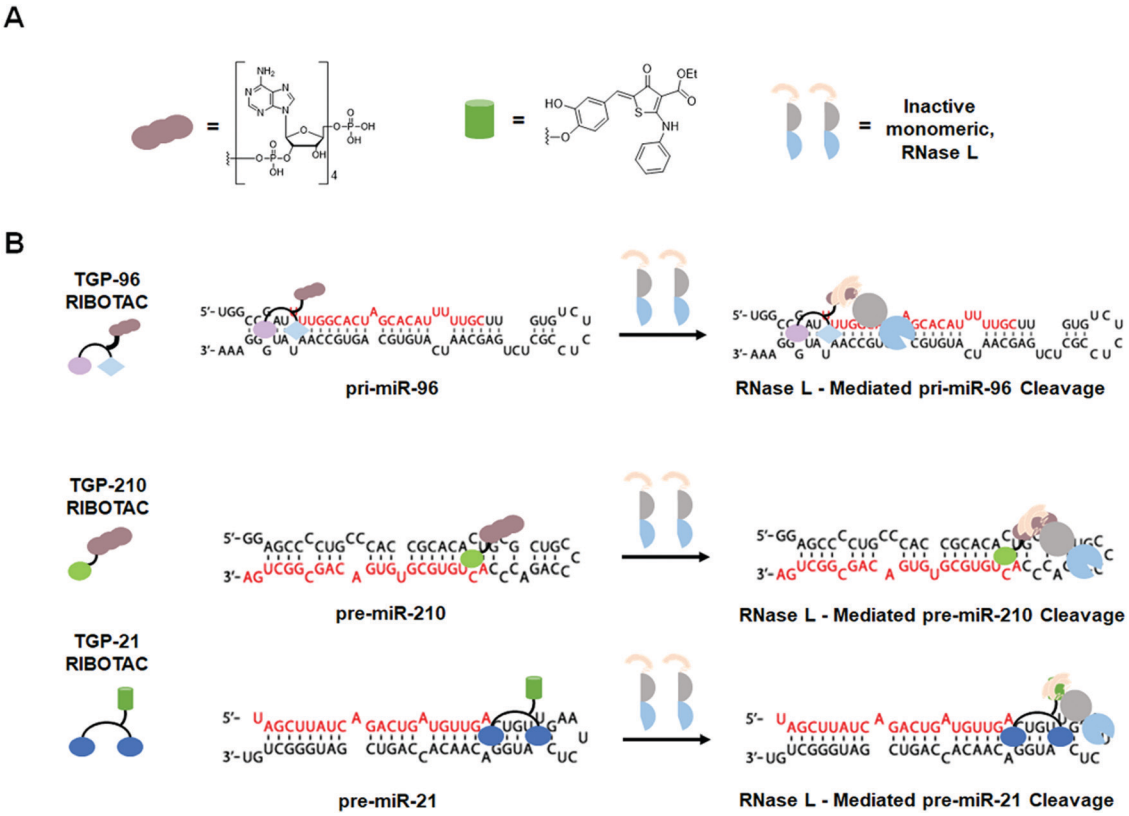

Fig. 17 Ribonuclease targeting chimeras (RIBOTACs) degrade disease-causing RNAs in a targeted manner. (A) Structures of first- and second-generation RNase L recruiting modules and schematized monomeric RNase L. (B) RIBOTAC-mediated degradation of oncogenic pri-miR-96, pre-miR-210, and pre-miR-21.

TGP-96 RIBOTAC has no effect on apoptosis in MCF-10a cells (healthy breast epithelial cells).[187] Further, **TGP-96 RIBOTAC** stimulated apoptosis to the same extent as its parent binding compound at a 2.5-fold lower dose. Combined with the decreased uptake of the compound, RNase L recruitment by **TGP-96 RIBOTAC** enhances the compound's activity by ~5-fold compared to **TGP-96**.[187] Most importantly, **TGP-96 RIBOTAC** acts catalytically and in a substoichiometric fashion to recruit RNase L for targeted RNA degradation, cleaving 3.1 pri-miR-96 molecules per molecule of RIBOTAC.[187]

11.2 Targapremir-210 RIBOTAC (TGP-210 RIBOTAC): Targeting pre-miR-210 for degradation

As discussed in Section 2.3 ("Design of Monomeric Small Molecules Targeting Disease-Causing miRNAs"), **TGP-210**, designed by Inforna, binds the Dicer processing site of pre-miR-210, inhibits its biogenesis and normalizes proteins in this circuit, ultimately inducing apoptosis in hypoxic cancer cells.[45] Costales *et al.*[189] optimized **TGP-210** by appending a 2′–5′ A_4 RNase L recruiting module to yield **TGP-210 RIBOTAC** (Fig. 17 and Table S1, ESI†). *In vitro* cleavage assays showed **TGP-210 RIBOTAC** cleaved pre-miR-210 and binding assays demonstrated **TGP-210 RIBOTAC** is more selective than **TGP-210**; an ~10-fold difference in affinity is observed between the Dicer processing site of pre-miR-210 and DNA while only an ~5-fold difference was observed for **TGP-210** (Table S1, ESI†).[189] Thus RNA degraders can show enhanced selectivity over their simple binding counterparts.

In hypoxic MDA-MB-231 cells, **TGP-210 RIBOTAC** decreased the levels of both pre-miR-210 and mature miR-210, consistent with its mode of action.[189] Upon treatment with **TGP-210 RIBOTAC**, *GPD1L* mRNA levels were significantly increased and *HIF1α* mRNA levels were decreased.[189] As a result of deactivation of the oncogenic circuit, **TGP-210 RIBOTAC** triggered apoptosis in hypoxic cancer cells, to a similar extent as **TGP-210**. However, because **TGP-210 RIBOTAC** is half as cell permeable as **TGP-210**, these results demonstrate the RIBOTAC has ~2-fold enhanced activity over **TGP-210**.[189]

Specific RNase L recruitment was confirmed *via*: (i) competitive cleavage assays, in which co-treatment of increasing amounts of **TGP-210** with **TGP-210 RIBOTAC** resulted in a dose-dependent decrease in pre-miR-210 cleavage; (ii) overexpression of RNase L, resulting in increased cleavage; (iii) overexpression of pre-miR-210, resulting in decreased cleavage; and (iv) siRNA ablation of RNase L, resulting in no **TGP-210 RIBOTAC**-mediated cleavage of pre-miR-210.[189] Additionally, immunoprecipitation of RNase L showed enrichment for pre-miR-210 only in cells treated with **TGP-210 RIBOTAC**.

RNA-seq and RT-qPCR profiling experiments revealed **TGP-210 RIBOTAC** has no significant off-targets trancriptome-wide (Table S1, ESI†).[189] Combined with its catalytic and substoichiometric mode of action, **TGP-210 RIBOTAC** demonstrates

 This journal is © The Royal Society of Chemistry 2020

Open Access Article. Published on 25 September 2020. Downloaded on 8/9/2025 2:37:59 AM. This article is licensed under a Creative Commons Attribution-NonCommercial 3.0 Unported Licence.

that enhanced activity and selectivity can be achieved through the targeted recruitment of nucleases *via* RIBOTAC compounds.

11.3 Targapremir-21 RIBOTAC (TGP-21 RIBOTAC): Targeting pre-miR-21 for degradation

A RIBOTAC targeting pre-miR-21, dubbed **TGP-21 RIBOTAC**, was recently reported that is based on the dimeric binding compound **TGP-21** (Table S1, ESI†).[190] **TGP-21** was first validated in MDA-MB-231 TNBC cells, reducing levels of mature miR-21 and increasing levels of pre-miR-21, in accordance with its mechanism of inhibiting Dicer processing (Table S1, ESI†).[190] The binding dimer also increased expression of programmed cell death protein 4 (PDCD4) and phosphatase and tension homolog (PTEN), two proteins that are translationally repressed by miR-21.[190] Additionally, invasion assays confirmed **TGP-21**'s ability to inhibit the invasive phenotype of MDA-MB-231 cells.[190]

TGP-21 was optimized by appending a heterocyclic small molecule recruiter of RNase L to create **TGP-21 RIBOTAC** (Fig. 17 and Table S1, ESI†). Previous studies by Thakur *et al.*[191] demonstrated the ability of a heterocyclic small molecule to recruit and activate RNase L in place of the traditional 2′–5′ poly(A) substrate. Extensive optimization of this structure by Costales *et al.*[190] yielded the small molecule RNase L-recruiting heterocycle that was incorporated in **TGP-21 RIBOTAC**.

In MDA-MB-231 cells, **TGP-21 RIBOTAC** showed a 20-fold enhancement in activity for reducing mature miR-21 levels compared to **TGP-21** and reduced pre-miR-21 levels in a substoichiometric manner (Table S1, ESI†).[190] RNase L recruitment was confirmed using the same assays as described for **TGP-210 RIBOTAC**, further supporting the mechanism of small molecule-targeted degradation.[190] A time course experiment in which reduction of mature miR-21 levels were monitored up to 96 h post-treatment revealed **TGP-21 RIBOTAC** has a more potent and prolonged effect than **TGP-21**.[190]

Importantly, **TGP-21 RIBOTAC** did not trigger an innate immune response, as monitored by mRNA and protein levels of innate immunity-associated biomarkers.[190] In contrast, transfection of 2′–5′ A_4 into MDA-MB-231 cells resulted in upregulation of several innate immunity biomarkers, such as interferon gamma (IFN-γ), 2′–5′-oligoadenylate synthase 1 (OAS1), retinoic acid-inducible gene 1 (RIG-1), and melanoma differentiation-associated protein 5 (MDA5).[190] These results support the hypothesis that **TGP-21 RIBOTAC** locally recruits and activates RNase L, instead of triggering a global antiviral innate immune response.[190]

Selectivity was also assessed miRNome-wide and quantified by calculating Gini coefficients. Gini coefficients were first introduced as a metric of biological selectivity by *Graczyk*[192] as a measure of kinase inhibitor selectivity, however the metric can be broadly applied to any biomolecule and small molecule modulator. A Gini coefficient of 0 represents a nonselective compound while a Gini coefficient of 1 represents an exquisitely selective compound. Gini coefficients for the monomer that comprises **TGP-21**, **TGP-21**, and **TGP-21 RIBOTAC**, by measuring their effects on the miRNome, are 0.52, 0.68, and 0.84 respectively, highlighting the increase in selectivity that is achieved by dimerization and by RNase L-mediated targeted degradation of RNA.[190] Proteome-wide analysis of the effects of **TGP-21 RIBOTAC** in MDA-MB-231 cells confirmed the selectivity of the compound with only 47 of 4181 proteins being significantly affected.[190]

TGP-21 RIBOTAC was also evaluated *in vivo* in a mouse model of metastatic breast cancer (NOD/SCID mice *i.v.* injected with MDA-MB-231-Luc cells). Treatment with **TGP-21 RIBOTAC** (10 mg kg^{-1}, every other day for 6 weeks) inhibited metastasis to lung, as evident by a significant decrease in the number of lung nodules present in **TGP-21 RIBOTAC**-treated mice.[190] Additionally, tissues from mice in the RIBOTAC treatment group displayed decreased hematoxylin and eosin (H&E) staining, decreased pre-miR-21 and mature miR-21 levels (as assayed by FISH and RT-qPCR), and increased levels of PDCD4 (as assayed by immunohistochemistry).[190] Thus, **TGP-21 RIBOTAC** selectivity and potently modulates the miR-21 pathway in a preclinical mouse model, resulting in inhibition of breast cancer metastasis.

12. Case study: direct comparison of bleomycin A5-mediated cleavage *versus* RNase L-mediated degradation of the pri-miR-17-92 cluster

The pri-miR-17-92 cluster is a direct target of the transcription factor c-MYC[193] and is upregulated in human diseases ranging from cancers[194–196] to fibrosis.[197] For each disease, the mature miRNA deregulated from the cluster and its downstream effects can be unique or overlap,[198] and the mature miRNAs can act either individually or synergistically to affect disease biology.[193,199] Through the use of Inforna and subsequent optimization steps, Liu *et al.*[200] developed a dimeric small molecule that binds to three miRNAs in the pri-miR-17-92 cluster (miR-17, miR-18a, and miR-20a) that share structural commonalities at and adjacent to their Dicer processing sites. They then appended the small molecule with either bleomycin A5, yielding **Targaprimir-17-92 Bleo** (**TGP-17-92 Bleo**) or the heterocyclic RNase L-recruiting module, yielding **TGP-17-92 RIBOTAC** (Fig. 16D and Table S1, ESI†).[200] The ability of these two compounds to reduce levels of pri-miR-17-92 was evaluated in MDA-MB-231 TNBC cells and DU-145 prostate cancer cells.[200] **TGP-17-92 Bleo** reduced pri-miR-17-92 levels and hence functionally inhibited all six miRNAs it encodes (Table S1, ESI†). Further, pre-miR17, pre-miR-18a, and pre-miR-20a levels were reduced. Cleavage of the cluster and the three pre-miRNAs that **TGP-17-92 Bleo** binds is consistent with the compound's cellular localization. In contrast, **TGP-17-92 RIBOTAC** only reduced levels of pre-miR17, pre-miR-18a, and pre-miR-20a and their mature miRNAs while not affecting the primary transcript (Table S1, ESI†).[200] That is, the RIBOTAC only cleaved the pre-miRNAs that bind **TGP-17-92** because of the co-localization of the RIBOTAC, RNase L, and the pre-miRNA, the three components required for cleavage, in the cytoplasm.[200] Thus, these

Open Access Article. Published on 25 September 2020. Downloaded on 8/9/2025 2:37:59 AM.
This article is licensed under a Creative Commons Attribution-NonCommercial 3.0 Unported Licence.

studies devised a facile design strategy to remove an entire pri-miRNA cluster, of importance since ~25% of all miRNAs are transcribed in clusters, or individual members of the cluster simply by careful selection of the cleavage module and by exploiting differences in cellular localization.

13. Conclusion

As this review showcases, various types of RNAs have been successfully targeted with small molecules including miRNAs, lncRNAs, splicing modifiers, repeat expansion disorders, and structured elements found within disease-causing RNAs. Since only 1–2% of the genome is translated into protein but ~80% is transcribed into RNA, it is not surprising that RNA is rapidly emerging as a promising target of small molecule therapeutics.[3,18,201] As illustrated by the examples discussed herein, RNA-targeting small molecules can display impressive potency (nM) and selectivity for their RNA targets, often rivaling those seen with traditional protein-targeting small molecules.

Current chemotherapeutic options come with a myriad of side-effects due to off-target effects of the drug. However, compounds such as **TGP-96 RIBOTAC**, **TGP-210 RIBOTAC**, **TGP-21 RIBOTAC** and **TGP-17-92 Bleo** demonstrate proteome- and transcriptome-wide selectivity while decreasing levels of oncogenic miRs. Thus, these compounds could offer a starting place for the development of novel anti-cancer treatments with fewer side effects.

In addition, this review highlights several RNA-targeting small molecules that affect neurodegenerative disease biology, further highlighting the potential of these small molecules to act as novel therapeutics. More importantly, RNA-targeting small molecules have unlocked therapeutic avenues against proteins of neurological relevance that were traditionally viewed as ''undruggable,'' such as the case of **Synucleozid** for α-synuclein and **A-5** for tau. Examples such as these highlight the importance of targeting RNA over traditional protein targets as a means of investigating the vast space of disease biology that has remained elusive to drug development. Additionally, RNA cleavers and degraders, such as bleomycin A5-conjugates and RIBOTACs, offer novel therapeutic modalities to reduce levels of disease-causing RNAs, whether oncogenic or neurodegenerative, further expanding the types of diseases that can be targeted with small molecules.

In comparison to antisense oligonucleotide (ASO) technology, the current leading therapeutic option for targeting RNA, small molecules are an attractive alternative due to their synthetic accessibility, on- and off-target optimization *via* structure–activity relationships, mode of action, and ease of administration. ASOs recognize RNA sequence, while small molecules recognize RNA structure; this essential difference gives small molecules many advantages over ASOs. For example, ASOs targeting repeat expansion disorders are often designed to target the coding region of the gene harboring the expansion, not the expansion itself due to off-target effects on transcripts that contain short repeats.[43,139,181] Thus, ASOs have to be specifically designed for each disease, even if the diseases are caused by the same RNA repeat expansion. In contrast, a single small molecule recognizing a disease-causing structure could be a potential treatment for all diseases that harbor the same repeat expansion. For example, DM1, Fuchs endothelial corneal dystrophy (FECD),[202] and Huntington's disease-like 2 (HDL-2)[203] are all caused by r(CUG)^{exp}. Therefore, small molecules targeting r(CUG)^{exp} could be applied broadly across these diseases as shorter, non-pathogenic repeats found in other transcripts typically lack structure. Another advantage of small molecules over ASOs is the route of therapeutic administration. ASOs are injected intrathecally, a painful and sometimes dangerous procedure for patients to endure. However, RNA-targeting small molecules have shown efficacy in mouse models with intraperitoneal injection[181] and success with oral bioavailability in clinical trials.[96]

Looking at the various classification of RNA-targeting small molecules that have emerged it is interesting to note the differences in affinity and bioactivity that result from appending bleomycin A5 or an RNase L-recruiting module to simple RNA-binding small molecules. While the conjugates tend to decrease the compounds' binding affinities for the target RNA, the overall biological effect observed upon treatment with the cleaving/degrading compounds far exceeds that of the simple RNA binder (Table S1, ESI†). This is demonstrated in the case of **TGP-96** (K_d = 39 nM) and **TGP-96 Bleo** (K_d = 64 nM), where **TGP-96 Bleo** demonstrates a greater biological effect than **TGP-96**. This trend was also observed for **TGP-210** (K_d = 160 nM) *versus* **TGP-210 RIBOTAC** (K_d = 340 nM) and **2H-K4NMeS** (K_d = 12 nM) *versus* **Cugamycin**, the bleomycin conjugate of **2H-K4NMeS** (EC_{50} = 365 nM). In all of these cases, the small decrease in affinity that results from appending a cleaving or degrading module to the compound is made up for by the large increase in biological activity (up to 20-fold) due to target RNA ablation, rather than simple binding.

Selectivity is also improved when an RNA-binding small molecule is converted to either a RIBOTAC or bleomycin A5 conjugate. Again, looking at the case of **TGP-210** and **TGP-210 RIBOTAC**, converting the small molecule to a RIBOTAC resulted in an increase in the selectivity window over DNA from 5-fold with the RNA binder to 10-fold with the degrader, despite **TGP-210 RIBOTAC** having decreased affinity for pre-miR-210.[189] Additionally, appending bleomycin A5 to RNA-binding small molecules decreases both the affinity of bleomycin A5 and the RNA binder itself for DNA, further enhancing the compound's selectivity. Thus, RNA-targeting small molecules demonstrate a novel avenue for achieving highly selective RNA-centric therapeutics.

The field of RNA-targeting small molecules is still in its infancy, as such the only FDA-approved small molecules on the market are anti-bacterials (targeting bacterial RNA), noting that **risdiplam**, which targets an RNA–protein interface, recently received FDA approval for the treatment of SMA (approved August 7th, 2020).[97] Additionally, **branaplam** (Novartis)[204] is also undergoing a Phase II clinical trial for the treatment of SMA. Both **risdiplam** and **branaplam** are administered orally, further supporting the advantages of using small molecules to target RNA. Despite the lack of branded ''RNA-targeting''

 This journal is © The Royal Society of Chemistry 2020

Open Access Article. Published on 25 September 2020. Downloaded on 8/9/2025 2:37:59 AM. This article is licensed under a Creative Commons Attribution-NonCommercial 3.0 Unported Licence.

FDA-approved small molecules it is important to note that many protein-targeting FDA-approved drugs, such as kinase and topoisomerase inhibitors, have been found to also bind RNA as off-targets. Thus, the future is exciting for the field of RNA-targeted small molecule therapeutics and will undoubtedly contribute to the advancement of modern, precision medicines.

Conflicts of interest

Matthew D. Disney is a founder of Expansion Therapeutics.

References

1 X.-D. Fu, *Natl. Sci. Rev.*, 2014, **1**, 190–204.
2 C. M. Connelly, M. H. Moon and J. S. Schneekloth, *Cell Chem. Biol.*, 2016, **23**, 1077–1090.
3 T. A. Cooper, L. Wan and G. Dreyfuss, *Cell*, 2009, **136**, 777–793.
4 R. R. Breaker, *Cold Spring Harbor Perspect. Biol.*, 2018, **10**, a032797.
5 Z. A. Jaafar and J. S. Kieft, *Nat. Rev. Microbiol.*, 2019, **17**, 110–123.
6 A. Bugaut and S. Balasubramanian, *Nucleic Acids Res.*, 2012, **40**, 4727–4741.
7 L. A. Macfarlane and P. R. Murphy, *Curr. Genomics*, 2010, **11**, 537–561.
8 K. Leppek, R. Das and M. Barna, *Nat. Rev. Mol. Cell Biol.*, 2018, **19**, 158–174.
9 M. B. Warf and J. A. Berglund, *Trends Biochem. Sci.*, 2010, **35**, 169–178.
10 E. Buratti and F. E. Baralle, *Mol. Cell. Biol.*, 2004, **24**, 10505–10514.
11 A. J. Zaug and T. R. Cech, *Science*, 1986, **231**, 470–475.
12 B. C. Stark, R. Kole, E. J. Bowman and S. Altman, *Proc. Natl. Acad. Sci. U. S. A.*, 1978, **75**, 3717–3721.
13 E. A. Doherty and J. A. Doudna, *Annu. Rev. Biophys. Biomol. Struct.*, 2001, **30**, 457–475.
14 S. Müller, B. Appel, D. Balke, R. Hieronymus and C. Nübel, *F1000Research*, 2016, **5**, 1511.
15 Z. Huang, J. Shi, Y. Gao, C. Cui, S. Zhang, J. Li, Y. Zhou and Q. Cui, *Nucleic Acids Res.*, 2019, **47**, 1013–1017.
16 A. M. Ardekani and M. M. Naeini, *Avicenna J. Med. Biotechnol.*, 2010, **2**, 161–179.
17 V. Bernat and M. D. Disney, *Neuron*, 2015, **87**, 28–46.
18 M. D. Disney, *J. Am. Chem. Soc.*, 2019, **141**, 6776–6790.
19 X.-H. Liang, H. Sun, J. G. Nichols and S. T. Crooke, *Mol. Ther.*, 2017, **25**, 2075–2092.
20 A. Ursu, J. L. Childs-Disney, R. J. Andrews, C. A. O'Leary, S. M. Meyer, A. J. Angelbello, W. N. Moss and M. D. Disney, *Chem. Soc. Rev.*, 2020, DOI: 10.1039/D0CS00455C.
21 M. M. Chong, G. Zhang, S. Cheloufi, T. A. Neubert, G. J. Hannon and D. R. Littman, *Genes Dev.*, 2010, **24**, 1951–1960.
22 L. F. R. Gebert and I. J. MacRae, *Nat. Rev. Mol. Cell Biol.*, 2019, **20**, 21–37.
23 T. A. Rand, S. Petersen, F. Du and X. Wang, *Cell*, 2005, **123**, 621–629.
24 H. A. Meijer, Y. W. Kong, W. T. Lu, A. Wilczynska, R. V. Spriggs, S. W. Robinson, J. D. Godfrey, A. E. Willis and M. Bushell, *Science*, 2013, **340**, 82–85.
25 T. Fukaya, H. O. Iwakawa and Y. Tomari, *Mol. Cell*, 2014, **56**, 67–78.
26 A. Fukao, Y. Mishima, N. Takizawa, S. Oka, H. Imataka, J. Pelletier, N. Sonenberg, C. Thoma and T. Fujiwara, *Mol. Cell*, 2014, **56**, 79–89.
27 M. Selbach, B. Schwanhausser, N. Thierfelder, Z. Fang, R. Khanin and N. Rajewsky, *Nature*, 2008, **455**, 58–63.
28 S. Uhlmann, H. Mannsperger, J. D. Zhang, E. A. Horvat, C. Schmidt, M. Kublbeck, F. Henjes, A. Ward, U. Tschulena, K. Zweig, U. Korf, S. Wiemann and O. Sahin, *Mol. Syst. Biol.*, 2012, **8**, 570.
29 M. Esteller, *Nat. Rev. Genet.*, 2011, **12**, 861–874.
30 S. Lin and R. I. Gregory, *Nat. Rev. Cancer*, 2015, **15**, 321–333.
31 C. P. Bracken, H. S. Scott and G. J. Goodall, *Nat. Rev. Genet.*, 2016, **17**, 719–732. 31.
32 D. D. Vo, C. Staedel, L. Zehnacker, R. Benhida, F. Darfeuille and M. Duca, *ACS Chem. Biol.*, 2014, **9**, 711–721.
33 V. Malnuit, M. Duca and R. Benhida, *Org. Biomol. Chem.*, 2011, **9**, 326–336.
34 M. Duca, V. Malnuit, F. Barbault and R. Benhida, *Chem. Commun.*, 2010, **46**, 6162–6164.
35 D. D. Vo, T. P. Tran, C. Staedel, R. Benhida, F. Darfeuille, A. Di Giorgio and M. Duca, *Chem. – Eur. J.*, 2016, **22**, 5350–5362.
36 D. D. Vo, C. Becquart, T. P. A. Tran, A. Di Giorgio, F. Darfeuille, C. Staedel and M. Duca, *Org. Biomol. Chem.*, 2018, **16**, 6262–6274.
37 S. Kumar and S. Maiti, *Biochimie*, 2013, **95**, 1422–1431.
38 J. P. Joly, G. Mata, P. Eldin, L. Briant, F. Fontaine-Vive, M. Duca and R. Benhida, *Chem. – Eur. J.*, 2014, **20**, 2071–2079.
39 C. Staedel, T. P. A. Tran, J. Giraud, F. Darfeuille, A. Di Giorgio, N. J. Tourasse, F. Salin, P. Uriac and M. Duca, *Sci. Rep.*, 2018, **8**, 1667.
40 C. Becquart, M. Le Roch, S. Azoulay, P. Uriac, A. Di Giorgio and M. Duca, *ACS Omega*, 2018, **3**, 16500–16508.
41 M. D. Disney, A. M. Winkelsas, S. P. Velagapudi, M. Southern, M. Fallahi and J. L. Childs-Disney, *ACS Chem. Biol.*, 2016, **11**, 1720–1728.
42 S. P. Velagapudi, Y. Luo, T. Tran, H. S. Haniff, Y. Nakai, M. Fallahi, G. J. Martinez, J. L. Childs-Disney and M. D. Disney, *ACS Cent. Sci.*, 2017, **3**, 205–216.
43 S. P. Velagapudi, S. M. Gallo and M. D. Disney, *Nat. Chem. Biol.*, 2014, **10**, 291–297.
44 I. K. Guttilla and B. A. White, *J. Biol. Chem.*, 2009, **284**, 23204–23216.
45 M. G. Costales, C. L. Haga, S. P. Velagapudi, J. L. Childs-Disney, D. G. Phinney and M. D. Disney, *J. Am. Chem. Soc.*, 2017, **139**, 3446–3455.
46 T. J. Kelly, A. L. Souza, C. B. Clish and P. Puigserver, *Mol. Cell. Biol.*, 2011, **31**, 2696–2706.
47 S. P. Velagapudi, M. D. Cameron, C. L. Haga, L. H. Rosenberg, M. Lafitte, D. R. Duckett, D. G. Phinney and

Open Access Article. Published on 25 September 2020. Downloaded on 8/9/2025 2:37:59 AM. This article is licensed under a Creative Commons Attribution-NonCommercial 3.0 Unported Licence.

M. D. Disney, *Proc. Natl. Acad. Sci. U. S. A.*, 2016, **113**, 5898–5903.
48 M. G. Costales, D. G. Hoch, D. Abegg, J. L. Childs-Disney, S. P. Velagapudi, A. Adibekian and M. D. Disney, *J. Am. Chem. Soc.*, 2019, **141**, 2960–2974.
49 H. Haniff, L. Knerr, X. Liu, G. Crynen, J. Boström, D. Abegg, A. Adibekian, M. Lemurell and M. Disney, *Nat. Chem.*, 2020, DOI: 10.1038/s41557-020-0514-4.
50 N. Ferrara, H. P. Gerber and J. LeCouter, *Nat. Med.*, 2003, **9**, 669–676.
51 N. Sun, B. Ning, K. M. Hansson, A. C. Bruce, S. A. Seaman, C. Zhang, M. Rikard, C. A. DeRosa, C. L. Fraser, M. Wagberg, R. Fritsche-Danielson, J. Wikstrom, K. R. Chien, A. Lundahl, M. Holtta, L. G. Carlsson, S. M. Peirce and S. Hu, *Sci. Rep.*, 2018, **8**, 17509.
52 S. Yla-Herttuala, T. T. Rissanen, I. Vajanto and J. Hartikainen, *J. Am. Coll. Cardiol.*, 2007, **49**, 1015–1026.
53 Z. Wen, W. Huang, Y. Feng, W. Cai, Y. Wang, X. Wang, J. Liang, M. Wani, J. Chen, P. Zhu, J. M. Chen, R. W. Millard, G. C. Fan and Y. Wang, *PLoS One*, 2014, **9**, 104666.
54 D. Joladarashi, V. N. S. Garikipati, R. A. Thandavarayan, S. K. Verma, A. R. Mackie, M. Khan, A. M. Gumpert, A. Bhimaraj, K. A. Youker, C. Uribe, S. Suresh Babu, P. Jeyabal, R. Kishore and P. Krishnamurthy, *J. Am. Coll. Cardiol.*, 2015, **66**, 2214–2226.
55 Z. Taimeh, J. Loughran, E. J. Birks and R. Bolli, *Nat. Rev. Cardiol.*, 2013, **10**, 519–530.
56 X. Guo, L. Gao, Y. Wang, D. K. Y. Chiu, T. Wang and Y. Deng, *Briefings Funct. Genomics*, 2015, **15**, 38–46.
57 F. Zhang, L. Zhang and C. Zhang, *Tumor Biol.*, 2016, **37**, 163–175.
58 C.-W. Wei, T. Luo, S.-S. Zou and A.-S. Wu, *Front. Behav. Neurosci.*, 2018, **12**, 348–358.
59 M. V. Neguembor, M. Jothi and D. Gabellini, *Skeletal Muscle*, 2014, **4**, 8.
60 S. Dahariya, I. Paddibhatla, S. Kumar, S. Raghuwanshi, A. Pallepati and R. K. Gutti, *Mol. Immunol.*, 2019, **112**, 82–92.
61 J. Chen, L. Ao and J. Yang, *Ann. Transl. Med.*, 2019, **7**, 494.
62 M. J. Delás and G. J. Hannon, *Open Biol.*, 2017, **7**, 170121.
63 R. Pedram Fatemi, S. Salah-Uddin, F. Modarresi, N. Khoury, C. Wahlestedt and M. A. Faghihi, *J. Biomol. Screening*, 2015, **20**, 1132–1141.
64 F. A. Abulwerdi, W. Xu, A. A. Ageeli, M. J. Yonkunas, G. Arun, H. Nam, J. S. Schneekloth, T. K. Dayie, D. Spector, N. Baird and S. F. J. Le Grice, *ACS Chem. Biol.*, 2019, **14**, 223–235.
65 N. F. Rizvi and E. B. Nickbarg, *Methods*, 2019, **167**, 28–38.
66 M. Hajjari and A. Salavaty, *Cancer Biol. Med.*, 2015, **12**, 1–9.
67 K. Zhang, X. Sun, X. Zhou, L. Han, L. Chen, Z. Shi, A. Zhang, M. Ye, Q. Wang, C. Liu, J. Wei, Y. Ren, J. Yang, J. Zhang, P. Pu, M. Li and C. Kang, *OncoTargets Ther.*, 2015, **6**, 537–546.
68 Y. Ren, Y.-F. Wang, J. Zhang, Q.-X. Wang, L. Han, M. Mei and C.-S. Kang, *Clin. Epigenet*, 2019, **11**, 29.
69 T. Gutschner, M. Hämmerle and S. Diederichs, *J. Mol. Med.*, 2013, **91**, 791–801.
70 R. Yoshimoto, A. Mayeda, M. Yoshida and S. Nakagawa, *Biochim. Biophys. Acta, Gene Regul. Mech.*, 2016, **1859**, 192–199.
71 C. Xu, M. Yang, J. Tian, X. Wang and Z. Li, *Int. J. Oncol.*, 2011, **39**, 169–175.
72 J. A. Brown, D. Bulkley, J. Wang, M. L. Valenstein, T. A. Yario, T. A. Steitz and J. A. Steitz, *Nat. Struct. Mol. Biol.*, 2014, **21**, 633–640.
73 J. E. Wilusz, C. K. JnBaptiste, L. Y. Lu, C.-D. Kuhn, L. Joshua-Tor and P. A. Sharp, *Genes Dev.*, 2012, **26**, 2392–2407.
74 A. Donlic, B. S. Morgan, J. L. Xu, A. Liu, C. Roble Jr. and A. E. Hargrove, *Angew. Chem., Int. Ed.*, 2018, **57**, 13242–13247.
75 W.-Y. Yang, R. Gao, M. Southern, P. S. Sarkar and M. D. Disney, *Nat. Commun.*, 2016, **7**, 11647.
76 J. B. Chaires, J. Ren, D. Hamelberg, A. Kumar, V. Pandya, D. W. Boykin and W. D. Wilson, *J. Med. Chem.*, 2004, **47**, 5729–5742.
77 D. Kumari, I. Gazy and K. Usdin, *Brain Sci.*, 2019, **9**, 39–57.
78 D. Colak, N. Zaninovic, M. S. Cohen, Z. Rosenwaks, W. Y. Yang, J. Gerhardt, M. D. Disney and S. R. Jaffrey, *Science*, 2014, **343**, 1002–1005.
79 M. D. Disney, B. Liu, W. Y. Yang, C. Sellier, T. Tran, N. Charlet-Berguerand and J. L. Childs-Disney, *ACS Chem. Biol.*, 2012, **7**, 1711–1718.
80 D. Kumari and K. Usdin, *Hum. Mol. Genet.*, 2016, **25**, 3689–3698.
81 P. Chiurazzi, M. G. Pomponi, R. Willemsen, B. A. Oostra and G. Neri, *Hum. Mol. Genet.*, 1998, **7**, 109–113.
82 B. Coffee, F. Zhang, S. T. Warren and D. Reines, *Nat. Genet.*, 1999, **22**, 98–101.
83 D. Kumari and K. Usdin, *Hum. Mol. Genet.*, 2014, **23**, 6575–6583.
84 Y. Lee and D. C. Rio, *Annu. Rev. Biochem.*, 2015, **84**, 291–323.
85 M. R. Lunn and C. H. Wang, *Lancet*, 2008, **371**, 2120–2133.
86 S. Lefebvre, L. Bürglen, S. Reboullet, O. Clermont, P. Burlet, L. Viollet, B. Benichou, C. Cruaud, P. Millasseau, M. Zeviani, D. Le Paslier, J. Frézal, D. Cohen, J. Weissenbach, A. Munnich and J. Melki, *Cell*, 1995, **80**, 155–165.
87 K. R. Brunden, J. Q. Trojanowski and V. M. Lee, *Nat. Rev. Drug Discovery*, 2009, **8**, 783–793.
88 M. Busslinger, N. Moschonas and R. A. Flavell, *Cell*, 1981, **27**, 289–298.
89 A. Shilo, F. A. Tosto, J. W. Rausch, S. F. J. Le Grice and T. Misteli, *Nucleic Acids Res.*, 2019, **47**, 5922–5935.
90 A. J. Bergsma, S. L. In't Groen, F. W. Verheijen, A. T. van der Ploeg and W. W. M. P. Pijnappel, *Mol. Ther. – Nucleic Acids*, 2016, **5**, 361.
91 C. F. Rochette, N. Gilbert and L. R. Simard, *Hum. Genet.*, 2001, **108**, 255–266.
92 C. L. Lorson, E. Hahnen, E. J. Androphy and B. Wirth, *Proc. Natl. Acad. Sci. U. S. A.*, 1999, **96**, 6307–6311.
93 B. G. Burnett, E. Muñoz, A. Tandon, D. Y. Kwon, C. J. Sumner and K. H. Fischbeck, *Mol. Cell. Biol.*, 2009, **29**, 1107–1115.

 This journal is © The Royal Society of Chemistry 2020

Open Access Article. Published on 25 September 2020. Downloaded on 8/9/2025 2:37:59 AM. This article is licensed under a Creative Commons Attribution-NonCommercial 3.0 Unported Licence.

94 T. Gidaro and L. Servais, *Dev. Med. Child Neurol.*, 2019, **61**, 19–24.
95 S. M. Hoy, *Drugs*, 2019, **79**, 1255–1262.
96 A. N. Calder, E. J. Androphy and K. J. Hodgetts, *J. Med. Chem.*, 2016, **59**, 10067–10083.
97 U.S. Food & Drug Administration, https://www.fda.gov/news-events/press-announcements/fda-approves-oral-treatment-spinal-muscular-atrophy, (accessed August 2020).
98 J. Palacino, S. E. Swalley, C. Song, A. K. Cheung, L. Shu, X. Zhang, M. Van Hoosear, Y. Shin, D. N. Chin, C. G. Keller, M. Beibel, N. A. Renaud, T. M. Smith, M. Salcius, X. Shi, M. Hild, R. Servais, M. Jain, L. Deng, C. Bullock, M. McLellan, S. Schuierer, L. Murphy, M. J. Blommers, C. Blaustein, F. Berenshteyn, A. Lacoste, J. R. Thomas, G. Roma, G. A. Michaud, B. S. Tseng, J. A. Porter, V. E. Myer, J. A. Tallarico, L. G. Hamann, D. Curtis, M. C. Fishman, W. F. Dietrich, N. A. Dales and R. Sivasankaran, *Nat. Chem. Biol.*, 2015, **11**, 511–517.
99 S. J. Kolb and J. T. Kissel, *Arch. Neurol.*, 2011, **68**, 979–984.
100 E. Goina, N. Skoko and F. Pagani, *Mol. Cell. Biol.*, 2008, **28**, 3850–3860.
101 D. A. Pomeranz Krummel, C. Oubridge, A. K. Leung, J. Li and K. Nagai, *Nature*, 2009, **458**, 475–480.
102 Y. Kondo, C. Oubridge, A. M. van Roon and K. Nagai, *eLife*, 2015, **4**, e04986.
103 S. Campagne, S. Boigner, S. Rudisser, A. Moursy, L. Gillioz, A. Knorlein, J. Hall, H. Ratni, A. Clery and F. H. Allain, *Nat. Chem. Biol.*, 2019, **15**, 1191–1198.
104 M. Sivaramakrishnan, K. D. McCarthy, S. Campagne, S. Huber, S. Meier, A. Augustin, T. Heckel, H. Meistermann, M. N. Hug, P. Birrer, A. Moursy, S. Khawaja, R. Schmucki, N. Berntenis, N. Giroud, S. Golling, M. Tzouros, B. Banfai, G. Duran-Pacheco, J. Lamerz, Y. Hsiu Liu, T. Luebbers, H. Ratni, M. Ebeling, A. Cléry, S. Paushkin, A. R. Krainer, F. H. Allain and F. Metzger, *Nat. Commun.*, 2017, **8**, 1476.
105 B. J. Blencowe, *Trends Biochem. Sci.*, 2000, **25**, 106–110.
106 A. Moursy, F. H. Allain and A. Cléry, *Nucleic Acids Res.*, 2014, **42**, 6659–6672.
107 J. Wang, P. G. Schultz and K. A. Johnson, *Proc. Natl. Acad. Sci. U. S. A.*, 2018, **115**, e4604–e4612.
108 N. N. Singh, R. N. Singh and E. J. Androphy, *Nucleic Acids Res.*, 2007, **35**, 371–389.
109 L. Debaize and M. B. Troadec, *Cell. Mol. Life Sci.*, 2019, **76**, 259–281.
110 P. Briata, D. Bordo, M. Puppo, F. Gorlero, M. Rossi, N. Perrone-Bizzozero and R. Gherzi, *Wiley Interdiscip. Rev.: RNA*, 2016, **7**, 227–240.
111 D. W. Cleveland, S. Y. Hwo and M. W. Kirschner, *J. Mol. Biol.*, 1977, **116**, 207–225.
112 M. Goedert, M. G. Spillantini, M. C. Potier, J. Ulrich and R. A. Crowther, *EMBO J.*, 1989, **8**, 393–399.
113 Q. Gao, J. Memmott, R. Lafyatis, S. Stamm, G. Screaton and A. Andreadis, *J. Neurochem.*, 2000, **74**, 490–500.
114 M. Hong, V. Zhukareva, V. Vogelsberg-Ragaglia, Z. Wszolek, L. Reed, B. I. Miller, D. H. Geschwind, T. D. Bird, D. McKeel, A. Goate, J. C. Morris, K. C. Wilhelmsen, G. D. Schellenberg, J. Q. Trojanowski and V. M. Lee, *Science*, 1998, **282**, 1914–1917.
115 A. Grover, H. Houlden, M. Baker, J. Adamson, J. Lewis, G. Prihar, S. Pickering-Brown, K. Duff and M. Hutton, *J. Biol. Chem.*, 1999, **274**, 15134–15143.
116 L. Varani, M. Hasegawa, M. G. Spillantini, M. J. Smith, J. R. Murrell, B. Ghetti, A. Klug, M. Goedert and G. Varani, *Proc. Natl. Acad. Sci. U. S. A.*, 1999, **96**, 8229–8234.
117 C. P. Donahue, C. Muratore, J. Y. Wu, K. S. Kosik and M. S. Wolfe, *J. Biol. Chem.*, 2006, **281**, 23302–23306.
118 S. Zheng, Y. Chen, C. P. Donahue, M. S. Wolfe and G. Varani, *Chem. Biol.*, 2009, **16**, 557–566.
119 Y. Liu, E. Peacey, J. Dickson, C. P. Donahue, S. Zheng, G. Varani and M. S. Wolfe, *J. Med. Chem.*, 2009, **52**, 6523–6526.
120 J. L. Chen, P. Zhang, M. Abe, H. Aikawa, L. Zhang, A. J. Frank, T. Zembryski, C. Hubbs, H. Park, J. Withka, C. Steppan, L. Rogers, S. Cabral, M. Pettersson, T. T. Wager, M. A. Fountain, G. Rumbaugh, J. L. Childs-Disney and M. D. Disney, *J. Am. Chem. Soc.*, 2020, **142**, 8706–8727.
121 Y. Luo and M. D. Disney, *ChemBioChem*, 2014, **15**, 2041–2044.
122 T. T. Wager, X. Hou, P. R. Verhoest and A. Villalobos, *ACS Chem. Neurosci.*, 2010, **1**, 435–449.
123 M. M. Scotti and M. S. Swanson, *Nat. Rev. Genet.*, 2016, **17**, 19–32.
124 G. Biamonti, A. Amato, E. Belloni, A. Di Matteo, L. Infantino, D. Pradella and C. Ghigna, *Aging: Clin. Exp. Res.*, 2019, DOI: 10.1007/s40520-019-01360-x.
125 M. Hecker, A. Rüge, E. Putscher, N. Boxberger, P. S. Rommer, B. Fitzner and U. K. Zettl, *Autoimmun. Rev.*, 2019, **18**, 721–732.
126 S. C. Lee and O. Abdel-Wahab, *Nat. Med.*, 2016, **22**, 976–986.
127 L. M. Urbanski, N. Leclair and O. Anczuków, *Wiley Interdiscip. Rev.: RNA*, 2018, **9**, e1476.
128 N. P. Mastroyiannopoulos, M. L. Feldman, J. B. Uney, M. S. Mahadevan and L. A. Phylactou, *EMBO Rep.*, 2005, **6**, 458–463.
129 J. L. Childs-Disney, J. Hoskins, S. G. Rzuczek, C. A. Thornton and M. D. Disney, *ACS Chem. Biol.*, 2012, **7**, 856–862.
130 S. G. Rzuczek, Y. Gao, Z. Z. Tang, C. A. Thornton, T. Kodadek and M. D. Disney, *ACS Chem. Biol.*, 2013, **8**, 2312–2321.
131 S. G. Rzuczek, L. A. Colgan, Y. Nakai, M. D. Cameron, D. Furling, R. Yasuda and M. D. Disney, *Nat. Chem. Biol.*, 2017, **13**, 188–193.
132 W. Y. Yang, H. D. Wilson, S. P. Velagapudi and M. D. Disney, *J. Am. Chem. Soc.*, 2015, **137**, 5336–5345.
133 J. F. Arambula, S. R. Ramisetty, A. M. Baranger and S. C. Zimmerman, *Proc. Natl. Acad. Sci. U. S. A.*, 2009, **106**, 16068–16073.
134 A. H. Jahromi, Y. Fu, K. A. Miller, L. Nguyen, L. M. Luu, A. M. Baranger and S. C. Zimmerman, *J. Med. Chem.*, 2013, **56**, 9471–9481.
135 L. M. Luu, L. Nguyen, S. Peng, J. Lee, H. Y. Lee, C. H. Wong, P. J. Hergenrother, H. Y. Chan and S. C. Zimmerman, *ChemMedChem*, 2016, **11**, 1428–1435.

Open Access Article. Published on 25 September 2020. Downloaded on 8/9/2025 2:37:59 AM.
This article is licensed under a Creative Commons Attribution-NonCommercial 3.0 Unported Licence.

136 J. Lee, Y. Bai, U. V. Chembazhi, S. Peng, K. Yum, L. M. Luu, L. D. Hagler, J. F. Serrano, H. Y. E. Chan, A. Kalsotra and S. C. Zimmerman, *Proc. Natl. Acad. Sci. U. S. A.*, 2019, **116**, 8709–8714.

137 J. Li, J. Matsumoto, L.-P. Bai, A. Murata, C. Dohno and K. Nakatani, *Chem. – Eur. J.*, 2016, **22**, 14881–14889.

138 M. M. Lee, A. Pushechnikov and M. D. Disney, *ACS Chem. Biol.*, 2009, **4**, 345–355.

139 R. I. Benhamou, A. J. Angelbello, R. J. Andrews, E. T. Wang, W. N. Moss and M. D. Disney, *ACS Chem. Biol.*, 2020, **15**, 485–493.

140 R. I. Benhamou, A. J. Angelbello, E. T. Wang and M. D. Disney, *Cell Chem. Biol.*, 2020, **27**, 223–231.

141 W. Y. Yang, F. He, R. L. Strack, S. Y. Oh, M. Frazer, S. R. Jaffrey, P. K. Todd and M. D. Disney, *ACS Chem. Biol.*, 2016, **11**, 2456–2465.

142 Z. Su, Y. J. Zhang, T. F. Gendron, P. O. Bauer, J. Chew, W. Y. Yang, E. Fostvedt, K. Jansen-West, V. V. Belzil, P. Desaro, A. Johnston, K. Overstreet, S. Y. Oh, P. K. Todd, J. D. Berry, M. E. Cudkowicz, B. F. Boeve, D. Dickson, M. K. Floeter, B. J. Traynor, C. Morelli, A. Ratti, V. Silani, R. Rademakers, R. H. Brown, J. D. Rothstein, K. B. Boylan, L. Petrucelli and M. D. Disney, *Neuron*, 2014, **83**, 1043–1050.

143 Z. F. Wang, A. Ursu, J. L. Childs-Disney, R. Guertler, W. Y. Yang, V. Bernat, S. G. Rzuczek, R. Fuerst, Y. J. Zhang, T. F. Gendron, I. Yildirim, B. G. Dwyer, J. E. Rice, L. Petrucelli and M. D. Disney, *Cell Chem. Biol.*, 2019, **26**, 179–190.

144 Ł. J. Sznajder, J. D. Thomas, E. M. Carrell, T. Reid, K. N. McFarland, J. D. Cleary, R. Oliveira, C. A. Nutter, K. Bhatt, K. Sobczak, T. Ashizawa, C. A. Thornton, L. P. W. Ranum and M. S. Swanson, *Proc. Natl. Acad. Sci. U. S. A.*, 2018, **115**, 4234–4239.

145 J. R. Hesselberth, *Wiley Interdiscip. Rev.: RNA*, 2013, **4**, 677–691.

146 P. E. Ash, K. F. Bieniek, T. F. Gendron, T. Caulfield, W. L. Lin, M. Dejesus-Hernandez, M. M. van Blitterswijk, K. Jansen-West, J. W. Paul, 3rd, R. Rademakers, K. B. Boylan, D. W. Dickson and L. Petrucelli, *Neuron*, 2013, **77**, 639–646.

147 T. F. Gendron, K. F. Bieniek, Y. J. Zhang, K. Jansen-West, P. E. Ash, T. Caulfield, L. Daughrity, J. H. Dunmore, M. Castanedes-Casey, J. Chew, D. M. Cosio, M. van Blitterswijk, W. C. Lee, R. Rademakers, K. B. Boylan, D. W. Dickson and L. Petrucelli, *Acta Neuropathol.*, 2013, **126**, 829–844.

148 K. Mori, T. Arzberger, F. A. Grasser, I. Gijselinck, S. May, K. Rentzsch, S. M. Weng, M. H. Schludi, J. van der Zee, M. Cruts, C. Van Broeckhoven, E. Kremmer, H. A. Kretzschmar, C. Haass and D. Edbauer, *Acta Neuropathol.*, 2013, **126**, 881–893.

149 T. Zu, B. Gibbens, N. S. Doty, M. Gomes-Pereira, A. Huguet, M. D. Stone, J. Margolis, M. Peterson, T. W. Markowski, M. A. C. Ingram, Z. Nan, C. Forster, W. C. Low, B. Schoser, N. V. Somia, H. B. Clark, S. Schmechel, P. B. Bitterman, G. Gourdon, M. S. Swanson, M. Moseley and L. P. W. Ranum, *Proc. Natl. Acad. Sci. U. S. A.*, 2011, **108**, 260–265.

150 P. K. Todd, S. Y. Oh, A. Krans, F. He, C. Sellier, M. Frazer, A. J. Renoux, K. C. Chen, K. M. Scaglione, V. Basrur, K. Elenitoba-Johnson, J. P. Vonsattel, E. D. Louis, M. A. Sutton, J. P. Taylor, R. E. Mills, N. Charlet-Berguerand and H. L. Paulson, *Neuron*, 2013, **78**, 440–455.

151 T. F. Gendron, V. V. Belzil, Y. J. Zhang and L. Petrucelli, *Acta Neuropathol.*, 2014, **127**, 359–376.

152 W.-Y. Yang, H. D. Wilson, S. P. Velagapudi and M. D. Disney, *J. Am. Chem. Soc.*, 2015, **137**, 5336–5345.

153 T. F. Gendron, J. Chew, J. N. Stankowski, L. R. Hayes, Y. J. Zhang, M. Prudencio, Y. Carlomagno, L. M. Daughrity, K. Jansen-West, E. A. Perkerson, A. O'Raw, C. Cook, L. Pregent, V. Belzil, M. van Blitterswijk, L. J. Tabassian, C. W. Lee, M. Yue, J. Tong, Y. Song, M. Castanedes-Casey, L. Rousseau, V. Phillips, D. W. Dickson, R. Rademakers, J. D. Fryer, B. K. Rush, O. Pedraza, A. M. Caputo, P. Desaro, C. Palmucci, A. Robertson, M. G. Heckman, N. N. Diehl, E. Wiggs, M. Tierney, L. Braun, J. Farren, D. Lacomis, S. Ladha, C. N. Fournier, L. F. McCluskey, L. B. Elman, J. B. Toledo, J. D. McBride, C. Tiloca, C. Morelli, B. Poletti, F. Solca, A. Prelle, J. Wuu, J. Jockel-Balsarotti, F. Rigo, C. Ambrose, A. Datta, W. Yang, D. Raitcheva, G. Antognetti, A. McCampbell, J. C. Van Swieten, B. L. Miller, A. L. Boxer, R. H. Brown, R. Bowser, T. M. Miller, J. Q. Trojanowski, M. Grossman, J. D. Berry, W. T. Hu, A. Ratti, B. J. Traynor, M. D. Disney, M. Benatar, V. Silani, J. D. Glass, M. K. Floeter, J. D. Rothstein, K. B. Boylan and L. Petrucelli, *Sci. Transl. Med.*, 2017, **9**, eaai7866.

154 T. F. Gendron, M. van Blitterswijk, K. F. Bieniek, L. M. Daughrity, J. Jiang, B. K. Rush, O. Pedraza, J. A. Lucas, M. E. Murray, P. Desaro, A. Robertson, K. Overstreet, C. S. Thomas, J. E. Crook, M. Castanedes-Casey, L. Rousseau, K. A. Josephs, J. E. Parisi, D. S. Knopman, R. C. Petersen, B. F. Boeve, N. R. Graff-Radford, R. Rademakers, C. Lagier-Tourenne, D. Edbauer, D. W. Cleveland, D. W. Dickson, L. Petrucelli and K. B. Boylan, *Acta Neuropathol.*, 2015, **130**, 559–573.

155 M. Clamp, B. Fry, M. Kamal, X. Xie, J. Cuff, M. F. Lin, M. Kellis, K. Lindblad-Toh and E. S. Lander, *Proc. Natl. Acad. Sci. U. S. A.*, 2007, **104**, 19428–19433.

156 A. Hopkins and C. Groom, *Nat. Rev. Drug Discovery*, 2002, **1**, 727–730.

157 C. V. Dang, E. P. Reddy, K. M. Shokat and L. Soucek, *Nat. Rev. Cancer*, 2017, **17**, 502–508.

158 J. Spiegel, P. M. Cromm, G. Zimmermann, T. N. Grossmann and H. Waldmann, *Nat. Chem. Biol.*, 2014, **10**, 613–622.

159 P. Zhang, H. J. Park, J. Zhang, E. Junn, R. J. Andrews, S. P. Velagapudi, D. Abegg, K. Vishnu, M. G. Costales, J. L. Childs-Disney, A. Adibekian, W. N. Moss, M. M. Mouradian and M. D. Disney, *Proc. Natl. Acad. Sci. U. S. A.*, 2020, **117**, 1457–1467.

160 V. M. Lee and J. Q. Trojanowski, *Neuron*, 2006, **51**, 33–38.

161 M. G. Spillantini, M. L. Schmidt, V. M.-Y. Lee, J. Q. Trojanowski, R. Jakes and M. Goedert, *Nature*, 1997, **388**, 839–840.

 This journal is © The Royal Society of Chemistry 2020

Open Access Article. Published on 25 September 2020. Downloaded on 8/9/2025 2:37:59 AM. This article is licensed under a Creative Commons Attribution-NonCommercial 3.0 Unported Licence.

162 K. C. Luk, V. Kehm, J. Carroll, B. Zhang, P. O'Brien, J. Q. Trojanowski and V. M.-Y. Lee, *Science*, 2012, **338**, 949–953.
163 A. B. Singleton, M. Farrer, J. Johnson, A. Singleton, S. Hague, J. Kachergus, M. Hulihan, T. Peuralinna, A. Dutra, R. Nussbaum, S. Lincoln, A. Crawley, M. Hanson, D. Maraganore, C. Adler, M. R. Cookson, M. Muenter, M. Baptista, D. Miller, J. Blancato, J. Hardy and K. Gwinn-Hardy, *Science*, 2003, **302**, 841.
164 E. Junn, K. W. Lee, B. S. Jeong, T. W. Chan, J. Y. Im and M. M. Mouradian, *Proc. Natl. Acad. Sci. U. S. A.*, 2009, **106**, 13052–13057.
165 D. M. Maraganore, *J. Mov. Disord.*, 2011, **4**, 1–7.
166 A. L. Friedlich, R. E. Tanzi and J. T. Rogers, *Mol. Psychiatry*, 2007, **12**, 222–223.
167 F. Febbraro, M. Giorgi, S. Caldarola, F. Loreni and M. Romero-Ramos, *NeuroReport*, 2012, **23**, 576–580.
168 J. L. Childs-Disney, T. Tran, B. R. Vummidi, S. P. Velagapudi, H. S. Haniff, Y. Matsumoto, G. Crynen, M. R. Southern, A. Biswas, Z. F. Wang, T. L. Tellinghuisen and M. D. Disney, *Chem*, 2018, **4**, 2384–2404.
169 J. R. Mazzulli, F. Zunke, O. Isacson, L. Studer and D. Krainc, *Proc. Natl. Acad. Sci. U. S. A.*, 2016, **113**, 1931–1936.
170 B. Liu, J. L. Childs-Disney, B. M. Znosko, D. Wang, M. Fallahi, S. M. Gallo and M. D. Disney, *BMC Bioinf.*, 2016, **17**, 112.
171 H. Pimentel, N. L. Bray, S. Puente, P. Melsted and L. Pachter, *Nat. Methods*, 2017, **14**, 687–690.
172 D. L. Boger and H. Cai, *Angew. Chem., Int. Ed.*, 1999, **38**, 448–476.
173 B. J. Carter, E. de Vroom, E. C. Long, G. A. van der Marel, J. H. van Boom and S. M. Hecht, *Proc. Natl. Acad. Sci. U. S. A.*, 1990, **87**, 9373–9377.
174 A. T. Abraham, J. J. Lin, D. L. Newton, S. Rybak and S. M. Hecht, *Chem. Biol.*, 2003, **10**, 45–52.
175 A. J. Angelbello and M. D. Disney, *ChemBioChem*, 2018, **19**, 43–47.
176 L. Ma, J. Teruya-Feldstein and R. A. Weinberg, *Nature*, 2007, **449**, 682–688.
177 Y. Li and M. D. Disney, *ACS Chem. Biol.*, 2018, **13**, 3065–3071.
178 Q. Ma, Z. Xu, B. R. Schroeder, W. Sun, F. Wei, S. Hashimoto, K. Konishi, C. J. Leitheiser and S. M. Hecht, *J. Am. Chem. Soc.*, 2007, **129**, 12439–12452.
179 Z.-D. Xu, M. Wang, S.-L. Xiao, C.-L. Liu and M. Yang, *Bioorg. Med. Chem. Lett.*, 2003, **13**, 2595–2599.
180 V. Agarwal, G. W. Bell, J.-W. Nam and D. P. Bartel, *eLife*, 2015, **4**, e05005.
181 A. J. Angelbello, S. G. Rzuczek, K. K. Mckee, J. L. Chen, H. Olafson, M. D. Cameron, W. N. Moss, E. T. Wang and M. D. Disney, *Proc. Natl. Acad. Sci. U. S. A.*, 2019, **116**, 7799–7804.
182 A. Mankodi, E. Logigian, L. Callahan, C. McClain, R. White, D. Henderson, M. Krym and C. A. Thornton, *Science*, 2000, **289**, 1769–1773.
183 A. Mankodi, M. P. Takahashi, H. Jiang, C. L. Beck, W. J. Bowers, R. T. Moxley, S. C. Cannon and C. A. Thornton, *Mol. Cell*, 2002, **10**, 35–44.
184 R. H. Blum, S. K. Carter and K. Agre, *Cancer*, 1973, **31**, 903–914.
185 Y. Katz, E. T. Wang, E. M. Airoldi and C. B. Burge, *Nat. Methods*, 2010, **7**, 1009–1015.
186 K. M. Sakamoto, K. B. Kim, A. Kumagai, F. Mercurio, C. M. Crews and R. J. Deshaies, *Proc. Natl. Acad. Sci. U. S. A.*, 2001, **98**, 8554–8559.
187 M. G. Costales, Y. Matsumoto, S. P. Velagapudi and M. D. Disney, *J. Am. Chem. Soc.*, 2018, **140**, 6741–6744.
188 R. H. Silverman, *J. Virol.*, 2007, **81**, 12720–12729.
189 M. G. Costales, B. Suresh, K. Vishnu and M. D. Disney, *Cell Chem. Biol.*, 2019, **26**, 1180–1186.
190 M. G. Costales, H. Aikawa, Y. Li, J. L. Childs-Disney, D. Abegg, D. G. Hoch, S. Pradeep Velagapudi, Y. Nakai, T. Khan, K. W. Wang, I. Yildirim, A. Adibekian, E. T. Wang and M. D. Disney, *Proc. Natl. Acad. Sci. U. S. A.*, 2020, **117**, 2406–2411.
191 C. S. Thakur, B. K. Jha, B. Dong, J. Das Gupta, K. M. Silverman, H. Mao, H. Sawai, A. O. Nakamura, A. K. Banerjee, A. Gudkov and R. H. Silverman, *Proc. Natl. Acad. Sci. U. S. A.*, 2007, **104**, 9585–9590.
192 P. P. Graczyk, *J. Med. Chem.*, 2007, **50**, 5773–5779.
193 P. Mu, Y. C. Han, D. Betel, E. Yao, M. Squatrito, P. Ogrodowski, E. de Stanchina, A. D'Andrea, C. Sander and A. Ventura, *Genes Dev.*, 2009, **23**, 2806–2811.
194 K. Conkrite, M. Sundby, S. Mukai, J. M. Thomson, D. Mu, S. M. Hammond and D. MacPherson, *Genes Dev.*, 2011, **25**, 1734–1745.
195 G. Huang, K. Nishimoto, Z. Zhou, D. Hughes and E. S. Kleinerman, *Cancer Res.*, 2012, **72**, 908–916.
196 K. Kim, G. Chadalapaka, S. O. Lee, D. Yamada, X. Sastre-Garau, P. A. Defossez, Y. Y. Park, J. S. Lee and S. Safe, *Oncogene*, 2012, **31**, 1034–1044.
197 V. K. Topkara and D. L. Mann, *Cardiovasc. Drugs Ther.*, 2011, **25**, 171–182.
198 E. Mogilyansky and I. Rigoutsos, *Cell Death Differ.*, 2013, **20**, 1603–1614.
199 S. P. Kabekkodu, V. Shukla, V. K. Varghese, J. D'Souza, S. Chakrabarty and K. Satyamoorthy, *Biol. Rev.*, 2018, **93**, 1955–1986.
200 X. Liu, H. S. Haniff, J. L. Childs-Disney, A. Shuster, H. Aikawa, A. Adibekian and M. D. Disney, *J. Am. Chem. Soc.*, 2020, **142**, 6970–6982.
201 M. G. Costales, J. L. Childs-Disney, H. S. Haniff and M. D. Disney, *J. Med. Chem.*, 2020, DOI: 10.1021/acs.jmedchem.9b01927.
202 E. D. Wieben, R. A. Aleff, X. Tang, M. L. Butz, K. R. Kalari, E. W. Highsmith, J. Jen, G. Vasmatzis, S. V. Patel, L. J. Maguire, K. H. Baratz and M. P. Fautsch, *Invest. Ophthalmol. Visual Sci.*, 2017, **58**, 343–352.
203 R. L. Margolis and D. D. Rudnicki, *Curr. Opin. Neurol.*, 2016, **29**, 743–748.
204 ClinicalTrials.gov, https://clinicaltrials.gov/ct2/show/NCT02268552, accessed July 2020.